# GEOPHYSICAL INVESTIGATIONS OF THE STRUCTURE AND TECTONICS OF SOUTHERN CALIFORNIA

Thesis by

David Milton Hadley

In Partial Fulfillment of the Requirements

for the Degree of

Doctor of Philosophy

California Institute of Technology

Pasadena, California

1978

(Submitted May 22, 1978)

ACKNOWLEDGMENTS

During my stay at the Seismological Laboratory, I have benefited most from the vigorous interaction, enthusiasm and support of the students, faculty and staff. In particular, I thank Dr. Hiroo Kanamori for his guidance and encouragement. His breadth of knowledge and ready willingness to assist have been great resources for me. Dr. Leon Silver has consistently encouraged and assisted this work through stimulating discussions on the geologic framework of southern California. Dr. Shawn Biehler first introduced me to the discipline of geophysics. His assistance and continuing personal support are greatly appreciated. Dr. David Harkrider assisted in the analysis of the surface wave data. I am very much indebted to Ralph Gilman, Francis Lehner and other members of the staff for their help in all phases of the field work. I thank Bob Hart, Carl Johnson and Sue Raikes for their support and critiques. Carl Johnson provided the computer software that produced the base maps in Chapter 3.

I thank Cheryl for her patience and encouragement. She has also helped edit the manuscript.

For their assistance in the preparation of the final draft of this thesis, I thank Marla Turner for the typing and Laszlo Lenches and Joe Galvan for their quality drafting.

Portions of this research were supported by the U. S. Geological Survey under contracts numbers: 14-08-0001-14563, 14-08-0001-15254, 14-08-0001-16711; and by the National Science Foundation under grant number DES75-03643.

ABSTRACT

Regional variations in the crustal structure of southern California are defined by travel-time data from natural and artificial events. We show that the crust of the Mojave, northeastern Peninsular Ranges, eastern Transverse Ranges and Colorado Desert is dominated by a velocity of 6.2±0.1 km/sec. The western Transverse Ranges and the western portion of the Peninsular Ranges are typified by a crustal velocity of 6.7 km/sec. The data indicate that the Transverse Ranges do not have a distinct crustal root. As the topography is not supported isostatically, the Range must be sustained by major north-south compression. A composite profile extending north from the southern end of the Salton Sea defines a crustal thickness for the Coachella Valley of less than 20 km. Through the inversion of Rayleigh wave dispersion data obtained from the analysis of teleseismic surface waves recorded across southern California, we have obtained average S-wave models for the southern Mojave-central Transverse Ranges and the Peninsular Ranges. The observed P-wave velocities and the calculated Poisson's ratio from both P- and S-wave data require a quartz rich crust for the Mojave and a more mafic crust for the Peninsular Ranges. All S-wave models suggest a slight mid-crustal velocity reversal that is approximately coincident with the bottom of the seismic zone.

Regional variations in $P_n$ velocities are obtained from several reversed refraction profiles. These data show that $P_n$ varies from 7.7 to 8.2 km/sec. The high $P_n$ values, 8.2 km/sec, are observed in

the eastern Mojave, the western Transverse Ranges and the Coast Ranges. The 7.8 km/sec $P_n$ velocity extends from the Imperial Valley, through the central Transverse Ranges, and across the western Mojave. $P_n$ profiles indicate that the Moho beneath the eastern Transverse Ranges and the southeastern Mojave dips 2-3$^o$ west.

P-delay studies of a vertically incident PKP phase indicate that a high velocity, 8.3 km/sec structure exists within the shallow upper mantle beneath much of the geomorphic Transverse Ranges. This feature is not offset by the San Andreas fault. We suggest that the continuity of this anomaly across the plate boundary indicates that if the upper mantle participates in plate motion, the mantle plate boundary must be laterally displaced from the crustal boundary. We suggest that the mantle boundary may extend northwest from the Salton Trough and across the eastern end of the velocity anomaly, in the vicinity of the active Helendale-Lenwood-Camprock faults. We propose that the horizontal decoupling between the crust and mantle, required by the lateral displacement at depth of the plate boundary, is accommodated, in part, within the 7.8 km/sec layer.

TABLE OF CONTENTS

# CHAPTER 1

## Introduction

The initial work leading to this thesis began with carefully repeated crustal travel-time measurements from quarries located throughout southern California to both temporary and permanent stations of the regional array. The initial goal was to document velocity variations that were reported by other investigators to precede local earthquakes. As the real, systematic variations in velocity have been less than a few percent, and as the region has not experienced a moderate earthquake ($M_L > 6$) since 1971, we have utilized the travel-time data collected as part of these studies, augmented with data from natural and artificial events, to define the velocity structure of the crust and upper mantle of southern California. Chapter 2 models the P-wave data from seismograms of 20 blasts that were recorded by 17 permanent and 20 temporary stations. The average structure determined for the region of the central Transverse Ranges and the southern Mojave consists of a 4 km thick 5.5 km/sec layer underlain successively by a 23.4 km thick 6.3 km/sec layer, a 5.0 km/sec thick 6.8 km/sec layer and a 7.8 km/sec half space. The details of the lower crust, as determined from this initial data set, are not well constrained. This structure models the travel-time data, corrected for local station and source delays, to ± 0.15 sec.

As the velocity structure derived in Chapter 2 is an average over several sub-provinces, we have compiled additional travel-time data from regional, natural and artificial events in order to define velocity variations within individual geologic provinces. In Chapter 3 we present a representative sample of both crust and upper mantle travel-time curves. A $P_g$ velocity of 6.2 ± 0.1 km/sec is observed for

the Mojave, eastern Transverse Ranges and Colorado desert. Within the western Transverse Ranges and the western portion of the Peninsular Ranges, first arrivals have an apparent velocity of 6.7 km/sec. With the constraints of a fixed array, a special effort has been made to select events that approximately reverse several $P_n$ profiles. These profiles show that $P_n$ varies from 7.7 to 8.2 km/sec. The low $P_n$ velocity of 7.8 km/sec extends northwest from the Imperial Valley, through the region of San Bernardino, and fans out across the central Mojave. Moho dips derived from $P_n$ profiles from the eastern Transverse Ranges and the Mojave indicate a relatively uniform westward dip. A composite profile extending across the Coachella Valley from a calibration blast at the south end of the Salton Sea defines an average crustal thickness of 16 to 19 km.

Although the P-wave velocity model for southern California is slowly becoming more detailed and precise, the S-wave structure has been virtually ignored. As suitable refraction data are not readily available, we have designed a technique, discussed in Chapter 4, for deriving local crustal structure that utilizes the dispersion characteristics of fundamental mode surface waves. Teleseismic Rayleigh waves, $M_s > 7.0$, in the period range 14 to 28 sec, are well recorded by the short period Benioff array within southern California. Multiple arrivals that hamper local dispersion analysis within this period range are detected by narrow band-pass filtering. The records are then windowed on distinct, coherent peaks that move uniformly across the array. Four to seven stations are included in the determination of both the phase velocity across the array and the incidence azimuth.

For earthquakes in the western Pacific, the derived incidence azimuths are systematically rotated counterclockwise by 2-16°. Most of the rotation results from refraction at the continental shelf. However, for events in the southern Pacific, the corrected azimuths for the first arrivals deviate several degrees from the great circle path. Phase velocity data for both the southern Mojave-central Transverse Ranges and the Peninsular Ranges are used in a damped, generalized inversion to obtain regional S-wave velocity models. The starting models are constructed from the travel-time studies described in Chapters 2 and 3. Poisson's ratio as a function of depth is calculated for these two regions. The comparison with laboratory ultrasonic studies requires a quartz-rich crust within the southern Mojave-central Transverse Ranges and a mafic crust within the Peninsular Ranges.

In Chapter 5 we return to the crustal P-wave structure of the Transverse Ranges. Modeling of a reversed, east-west profile indicates that this mountain range does not have a distinct crustal root. As the topography is not supported isostatically, the observed style of deformation requires major north-south compression. Unlike other provinces within southern California, the Transverse Ranges are underlain at a depth of about 40 km by a refractor with a P-velocity of 8.3 km/sec. P-delays from a vertically incident, well-recorded teleseism suggest that this velocity anomaly extends to a depth of 100 km. These data indicate that this high velocity, ridge-like structure is coincident with much of the areal extent of the geomorphic Transverse Ranges and is not offset by the San Andreas fault. Four hypotheses are advanced to explain the continuity of this feature

across the plate boundary: 1) Dynamic phase change, 2) A coincidental alignment of crust or mantle anomalies, 3) Restriction of the lithosphere to the crust, 4) Displacement of plate boundary at depth from the San Andreas fault at the surface. Within the context of the last hypothesis, we suggest the plate boundary at depth is at the eastern end of the velocity anomaly, in the vicinity of the active Helendale-Lenwood-Camprock faults. The 7.8 km/sec layer, observed in the regions of the Salton Trough, northeastern Peninsular Ranges, central Transverse Ranges and the western Mojave, is suggested as a zone of decoupling necessary to accommodate the horizontal shear that results from the divergence of the crust and upper mantle plate boundaries. We suggest that the Transverse Ranges may be, in part, the result of enhanced coupling between the crust and upper mantle suggested by the locally thin 7.8 km/sec layer.

After discussing the implications of the observed mantle velocity anomaly, we conclude in Chapter 6 by discussing the recent seismicity in the west-central Transverse Ranges. Since the San Fernando earthquake, February 1971, the density of the southern California seismic array has increased by an order of magnitude. The enhanced coverage provides an ideal setting for the study of the long-term seismicity of the San Fernando aftershock zone and the adjacent regions. Most of the recent activity within the aftershock zone has been thrust faulting at depths shallower than and south of the mainshock. One event located slightly deeper than and several km north of the main event suggests shear along a flat plane. Transport of the upper block is south. This event is very similar to another deep, $M_L = 4.5$,

earthquake 30 km west of San Fernando. If these events are typical of midcrustal deformation, the west-central Transverse Ranges may be a form of decollement; the horizontal decoupling zone, suggested in Chapter 5 to be localized in the 7.8 km/sec layer, may extend into the crust. A rapid increase in seismicity ($M_L > 3.0$) in the region south of San Fernando suggests an increase in regional strain that was either contemporaneous with or immediately followed the San Fernando earthquake.

# CHAPTER 2

## Average P-wave Structure for Southern California: A Starting Model

ABSTRACT

About twenty blasts are used to determine an average crustal structure for the western Mojave, central Transverse Ranges and northern Peninsular Ranges of Southern California. The shot time is determined up to 10 msec by using a disposable pick-up placed directly on the explosive. About 17 permanent stations and 20 temporary stations are used for the recordings. With a fast paper speed (typically 1 cm/sec) and the WWVB radio signals superposed on the seismic trace, absolute timing accuracy of up to 10 msec is achieved. A representative structure thus determined consists of a 4 km thick 5.5 km/sec layer underlain successively by 23.4 km thick 6.3 km/sec layer, 5.0 km thick 6.8 km/sec layer and 7.8 km/sec half space. The details of the lower crust are somewhat uncertain. This structure can explain the travel time data, corrected for the station and source elevations and for the station delays, to ± 0.15 sec.

# INTRODUCTION

Implicit in earthquake prediction studies, in modeling ground motions from various expected ruptures and in placing boundary conditions on the mechanisms of rapid crustal deformation, such as the Palmdale uplift, is the requirement of a detailed understanding of the structure of the crust and upper mantle within Southern California. Pioneer works on this subject in southern California include those by Gutenberg (1944, 1951, 1952, 1955), Richter (1950), Shor (1955), Press (1956, 1960), and Roller and Healy (1963).

The structure determined by Press (1960) has long been used in the earthquake location program by the Seismological Laboratory, California Institute of Technology (Hileman et al., 1973) (Press's model has an upper layer 26.2 km thick with P velocity of 6.11 km/sec; a second layer 25.6 km thick with P velocity of 7.66 km/sec and an underlying half-space with P velocity of 8.11 km/sec). The recent increase in the number of seismic stations as well as the improved timing accuracy warrant a more detailed study of the crust.

## DATA

Figure 2.1 shows the locations of the explosions used in this phase of the study. The coordinates and nature of the blasts are listed in Table 2.1. In most cases, the shot was timed with a disposable pick-up placed directly on the explosive. The signal was recorded on a Kinemetrics PS-1 portable seismograph unit together with the WWVB radio signal. This method permits a determination of the shot time to within ±10 msec. The shot point location was determined to 1/100 minute from U.S. Geological Survey quadrangles. These events were recorded by permanent seismic stations belonging to the southern California seismic network and temporary stations consisting of the Kinemetrics portable units and Caltech seismographic trailers (Figure 2.1). Except on few occasions, the signals recorded by the permanent stations were telemetered through telephone lines to Pasadena and recorded on 16 mm films (Develocorder) with the WWVB radio signal superimposed on the seismic trace. The portable Kinemetrics units are run with 1 cm/sec paper speed with the WWVB radio signal superimposed on the trace. In some cases a strip-chart recorder was used with 1 to 2 cm/sec paper speed. The trailer recordings are also timed with either WWVB or WWV radio signals. Figure 2.2 shows typical examples of the seismograms. With these recording systems, a timing accuracy of up to 10 msec is achieved when the signal onset is clear.

Figure 2.1 also shows the source-station combinations used in the present study and several profiles which were established specifically for the determination of crustal structure.

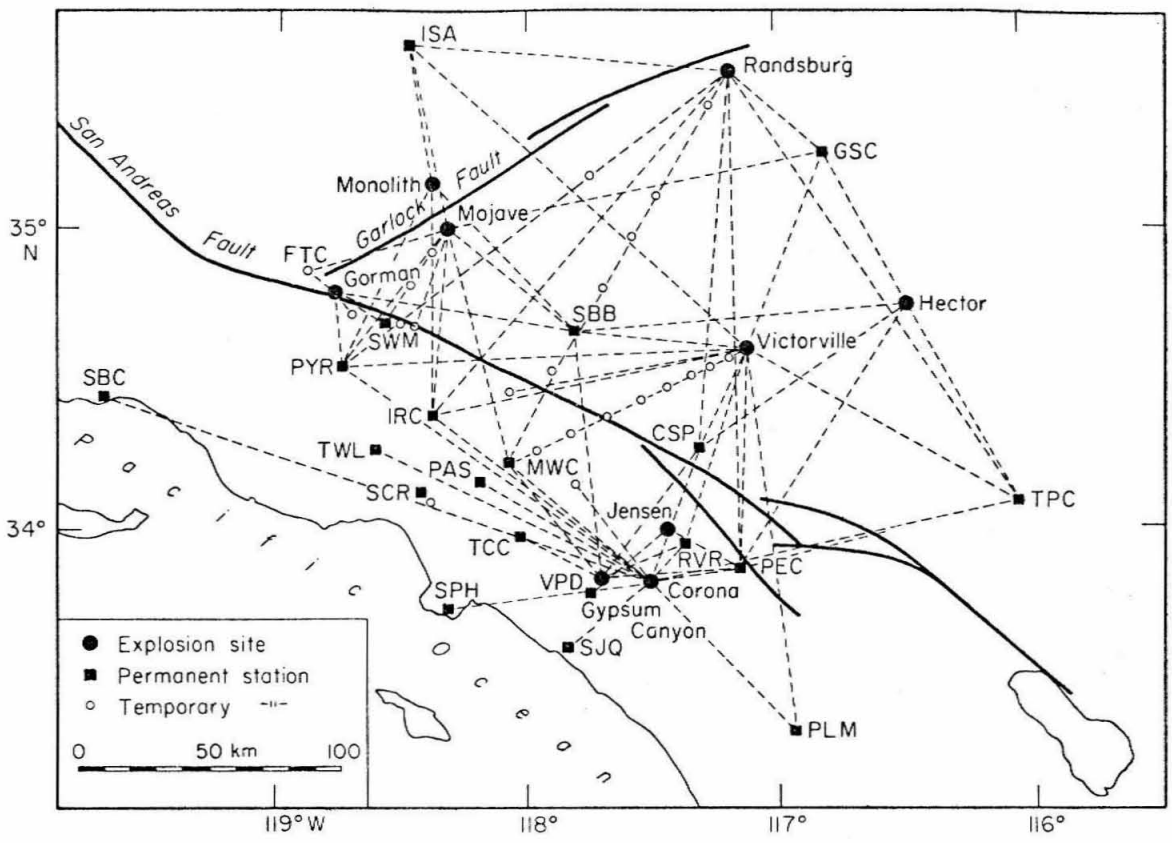


Figure 2.1 Source-station combinations used in the present study. Explosion sites are shown by large circles and stations are shown by squares (permanent stations) and open circles (temporary stations).

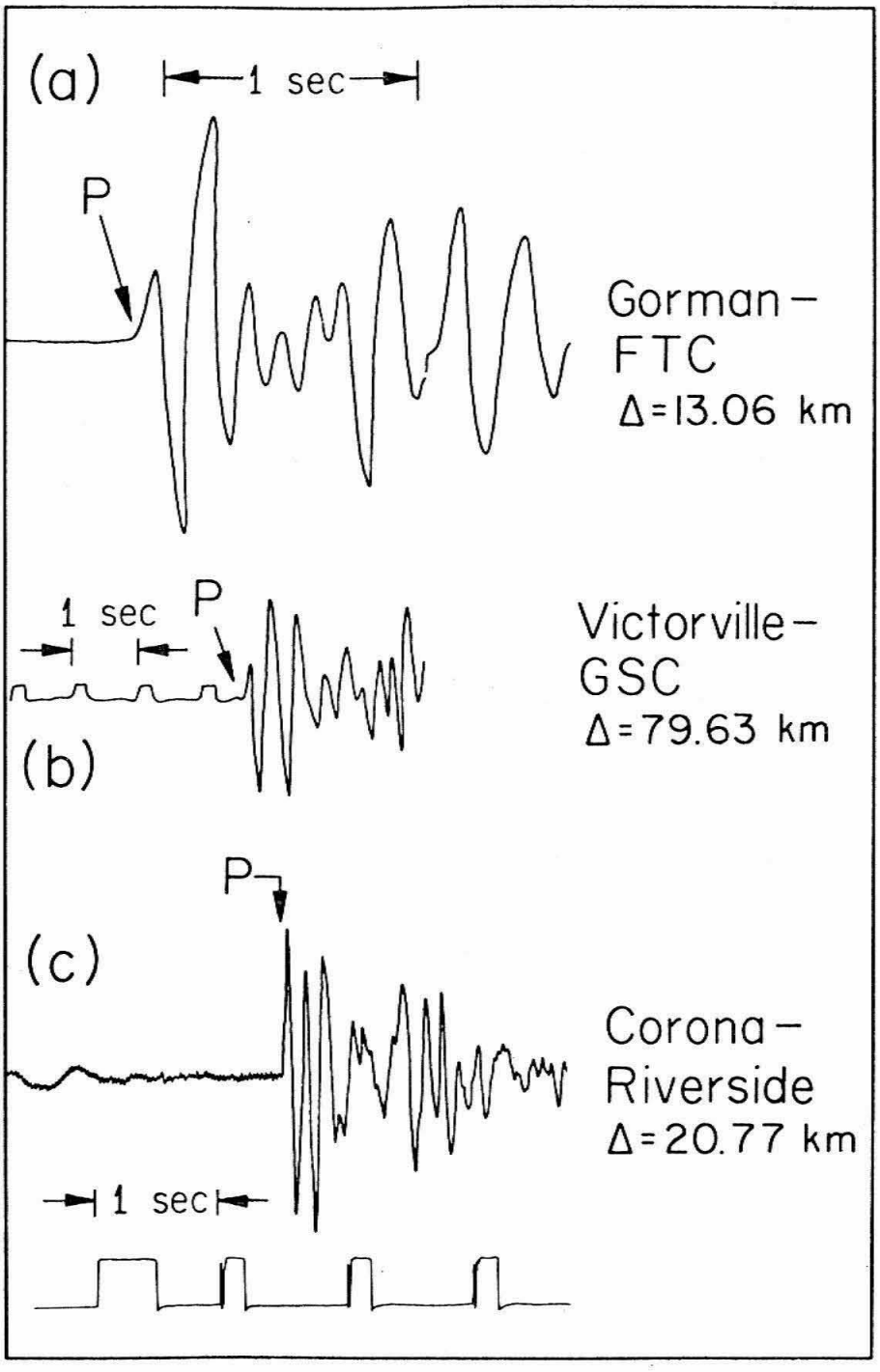


Figure 2.2 Examples of the records. (A) Kinemetrics (PS-1) portable unit (paper speed: 1 cm/sec) used at temporary stations. (B) Telemetered record on Develocorder from permanent stations (film speed: 1 cm/sec on a viewer). (C) Strip chart recording at temporary stations (paper speed: 2 cm/sec).

Table 2.1 *Explosion data*

| Location | Approximate Coordinates | Elevation (m) | Note |
|---|---|---|---|
| Victorville | 34.63°N, 117.11°W | 1280 | Cement Quarry |
| Corona | 33.84°N, 117.51°W | 300 | Dacite Porphyry |
| Jensen | 34.03°N, 117.43°W | 360 | Cement Quarry |
| Gypsum Canyon | 33.86°N, 117.71°W | 150 | Sand and Gravel |
| Randsburg | 38.52°N, 117.17°W | 750 | Navy Testing |
| Gorman | 34.83°N, 118.76°W | 1290 | Cement Quarry |
| Mojave | 35.03°N, 118.32°W | 1190 | Cement Quarry |
| Monolith | 35.15°N, 118.39°W | 1350 | Cement Quarry |
| Hector | 34.75°N, 116.42°W | 600 | Bentonite Quarry |

The travel time data, summarized in Table 2.2, are assigned grades A (± 10 msec), B (± 30 sec), and C (± 100 msec).

## UPPER CRUST

All of the travel time data obtained for the source-station combinations shown in Figure 2.1 are plotted, regardless of the azimuth, on the reduced travel time curve given by Figure 2.3. Since the altitude of the shot points and the stations varies from 350 to 2280 m, and also the local geologic structure differs beneath individual shot points and stations, these data are not homogeneous. Nevertheless, in view of the fairly random coverage of the paths as shown in Figure 2.1, this figure depicts the overall variation of the short-distance ($\Delta < 220$ km) travel times in southern California. The scatter is surprisingly small in view of the vast variability of geology in this area. With a few exceptions, the scatter is within ± 0.3 sec of the average. The straight line segments shown in Figure 2.3 correspond to a structure determined for a more restricted profile which will be discussed in the following.

### Victorville Blast

The Victorville blasts have been used to establish a fairly complete profile extending from the quarry to the station MWC (Figure 2.1). Figure 2.4a shows the data uncorrected for station elevation and local geology. The data along the profile (closed circles) can be fit very well by two segments having apparent velocities of 5.32 km/sec and 6.35 km/sec, the cross-over being at 37.5 km. This indicates a structure

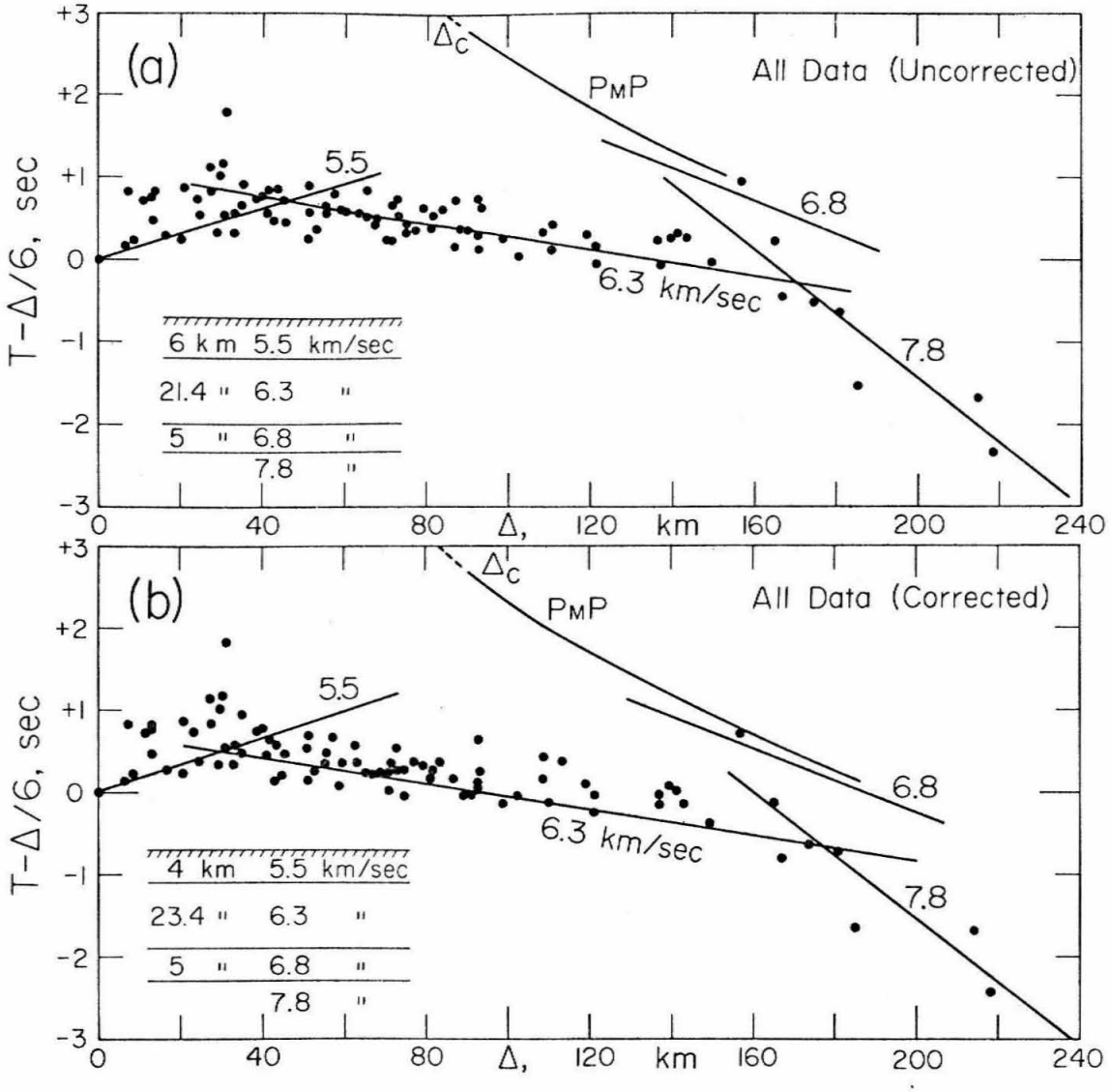


Figure 2.3 (a) Reduced travel times for all data except those for the Hector blast. Travel time curves are for the structure shown in the inset. $P_MP$ branch shows the Moho reflection. (b) Reduced travel times corrected for the elevations at both source and stations. The structure is shown in the inset.

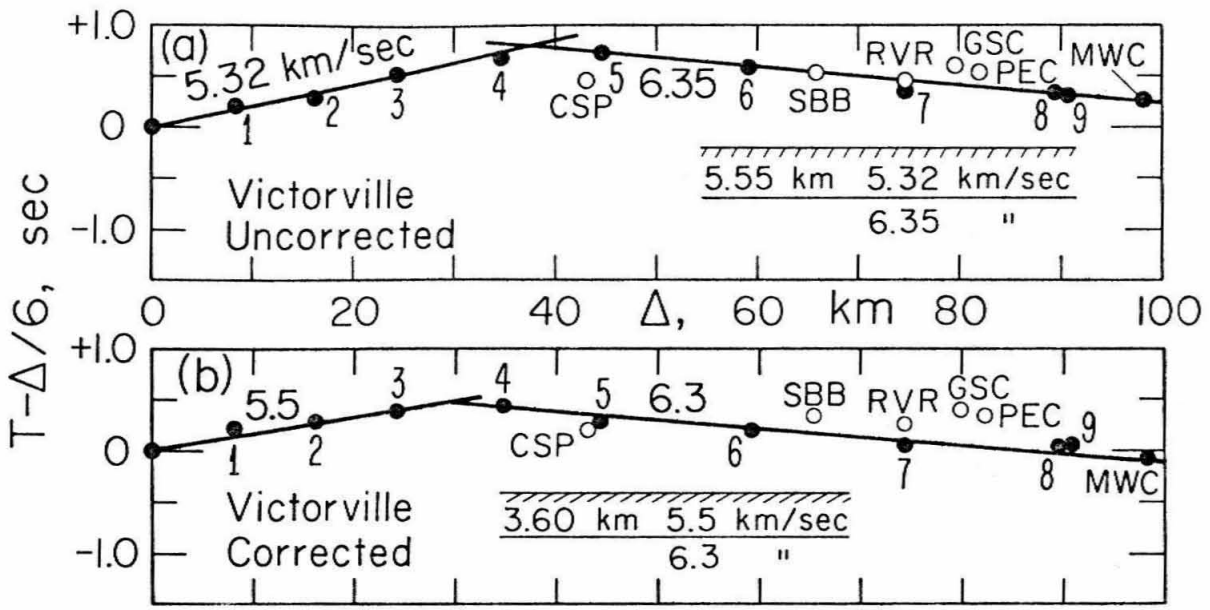


Figure 2.4 Uncorrected (a) and corrected (b) travel times for the Victorville blast. The corresponding structures are given in the inset. Numbered stations are; 1: Navajo; 2: UICT; 3: Trash; 4: Baldy Mesa; 5: EXP-O; 6: Table Mt.; 7: Crystal Lake; 8: Charlton Flats; 9: Mt. Emma.

Table 2.2a *Victorville blast*

| Station | $\Delta$ (km) | Azimuth (deg) | $T-\Delta/6$ (sec) | Corrected $T-\Delta/6$ (sec) | Grade |
|---|---|---|---|---|---|
| Navajo | 8.24 | 237.8 | 0.21 | 0.21 | C |
| UICT | 16.18 | 241.1 | 0.28 | 0.28 | B |
| Trash | 24.39 | 245.1 | 0.52 | 0.39†) | B |
| Baldy Mesa | 34.82 | 242.6 | 0.68 | 0.47†) | C |
| EXP-O | 44.55 | 244.8 | 0.74 | 0.29 | A |
| Table Mt. | 59.08 | 242.4 | 0.60 | 0.24 | A |
| Crystal Lake | 74.63 | 243.1 | 0.37 | 0.06 | B |
| Charlton Flats | 89.55 | 245.0 | 0.36 | 0.07 | C |
| MWC | 98.03 | 242.9 | 0.26 | –0.05 | C |
| Mt. Emma | 90.62 | 258.8 | 0.34 | 0.08 | B |
| CSP | 43.12 | 211.6 | 0.46 | 0.20 | A |
| SBB | 65.64 | 275.9 | 0.54 | 0.33 | A |
| RVR | 74.64 | 199.0 | 0.44 | 0.28 | B |
| GSC | 79.63 | 20.5 | 0.62 | 0.39 | B |
| PEC | 81.97 | 183.2 | 0.54 | 0.35 | B |
| VPD | 108.43 | 213.7 | 0.33 | 0.18 | C |
| TPC | 113.92 | 120.5 | 0.66 | 0.46 | C |
| IRC | 121.29 | 257.7 | 0.19 | 0.00 | C |
| PLM | 143.44 | 170.7 | 0.25 | –0.05 | C |
| PYR | 149.71 | 267.8 | –0.04 | –0.30 | C |
| ISA | 167.58 | 312.5 | –0.49 | –0.71 | C |

For station coordinates, see HILEMAN *et al.* (1973) for permanent stations (three-letter abbreviation) and Table 2j for temporary stations.

† Corrected for local structure.

Table 2.2b *Corona blast*

| Station | $\Delta$ (km) | Azimuth (deg) | $T-\Delta/6$ (sec) | Corrected $T-\Delta/6$ (sec) | Grade |
|---|---|---|---|---|---|
| RVR | 20.77 | 35.8 | 0.23 | 0.23 | A |
| VPD | 23.81 | 263.0 | 0.72 | 0.72 | B |
| PEC | 32.48 | 80.0 | 0.32 | 0.32 | B |
| SJQ | 39.85 | 232.0 | 0.77 | 0.77 | B |
| Dalton Lake | 45.85 | 322.3 | 0.47 | 0.39 | A |
| CSP | 52.53 | 15.2 | 0.40 | 0.24 | B |
| MWC | 66.27 | 309.9 | 0.44 | 0.23 | B |
| PAS | 70.25 | 299.2 | 0.25 | 0.19 | B |
| SPH | 77.42 | 262.4 | 0.37 | 0.30 | B |
| PLM | 80.71 | 132.0 | 0.38 | 0.19 | B |
| UCLA-1 | 86.67 | 290.2 | 0.16 | 0.09 | — |
| SCR | 92.37 | 288.8 | 0.11 | 0.05 | C |
| IRC | 102.46 | 306.7 | 0.02 | −0.07 | B |
| TWL | 111.53 | 296.1 | 0.41 | 0.35 | C |
| TPC | 137.89 | 77.4 | −0.08 | −0.17 | B |
| PYR | 139.48 | 305.6 | 0.25 | 0.10 | C |
| GSC | 174.3 | 21.5 | −0.52 | −0.70 | B |
| IKP | 185.7 | 135.0 | −1.55 | −1.72 | C |
| SBC | 214.15 | 288.7 | −1.69 | −1.74 | C |
| ISA | 218.74 | 336.3 | −2.36 | −2.52 | C |

Table 2.2c *Jensen blast*

| Station | $\Delta$ (km) | Azimuth (deg) | $T-\Delta/6$ (sec) | Corrected $T-\Delta/6$ (ec) | Grade |
|---|---|---|---|---|---|
| RVR | 6.45 | 124.3 | 0.14 | 0.14 | B |
| PEC | 29.23 | 120.6 | 0.33 | 0.33 | B |
| CSP | 30.99 | 13.0 | 0.54 | 0.54 | B |
| VPD | 38.40 | 232.5 | 0.74 | 0.74 | B |

Table 2.2d *Gypsum Canyon*

| Station | $\Delta$ (km) | Azimuth (deg) | $T-\Delta/6$ (sec) | Corrected $T-\Delta/6$ (sec) | Grade |
|---|---|---|---|---|---|
| VPD | 7.52 | 223.3 | 0.83 | 0.83 | A |
| SJQ | 30.01 | 205.5 | 1.18 | 1.18 | B |
| TCC | 31.84 | 297.1 | 1.82 | 1.82 | B |
| RVR | 33.71 | 65.1 | 0.57 | 0.57 | C |
| PEC | 50.55 | 86.4 | 0.60 | 0.52 | A |
| MWC | 51.42 | 320.8 | 0.91 | 0.71 | C |
| CSP | 57.94 | 33.7 | 0.82 | 0.67 | B |
| SBB | 92.07 | 353.3 | 0.74 | 0.64 | B |

Table 2.2e *Randsburg blast*

| Station | $\Delta$ (km) | Azimuth (deg) | $T-\Delta/6$ (sec) | Corrected $T-\Delta/6$ (sec) | Grade |
|---|---|---|---|---|---|
| Navy Test Range—1 | 13.90 | 237.8 | 0.47 | 0.47 | B |
| Galileo Hill | 63.29 | 237.6 | 0.58 | 0.40 | B |
| Kramer Hill | 71.11 | 213.1 | 0.22 | 0.06 | A |
| Jackrabbit Hill | 92.46 | 212.8 | 0.30 | 0.14 | A |
| SBB | 110.14 | 213.1 | 0.10 | –0.06 | B |
| Lovejoy Buttes | 121.01 | 211.3 | –0.04 | –0.21 | A |
| GSC | 40.95 | 126.5 | 0.58 | 0.48 | A |
| CLC | 50.84 | 310.2 | 0.23 | 0.07 | C |
| ISA | 119.47 | 276.9 | 0.32 | 0.15 | B |
| CSP | 136.82 | 187.3 | 0.24 | –0.03 | B |
| SWM | 156.67 | 235.8 | 0.97 | 0.77 | C |
| MWC | 165.49 | 209.8 | 0.22 | –0.04 | C |
| PEC | 180.81 | 179.8 | –0.64 | –0.85 | C |

Table 2.2f *Mojave blast*

| Station | $\Delta$ (km) | Azimuth (deg) | $T-\Delta/6$ (sec) | Corrected $T-\Delta/6$ (sec) | Grade |
|---|---|---|---|---|---|
| Willow Springs | 11.71 | 211.0 | 0.73 | 0.73 | A |
| Rosamond | 26.93 | 214.2 | 1.13 | 1.13 | B |
| Lake Hughes | 41.95 | 194.1 | 0.85 | 0.63 | B |
| SWM | 43.16 | 214.0 | 0.90 | 0.66 | A |
| FTC | 55.47 | 250.8 | 0.79 | 0.57 | B |
| SBB | 59.78 | 130.4 | 0.61 | 0.41 | A |
| PYR | 65.24 | 216.6 | 0.90 | 0.66 | A |
| ISA | 68.54 | 348.1 | 0.51 | 0.31 | C |
| IRC | 72.37 | 185.8 | 0.77 | 0.59 | B |
| MWC | 93.62 | 165.1 | 0.66 | 0.36 | B |
| GSC | 141.09 | 77.6 | 0.32 | 0.10 | C |

Table 2.2g *Gorman blast*

| Station | $\Delta$ (km) | Azimuth (deg) | $T-\Delta/6$ (sec) | Corrected $T-\Delta/6$ (sec) | Grade |
|---|---|---|---|---|---|
| FTC | 12.88 | 288.9 | 0.78 | 0.78 | A |
| West Liebre Mt. | 13.21 | 153.2 | 0.82 | 0.82 | B |
| SWM | 20.89 | 128.6 | 0.88 | 0.88 | A |
| Pine Canyon | 27.81 | 123.1 | 0.82 | 0.82 | A |
| PYR | 29.76 | 176.8 | 1.01 | 1.01 | A |
| Lake Hughes | 35.20 | 120.5 | 0.92 | 0.92 | A |

Table 2.2h *Monolith blast*

| Station | $\Delta$ (km) | Azimuth (deg) | $T-\Delta/6$ (sec) | Corrected $T-\Delta/6$ (sec) | Grade |
|---|---|---|---|---|---|
| ISA | 55.76 | 351.7 | 0.64 | 0.41 | B |
| PYR | 71.81 | 206.9 | 0.68 | 0.41 | B |
| SBB | 72.36 | 134.4 | 0.54 | 0.32 | C |
| IRC | 83.88 | 180.7 | 0.62 | 0.42 | C |

Table 2.2i *Hector blast*

| Station | $\Delta$ (km) | Azimuth (deg) | $T-\Delta/6$ (sec) | Corrected $T-\Delta/6$ (sec) | Grade |
|---|---|---|---|---|---|
| GSC | 70.71 | 330.7 | 1.16 | 1.00 | B |
| TPC | 79.12 | 154.0 | 1.01 | 0.88 | B |
| CSP | 98.98 | 240.1 | 0.77 | 0.58 | B |
| PEC | 116.53 | 215.8 | 0.72 | 0.60 | B |
| SBB | 128.35 | 267.5 | 0.60 | 0.46 | B |

Table 2.2j *Station coordinates*

| Station | Latitude | Longitude | Height |
|---|---|---|---|
| Navajo | 34°35.41′N | 117°11.25′W | 910 |
| UICT | 34°33.54′N | 117°15.95′W | 900 |
| Trash | 34°32.22′N | 117°21.15′W | 870 |
| Baldy Mesa | 34°29.11′N | 117°26.88′W | 1012 |
| EXP-O | 34°27.47′N | 117°33.00′W | 1130 |
| Table Mt. | 34°22.91′N | 117°40.84′W | 2280 |
| Crystal Lake | 34°19.39′N | 117°50.07′W | 1736 |
| Charlton Flats | 34°17.09′N | 117°59.53′W | 1556 |
| Mt. Emma | 34°28.07′N | 118°04.74′W | 1305 |
| SBB | 34°41.31′N | 117°49.43′W | 829 |
| Dalton Lake | 34°10.20′N | 117°48.56′W | 523 |
| UCLA—1 | 34°06.52′N | 118°23.27′W | 347 |
| Navy Test Range—1 | 35°27.29′N | 117°17.79′W | 867 |
| Galileo Hill | 35°12.87′N | 117°45.23′W | 945 |
| Kramer Hill | 34°59.03′N | 117°35.52′W | 774 |
| Jackrabbit Hill | 34°49.21′N | 117°42.89′W | 830 |
| Lovejoy Buttes | 34°35.27′N | 117°51.14′W | 879 |
| Willow Springs | 34°57.03′N | 118°23.04′W | 1180 |
| Rosamond | 34°50.40′N | 118°29.00′W | 872 |
| Lake Hughes | 34°40.43′N | 118°25.76′W | 1000 |
| Lake Hughes—2 | 34°40.59′N | 118°26.07′W | 1024 |
| West Liebre Mt. | 34°43.77′N | 118°41.70′W | 1627 |
| Pine Canyon | 34°41.93′N | 118°30.34′W | 1146 |

as shown in the inset. The off-profile stations (open circle) are within $\pm$ 0.3 sec of the above travel time curves indicating a lateral uniformity of the structure.

Next we will consider corrections for elevation and local structure at both the source and the station. These corrections are very difficult to make precisely. Utilizing the structure given in the inset of Figure 2.4a, the station and the source height corrections can be given by $\Delta t = -h \cos i_o/v_o$ where h is the height, $v_o$ is the velocity at the surface, here 5.32 km/sec, and $i_o$ is the incidence angle at the station or the take-off angle at the source. For $\overline{P}$, $i_o = 90^o$, for $P_g$, $i_o = 57^o$, and for $P_n$, $i_o = 42^o$.

The effect of the local geology cannot be estimated unless the structure is known. The correction is probably negligible for stations on bedrock, but it can become considerably large for stations on alluvium. For estimating this correction, we have made short range (up to 1.4 km) refraction measurements at stations 3 (Trash), 4 (Baldy Mesa) and 5 (EXP-O) shown in Figure 2.4. These profiles were recorded with a 24-channel refraction system. Small charges were used as seismic sources. The profiles are shown in Figures 2.5a, b, and c. Since these structures are used only for correction purposes, the dip of the layers is not considered and the insets represent the average structure. The corrections are then computed as the difference of the travel times for a vertical path between this structure and a homogeneous 5.32 km/sec layer. The largest height correction amounts to 0.23 sec (Table Mountain, 2280 m) and the largest station correction amounts to 0.21 sec (EXP-O). Although these corrections are

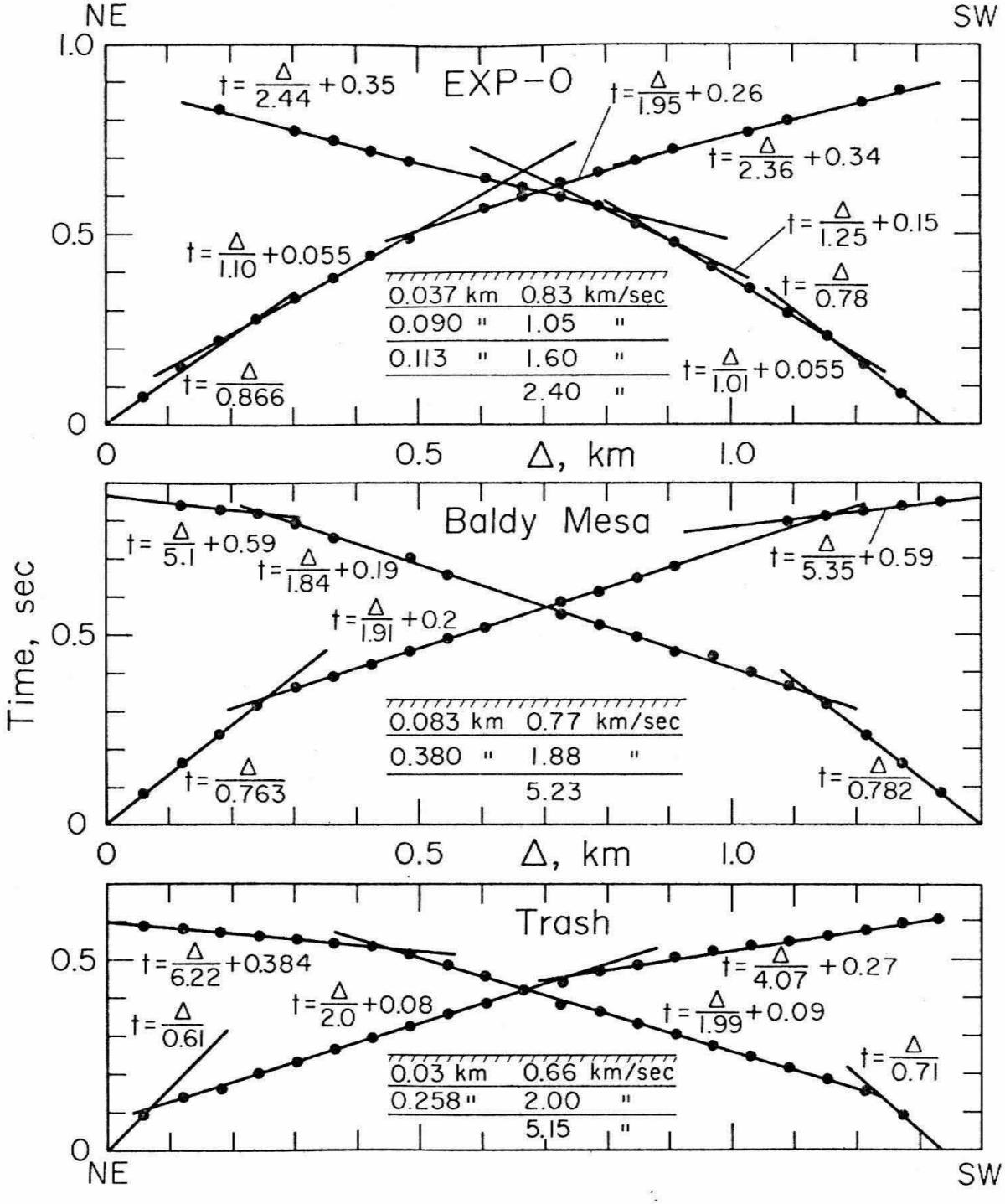


Figure 2.5 Short range refraction measurements at temporary stations EXP-0 (a), Baldy Mesa (b) and Trash (c). Structures (averaged) are given in the inset.

significant, they are still small enough so that the errors arising from the crude correction method are probably insignificant. Figure 2.4b shows the corrected travel times. These data can be fit very well by two straight segments having apparent velocities of 5.5 km/sec, and 6.3 km/sec; the cross-over is at 28.0 km. The corresponding structure is given in the inset. In this structure, any feature above the sea level has been stripped off. Considering the source-station combinations shown in Figure 2.1, this structure can be considered to represent the structure north of the San Andreas fault in this area. We will use these travel time curves as a standard for comparison with the results from other profiles.

Corona, Jensen and Gypsum Canyon Blast

For these blasts (Figure 2.6a), no attempt has been made to align stations to make up a profile. However, it is remarkable that the combined travel times for the Corona and Jensen blasts are very consistent with those determined by the Victorville blast. If the 6.3 km/sec branch is shifted upward by 0.1 sec, the agreement would be even better. This indicates that the 5.5 km/sec layer is 0.5 km thicker in this region than the Victorville profile. It should also be noted that the arrivals at stations VPD, SJQ, SPH and TWL for the Corona blast and at VPD for the Jensen blast are delayed by 0.3 sec to 0.7 sec, the average being 0.5 sec. All of these stations are located on the alluvium of the Los Angeles basin. Although the details of the local structure beneath these stations are unknown, a delay of 0.5 sec seems reasonable for the alluvium. If we use this value for

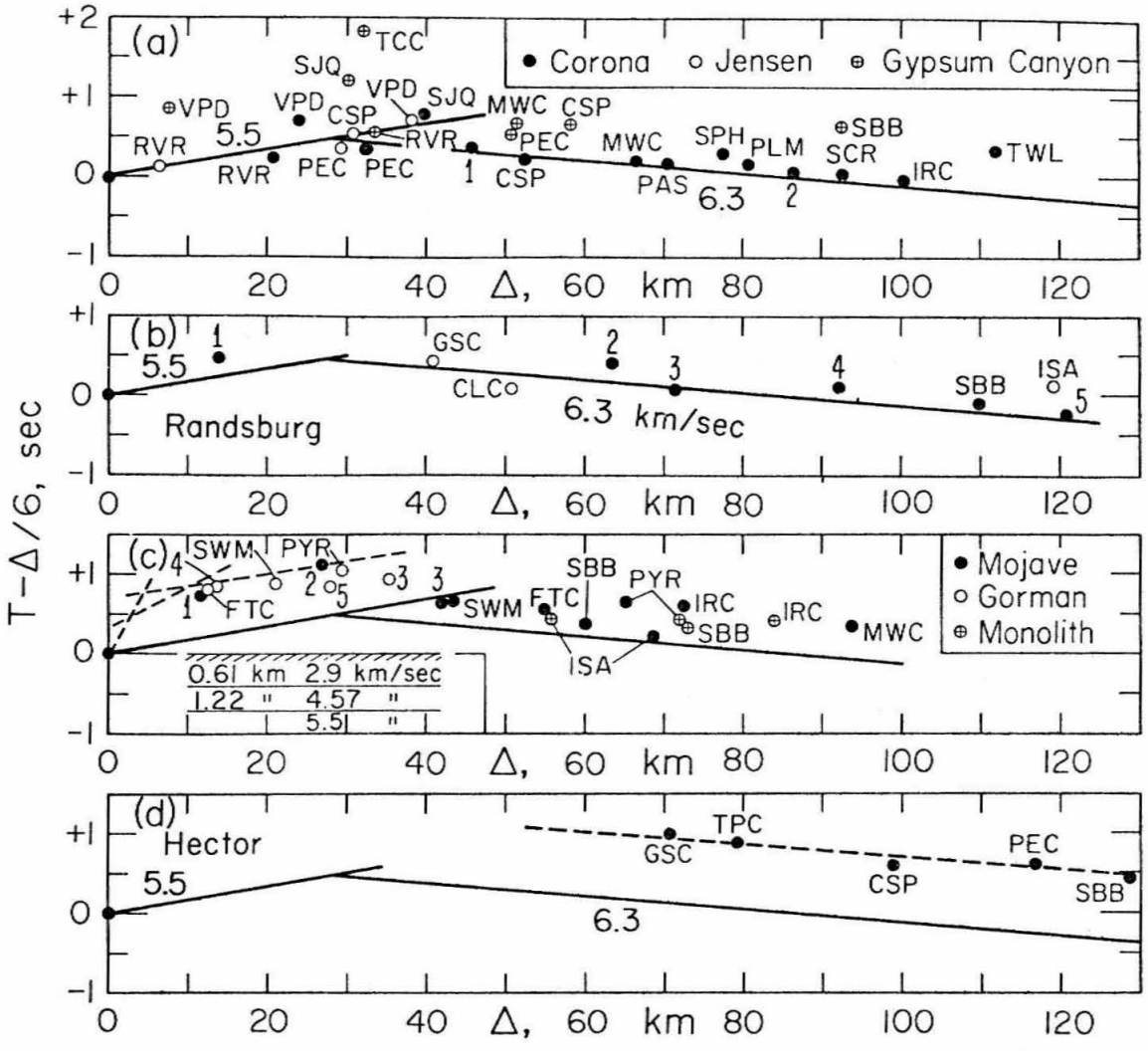


Figure 2.6 Travel times for various blasts. Height corrections are applied for both source and stations. Solid travel time curves are for the structure fitted to the corrected Victorville data. (a) Corona, Jensen and Gypsum Canyon blasts. Numbered stations are; 1: Dalton Lake; 2: UCLA-1. (b) Randsburg blast. Numbered stations are; 1: Navy Test Range-1; 2: Galileo Hill; 3: Kramer Hill; 4: Jackrabbit Hill; 5: Lovejoy Buttes. (c) Mojave, Gorman and Monolith blasts. Dotted travel time curves correspond to the structure shown in the inset. Numbered stations are; 1: Willow Springs; 2: Rosamond; 3: Lake Hughes; 4: West Liebre Mt.; 5: Pine Canyon. (d) Hector blast. The dotted line shows the 6.3 km/sec line displaced upward by 0.9 sec from the Victorville curve.

the time delay at these stations, the data for the Corona and the Jensen blasts become very consistent with the structure obtained for the Victorville profile.

For the Gypsum Canyon blast, the data, though scattered considerably, show systematically late arrivals. However, if we assume a delay of 0.5 sec for the Los Angeles basin alluvium, these delays can readily be explained. Since in this case, the shot point itself is on the alluvium, allowance should be made for an additional delay of 0.5 sec. Thus if we subtract 1.0 sec from the times at stations on the Los Angeles basin alluvium (VPD, TCC, SJQ) and 0.5 sec from other stations (RVR, MWC, PEC, CSP, SBB), the general trend for the Gypsum Canyon blast becomes consistent with that for the Corona and the Jensen blasts. These source-station combinations represent primarily the structure south of the San Andreas fault. We therefore conclude that, except for the delay of about 0.5 sec beneath the stations on the Los Angeles basin alluvium, the upper crustal structure of the central Transverse Ranges and the northern Peninsula Ranges is nearly the same, velocitywise, as that in the south-central Mojave.

Randsburg Blast

Figure 2.6b shows the travel time data for the Randsburg blast. The height corrections are made, but no corrections are made for the local structure. The closed circles represent the stations along the profile to Mount Wilson, and the open circles, off-profile stations. There is no obvious difference between these two groups of stations, and they are, as a whole, consistent with the Victorville travel time

curves. If the whole curve were shifted upwards by 0.1 sec, the agreement would become even better. It is possible that this 0.1 sec delay is due to the local structure beneath the source. However, owing to the lack of short-distance data, it is not resolvable whether the delay is due to the source or to a thickening of the top, presumably 5.5 km/sec, layer.

Mojave, Monolith and Gorman Blast

Figure 2.2 shows the composite travel-time data for the Mojave, Monolith and Gorman blasts together with the travel-time curves obtained for the Victorville profile. The observed arrivals at $\Delta < 40$ km are delayed by nearly 0.5 sec. Most of these data are obtained from the Gorman blast for which the paths are essentially within the fault zone of either the Garlock or the San Andreas faults. Refraction measurements made in 1965 in this area (Don L. Anderson, personal communication, 1973) suggest low-velocity, presumably highly shattered, surface layers to a depth of 600 m as shown in the inset of Figure 2.6c. The dotted lines in Figure 2.6c are the travel time curves corresponding to this structure; the delay can be accounted for by this low-velocity surface layer.

The arrival times at $\Delta > 40$ km are delayed by 0.25 sec. Both Mojave and Monolith are cement quarries. Usually the in-situ velocity in limestones is relatively high, about 4 km/sec, so that a large source delay is unlikely. It seems that the above delay can be explained most reasonably by a thickening of about 1.5 km of the 5.5 km/sec layer.

Hector

Figure 2.6d shows the travel time data for the Hector blast. Unlike other blasts, all the arrivals are consistently late by 0.9 sec. Although the lack of short-distance data does not permit the determination of the structure, the above delay seems to be mostly due to the source. Hector mine is quarrying bentonite, a very soft clay mineral (ultrasonic velocity $\sim$ 1.7 km/sec), and an excessively large delay is quite possible. In view of this possible large source delay, the data obtained by this blast may not be adequate for crustal studies unless the structure beneath the quarry can be determined. In the interpretation that follows, these data will not be used directly. However, the consistent 6.3 km/sec branch strengthens the evidence for the existence of a layer with this velocity.

In summary, if we remove all the structures above the sea level, and are to find a single upper crustal structure that represents the whole area, we obtain a model consisting of a 4 km thick 5.5 km/sec layer underlain by a 6.3 km/sec layer. There is an indication that the 5.5 km/sec layer is about 1 to 1.5 km thinner along the Victorville to Mount Wilson path than elsewhere. The well defined 6.3 km/sec branch up to 150 km suggests a substantial thickness of at least 10 km for this layer. This model will be used in the following.

## LOWER CRUST

Since most of the blasts are not large enough to be recorded at distances beyond 150 km, the data for the lower crust are incomplete. As shown in Figure 2.3, there are arrivals at $\Delta > 160$ km which indicate the $P_n$ branch, but the slope cannot be well defined. It is also not clear whether there is another branch intermediate between the 6.3 km/sec and the $P_n$ branch. However, there are several constraints which are useful for determining the lower crustal structure. These constraints come from the following observations:

(1) The round-trip travel time for the clear near-vertical Moho reflections, $P_MP$, observed at Corona is 10.5 sec (Shor, 1955; see also Richter, 1958). (2) For the Victorville blast, a very large second arrival was observed at Mt. Wilson ($\Delta$ = 98 km), but it was not observed at Crystal Lake ($\Delta$ = 75 km) nor Charlton Flats ($\Delta$ = 90 km) (see Figure 2.7); we consider this strong phase as the Moho reflection near the critical distance $\Delta c$, and set $\Delta c$ at 90 to 98 km. (3) This strong phase is also observed for other blasts at stations from $\Delta$ = 90 to 110 km. $P_MP$ - P times are 1.5 sec to 3 sec depending on the distance (see Figure 2.7). (4) The $P_n$ velocity is determined as 7.66 km/sec by Press (1960), while 8.0 to 8.2 km/sec has been suggested by Gutenberg (1955). We examined a Nevada event to determine the $P_n$ velocity over a distance range 200 to 400 km beneath the area considered. The origin time and the location of this event are known sufficiently well for this purpose. Figure 2.8 shows the reduced travel time curve. The station corrections suggested in the earlier section have been applied. The $P_n$ velocity of about 7.8 km/sec appears appropriate for the central

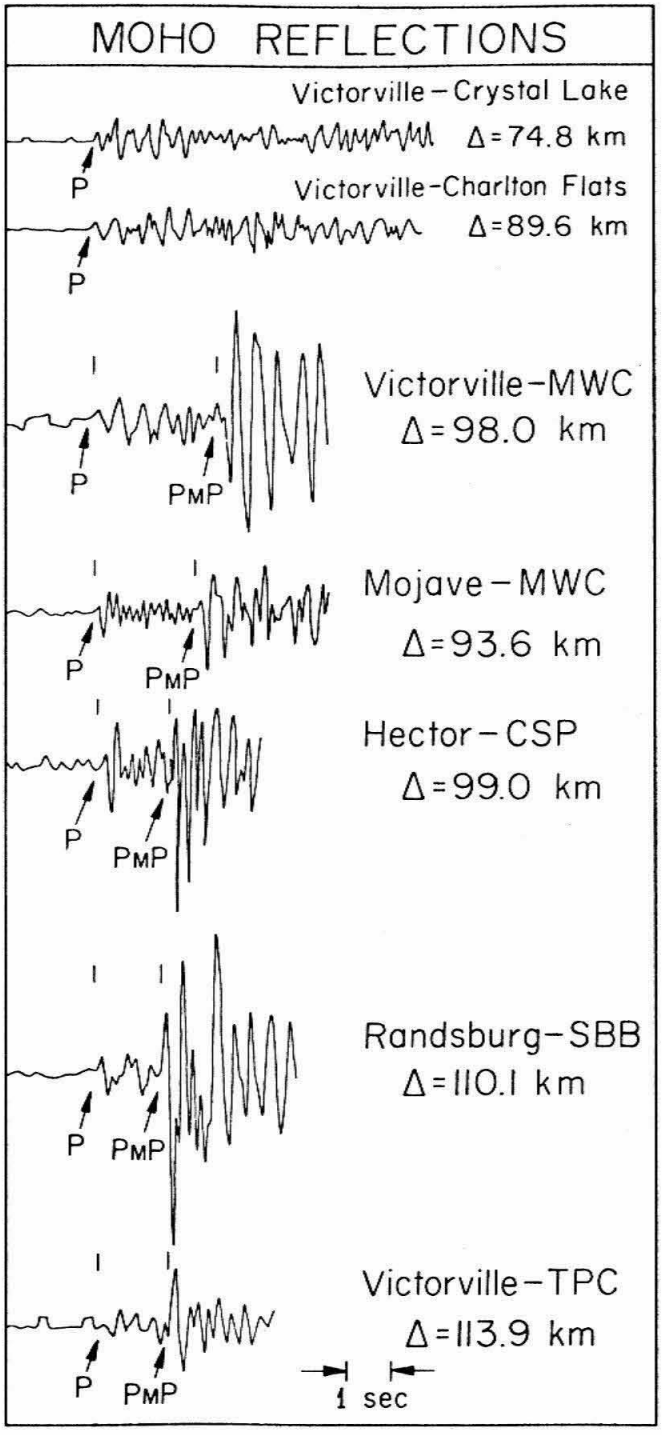


Figure 2.7 Examples of the Moho reflection ($P_MP$) near the critical distance. Note the absence of the $P_MP$ phase at Crystal Lake ($\Delta$ = 74.8 km) and Charlton Flats ($\Delta$ = 89.6 km).

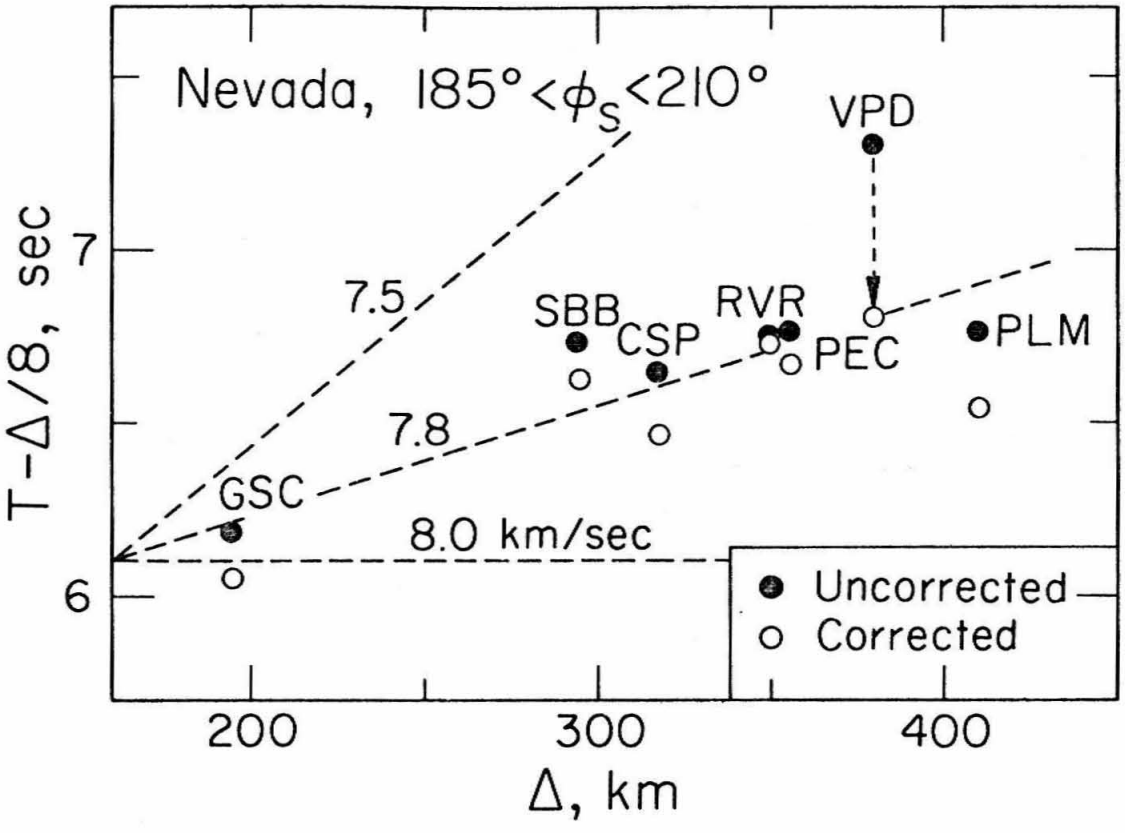


Figure 2.8 Travel times for a Nevada event. The stations within the azimuth range from 185° to 210° are used.

Mojave. This value, which is intermediate between Press (1960) and Gutenberg (1955), will be used in the following.

First, we assume that the 6.3 km/sec layer extends to the Moho. Then to satisfy (1), the thickness of the 6.3 km/sec layer should be approximately 28 km, the height correction having been considered. However, simple calculation shows that this structure brings $\Delta_c$ at 85 km which is slightly too small. One possible way of increasing $\Delta_c$ is to insert an intermediate layer at the bottom of the crust. For example, replacing the bottom 4.6 km of the 6.3 km/sec layer by a 5 km thick 6.8 km/sec layer brings $\Delta_c$ up to 90 km and still satisfies (1).

This model gives $P_M P$ - P times of 2.7 sec and 2.1 sec, at $\Delta$ = 90 km and 110 km respectively, and therefore satisfies (2) and (3). Of course, this is not the only possibility. However, since the structure down to 15 km is fairly well constrained by the data for $\Delta < 150$ km, the range of the possible models is not large. The least certain is the velocity of the intermediate layer. The travel time curves for this structure are given in Figure 2.3b which shows the overall consistency of this model with the data. The phase refracted in the 6.8 km/sec layer never appears as the first arrival for shallow focus events.

The structure obtained here differs from that of Press (1960). In particular, the 4 km thick upper layer (5.5 km/sec) found in the present study does not exist in Press (1960). Since Press's emphasis was on the regional structure rather than the local structure, he had only two stations at $\Delta \leq 50$ km, which are too few to determine this layer. Press's model includes a 8.11 km/sec layer at about 50 km depth. None of the above discussed profiles is long enough to detect

this layer.

## DISCUSSION AND CONCLUSIONS

The crustal structure obtained here (see the inset of Figure 2.3b) is not unique, particularly the lower crust, but it fits the travel-time data within ± 0.3 sec. If corrections are made for station and the source delays, the fit would be better than ± 0.15 sec, and therefore it will serve as a useful model for the location of local earthquakes and as a basis of comparison for other regions within southern California. It may be suggested that, if no corrections for station height and delay are included in the location program, use of the structure given in Figure 2.3 is appropriate. If the station corrections for height and possibly for station delays are included in the location program the structure shown in Figure 2.3b would be more appropriate. (0.5 sec may be tentatively used for the stations in the Los Angeles basin. This delay is consistent with that calculated for the velocity-depth functions obtained from sonic logs from oil explorations. The calculated delay ranges from 0.47 to 0.69 sec for several locations in the Los Angeles basin.)

The present data do not preclude a possibility of a velocity reversal in the mid to lower crust. More detailed analyses of the amplitude and the waveform of the first as well as later arrivals are necessary for the determination of the details of the lower crust.

It is rather surprising that the structure is very homogeneous in the entire area. Press (1960) also pointed out this fact. The velocity of the upper 3 to 5 km thick layer is fairly well defined at 5.5 km/sec (see Figures 2.3b and 2.4b). It is instructive to compare the crustal velocities with laboratory velocity-pressure data

for typical granites. Figure 2.9 shows such comparison. The crustal velocity to a depth of 4 km is significantly lower than that for granites. If we accept the prevalent notion that the upper crustal layer consists of granitic rocks, this discrepancy requires explanation. The most obvious is that the upper crustal rocks are both highly fractured and weathered.

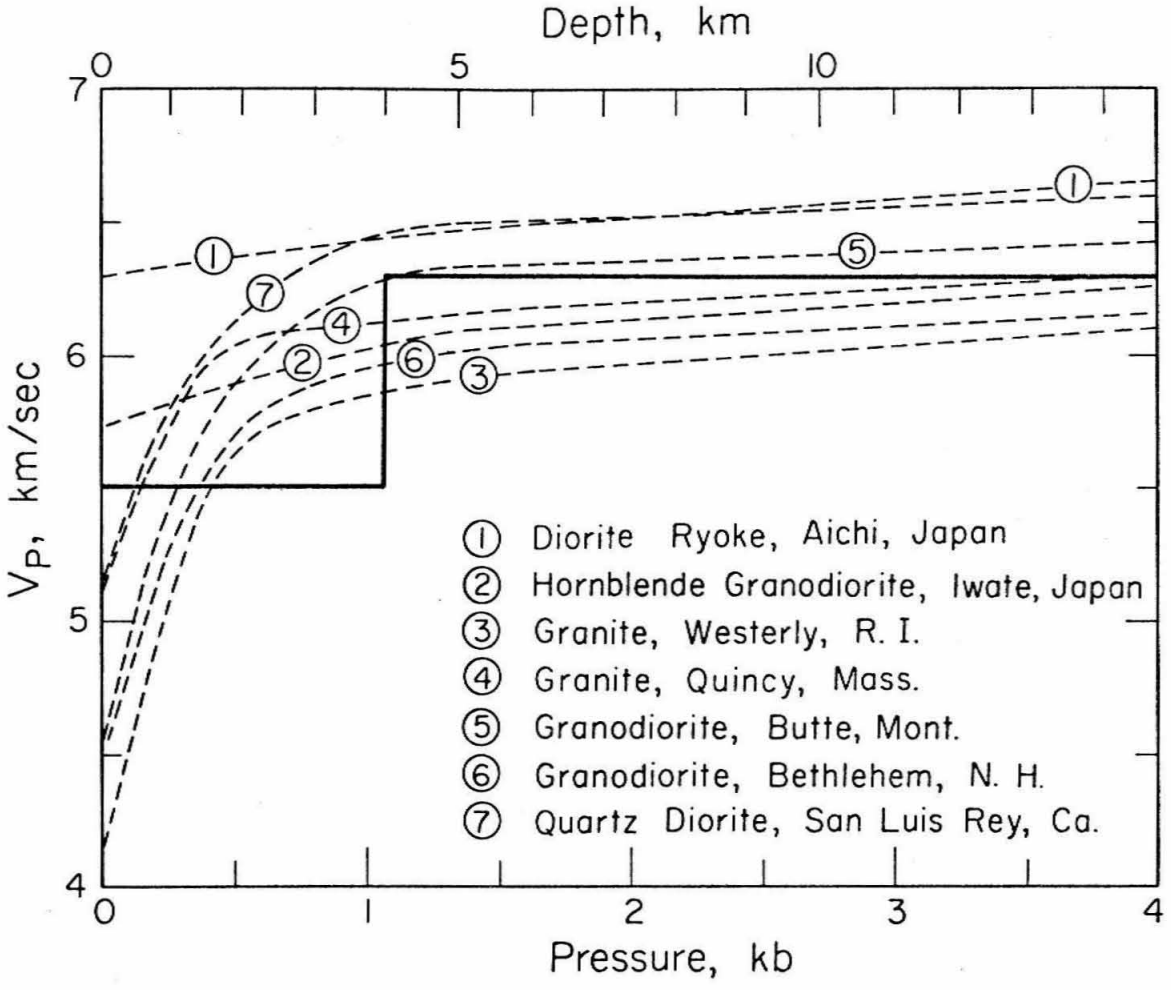


Figure 2.9 Comparison of crustal velocity with velocities of granites. Data for rocks are from Birch (1960) ((3), (4), (5), (6), and Kanamori and Mizutani (1965) ((1) and (2)).

REFERENCES

Allen, C. R., and D. V. Helmberger (1973). Search for temporal changes in seismic velocities using large explosions in southern California, in Proceedings of Conference on Tectonic Problems of the San Andreas Fault System, June 20-23, 1973, Stanford, California, ed. R. B. Kovach and A. Nur, 436-445.

Birch, F. (1960). The velocity of compressional waves in rocks to 10 kilobars, 1, J. Geophys. Res., 65, 1083-1102.

Gutenberg, B. (1944). Travel times of principal P and S waves over small distances in southern California, Bull. Seismol. Soc. Am., 34, 13-32.

Gutenberg, B. (1951). Revised travel times in southern California, Bull. Seismol. Soc. Am., 62, 427-439.

Gutenberg, B. (1952). Waves from blasts recorded in southern California, Trans. Am. Geophys. Union, 33, 427-431.

Gutenberg, B. (1955). Wave velocities in the earth's crust, Geol. Soc. Am., Special Paper 62, 19-34.

Hileman, J. A., C. R. Allen, and J. M. Nordquist (1973). Seismicity of the southern California region, 1 January 1932 to 31 December 1972, Seismological Laboratory, California Institute of Technology, Pasadena, pp. 83.

Kanamori, H., and W. Y. Chung (1974). Temporal changes in P-wave velocity in southern California, Tectonophysics, 23, 67-68.

Kanamori, H., and H. Mizutani (1965). Ultrasonic measurements of elastic constants of rocks under high pressures, Bull. Earthq. Res. Inst. Tokyo Univ., 43, 173-194.

Press, F. (1956). Determination of crustal structure from phase velocity of Rayleigh waves, 1., Bull. Geol. Soc. Am., 67, 1647-1658.

Press, F. (1960). Crustal structure in the California-Nevada region, J. Geophys. Res., 65, 1039-1051.

Richter, C. F. (1950). Velocities of P at short distances, Bull. Seismol. Soc. Am., 40, 281-289.

Richter, C. F. (1958). Elementary Seismology, W. H. Freeman and Company, San Francisco, pp. 44-45.

Roller, J. C., and J. H. Healy (1963). Seismic-refraction measurements of crustal structure between Santa Monica Bay and Lake Mead, J. Geophys. Res., 68, 5837, 5849.

Shor, G. G., Jr. (1955). Deep reflections from southern California blasts, Trans. Am. Geophys. Union, 36, 133-138.

Whitcomb, J. H., H. Kanamori, and D. Hadley (1974). Earthquake prediction: Variation of seismic velocities in southern California, abstract, EOS, 55, 355.

# CHAPTER 3

## Regional Variations in Crust and Mantle P-Wave Velocities

ABSTRACT

Seismograms of natural and artificial events recorded by the southern California array, in conjunction with several portable stations, define travel-time curves for both crust and upper mantle P-wave phases. A $P_g$ velocity of $6.2 \pm 0.1$ km/sec is observed for the Mojave, eastern Transverse Ranges and Colorado desert. Within the western Transverse Ranges and the western portion of the Peninsular Ranges, first arrivals have an apparent velocity of 6.7 km/sec. With the constraints of a fixed array, a special effort has been made to select events that approximately reverse several $P_n$ profiles. These profiles show that $P_n$ varies from 7.7 to 8.2 km/sec. The low $P_n$ velocity of 7.8 km/sec extends northwest from the Imperial Valley, through the region of San Bernardino, and fans out across the central Mojave. Moho dips, derived from $P_n$ profiles from the eastern Transverse Ranges and the Mojave, indicate a relatively uniform westward dip. A composite profile extending across the Coachella Valley from a calibration blast at the south end of the Salton Sea defines an average crustal thickness of 16 to 19 km.

## INTRODUCTION

Before the expansion of the southern California array, crust and upper mantle velocity studies required elaborate, expensive field operations. Those studies involved both relatively large explosions and portable arrays of seismometers. The studies of Roller and Healy (1963) and Healy (1963) are classic examples of long-line seismic refraction studies within southern California. With the expanded, present array, Figure 3.1, we are frequently able to inexpensively compile composite profiles throughout the region by using both earthquakes ($M_L > 3$) and quarry blasts as sources. As the stations seldom fall into perfect, linear arrays, these profiles tend to average structure within a sub-province. Although this technique does not define the fine details of the crust, such as can be determined from special refraction profiles, the abundant source-station combinations can provide significant new data on the average structure within each sub-province of southern California.

All of the travel-time data used in this study have been read from either 16 mm film, at a magnification of 1 sec/cm, or from digital recordings from the Caltech online system (Johnson, 1978). Average timing accuracy is slightly better than 100 msec. All data have been corrected to an elevation of sea level, Table 3.1, as discussed in Chapter 2. These corrections have been based on an average upper crustal velocity of 5 km/sec. Stations situated on deep accumulations of sediments, such as the Los Angeles basin and the Imperial Valley, have not been used in the determination of crustal and reversed upper mantle velocities.

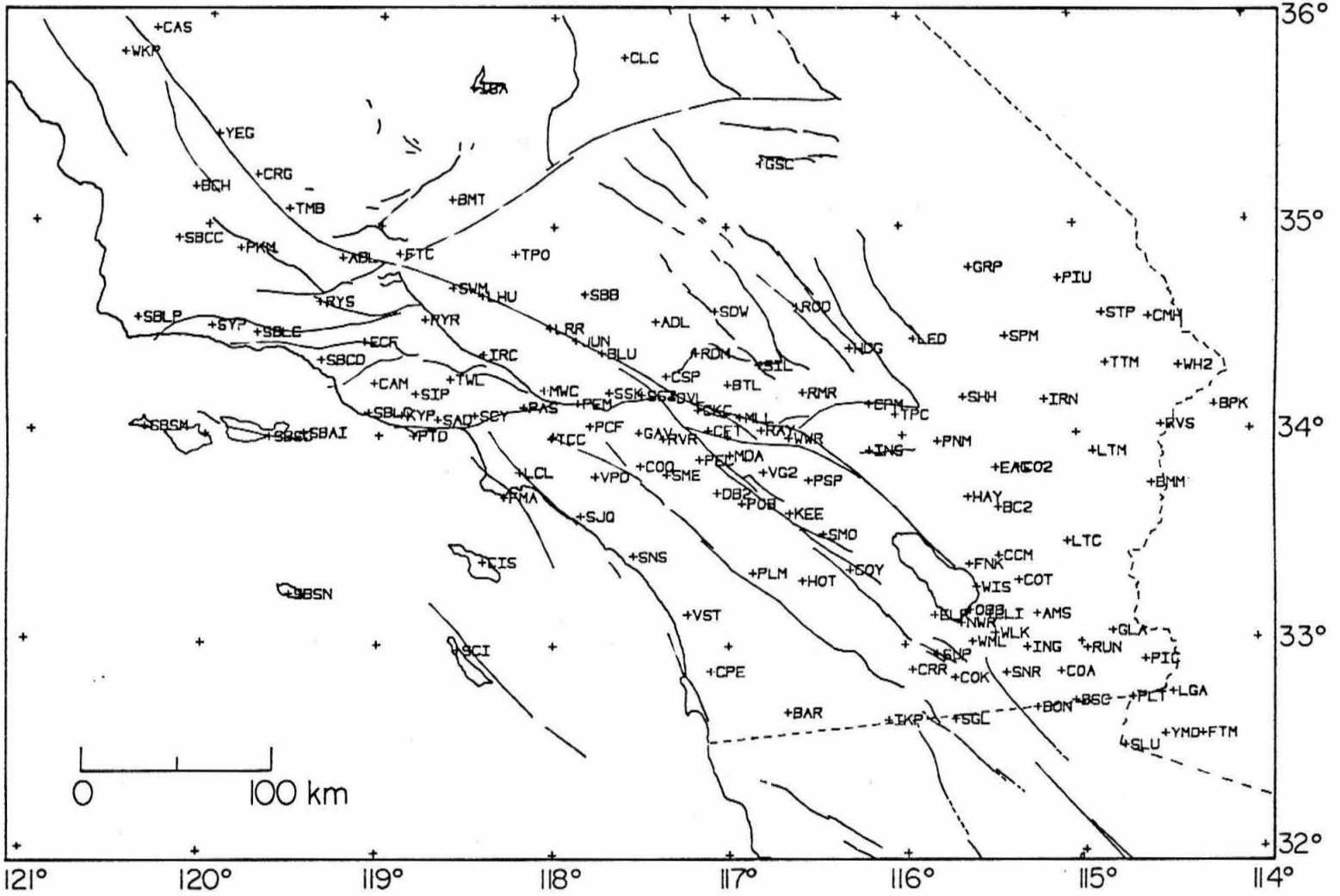


Figure 3.1 Stations of the permanent southern California array.

Table 3.1 Station location data.

| STATION | LATITUDE | LONGITUDE | HEIGHT |
|---|---|---|---|
| ABL | 34 51.04 | 119 13.25 | 1980 |
| ADL | 34 33.37 | 117 25.01 | 900 |
| AGCT | 32 56.46 | 116 16.53 | 366 |
| ALBT | 33 44.17 | 117 24.15 | 396 |
| AMS | 33 8.48 | 115 15.25 | 140 |
| BAR | 32 40.79 | 116 40.29 | 510 |
| BCH | 35 11.10 | 120 5.04 | 1140 |
| BC2 | 33 39.42 | 115 27.67 | 1185 |
| BHM | 34 16.73 | 116 36.90 | 1850 |
| BHR | 34 0.51 | 118 21.71 | 149 |
| BLPT | 32 41.29 | 117 10.60 | 0 |
| BLU | 34 24.40 | 117 43.60 | 1880 |
| BMM | 33 45.40 | 114 35.14 | 564 |
| BMT | 35 8.15 | 118 35.81 | 1237 |
| BON | 32 41.67 | 115 16.10 | 14 |
| BPK | 34 7.48 | 114 12.58 | 504 |
| BSC | 32 43.48 | 115 2.64 | 43 |
| BTL | 34 15.43 | 117 0.29 | 2526 |
| BWLT | 32 50.51 | 116 13.52 | 292 |
| CADT | 34 57.23 | 119 25.09 | 1010 |
| CAM | 34 15.27 | 119 2.00 | 268 |
| CAS | 35 55.90 | 120 20.21 | 1189 |
| CCDT | 34 51.45 | 119 12.50 | 1880 |
| CCM | 33 25.75 | 115 27.87 | 488 |
| CFT | 34 2.11 | 117 6.66 | 671 |
| CHM | 34 33.17 | 114 34.31 | 940 |
| CHMT | 33 0.08 | 116 31.56 | 1170 |
| CIS | 33 24.40 | 118 24.20 | 485 |
| CJP | 34 10.92 | 118 59.18 | 314 |
| CKC | 34 8.17 | 117 10.48 | 550 |
| CLC | 35 49.00 | 117 35.79 | 766 |
| CLI | 33 8.45 | 115 31.64 | -59 |
| CLP | 34 5.33 | 118 57.84 | 545 |
| CMH | 34 33.17 | 114 34.31 | 940 |
| COA | 32 51.81 | 115 7.36 | -35 |
| COK | 32 50.95 | 115 43.60 | -15 |
| COQ | 33 51.62 | 117 30.57 | 250 |
| COT | 33 18.28 | 115 21.20 | 293 |
| COY | 33 21.84 | 116 18.62 | 210 |
| CO2 | 33 50.82 | 115 20.67 | 276 |

| STATION | LATITUDE | LONGITUDE | HEIGHT |
|---|---|---|---|
| CPE | 32 52.79 | 117 6.00 | 213 |
| CPGT | 32 58.67 | 116 25.60 | 620 |
| CPM | 34 9.24 | 116 11.80 | 937 |
| CRAT | 35 3.25 | 119 31.17 | 733 |
| CRBT | 35 8.49 | 119 38.78 | 733 |
| CRCT | 35 13.48 | 119 42.57 | 1020 |
| CRG | 35 14.53 | 119 43.40 | 1204 |
| CRR | 32 53.17 | 115 58.09 | 93 |
| CSP | 34 17.87 | 117 21.32 | 1266 |
| CWC | 36 26.34 | 118 4.68 | 1620 |
| DAC | 36 16.62 | 117 35.62 | 1432 |
| DB2 | 33 44.09 | 117 3.71 | 625 |
| DRST | 33 27.84 | 116 58.20 | 488 |
| DVH | 34 1.04 | 118 23.12 | 1371 |
| DVL | 34 11.99 | 117 19.68 | 598 |
| DYCT | 33 17.10 | 116 49.34 | 1380 |
| EAG | 33 50.93 | 115 28.39 | 366 |
| ECF | 34 27.48 | 119 5.44 | 1000 |
| ELR | 33 8.83 | 115 49.95 | -63 |
| EMST | 34 59.00 | 117 34.73 | 775 |
| FMA | 33 42.75 | 118 17.12 | 15 |
| FNK | 33 22.98 | 115 38.26 | 12 |
| FRET | 35 11.51 | 117 34.59 | 856 |
| FTC | 34 52.25 | 118 53.51 | 924 |
| FTM | 32 33.28 | 114 20.01 | 263 |
| GAV | 34 1.35 | 117 30.73 | 186 |
| GLA | 33 3.10 | 114 49.59 | 627 |
| GLDT | 34 43.70 | 118 54.64 | 1290 |
| GRP | 34 48.26 | 115 36.26 | 1238 |
| GRTT | 34 7.10 | 118 17.90 | 400 |
| GSC | 35 18.09 | 116 48.29 | 990 |
| HAY | 33 42.40 | 115 38.20 | 439 |
| HCM | 33 59.64 | 118 22.98 | 56 |
| HDB | 34 31.59 | 118 9.41 | 1286 |
| HDC | 34 25.73 | 116 18.29 | 1347 |
| HID | 34 25.73 | 116 18.29 | 1347 |
| HGT | 33 18.84 | 116 34.89 | 1975 |
| IKP | 32 38.92 | 116 6.48 | 957 |
| ING | 32 59.29 | 115 18.60 | 2 |
| INS | 33 56.14 | 116 11.66 | 1700 |

Table 3.1 Station location data (continued).

| STATION | LATITUDE | LONGITUDE | HEIGHT |
|---|---|---|---|
| IPC | 33 58.23 | 118 20.87 | 57 |
| IRC | 34 23.40 | 118 24.00 | 579 |
| IRN | 34 9.60 | 115 11.04 | 980 |
| ISA | 35 39.79 | 118 28.40 | 835 |
| JBF | 33 59.57 | 118 20.67 | 82 |
| JKHT | 34 48.50 | 117 41.50 | 855 |
| JNH | 34 26.87 | 117 57.35 | 1314 |
| JUN | 34 28.17 | 117 52.67 | 1210 |
| KEE | 33 38.29 | 116 39.18 | 1366 |
| KYP | 34 6.11 | 118 52.76 | 700 |
| LAJT | 32 51.79 | 117 15.20 | 0 |
| LCL | 33 50.00 | 118 11.55 | 8 |
| LCM | 34 1.07 | 118 17.21 | 53 |
| LED | 34 28.06 | 115 56.18 | 853 |
| LGA | 32 45.57 | 114 29.56 | 68 |
| LHU | 34 40.29 | 118 24.70 | 1036 |
| LJBT | 34 36.31 | 117 51.87 | 885 |
| LKWT | 34 48.70 | 119 1.00 | 1610 |
| LOV | 34 35.45 | 117 50.87 | 899 |
| LRR | 34 31.56 | 118 1.66 | 908 |
| LSM | 36 44.31 | 116 16.67 | 1146 |
| LTC | 33 29.34 | 115 4.20 | 458 |
| LTM | 33 54.90 | 114 55.09 | 744 |
| MDA | 33 54.78 | 116 59.96 | 845 |
| MLL | 34 5.48 | 116 56.17 | 1513 |
| MTST | 32 50.40 | 117 14.90 | 0 |
| NWC | 34 13.40 | 118 3.50 | 1730 |
| NWR | 33 6.10 | 115 41.01 | -69 |
| OBB | 33 10.04 | 115 38.20 | -61 |
| OTRT | 32 37.40 | 117 0.10 | 0 |
| PAS | 34 8.95 | 118 10.29 | 308 |
| PCF | 34 3.19 | 117 47.43 | 163 |
| PEC | 33 53.51 | 117 9.60 | 616 |
| PEM | 34 10.04 | 117 52.17 | 500 |
| PIC | 32 54.84 | 114 38.59 | 263 |
| PIST | 33 31.42 | 117 12.78 | 402 |
| PIU | 34 44.42 | 115 5.64 | 1209 |
| PKM | 34 53.75 | 119 49.12 | 1704 |
| PLM | 33 21.20 | 116 51.70 | 1692 |
| PLT | 32 43.87 | 114 43.76 | 61 |
| PMAT | 34 6.00 | 117 42.85 | 369 |
| PNM | 33 58.64 | 115 48.04 | 1147 |
| POB | 33 41.20 | 116 55.40 | 0 |
| PSP | 33 47.62 | 116 32.92 | 195 |
| PTD | 34 0.25 | 118 48.37 | 40 |
| PYR | 34 34.07 | 118 44.50 | 1247 |
| QZH | 34 38.76 | 118 12.55 | 772 |
| RAY | 34 2.18 | 116 48.67 | 2342 |
| RCP | 33 46.65 | 118 8.00 | 10 |
| RDM | 34 24.00 | 117 11.10 | 1426 |
| RLCT | 33 39.92 | 117 17.48 | 412 |
| RMR | 34 12.77 | 116 34.51 | 1702 |
| ROD | 34 37.78 | 116 36.28 | 1292 |
| RUN | 32 58.32 | 114 58.62 | 152 |
| RVR | 33 59.59 | 117 22.50 | 260 |
| RVS | 34 2.08 | 114 31.07 | 677 |
| RYS | 34 38.59 | 119 21.09 | 1841 |
| SAD | 34 4.86 | 118 39.90 | 732 |
| SBAI | 34 0.80 | 119 26.23 | 113 |
| SBB | 34 41.29 | 117 49.50 | 850 |
| SBCC | 34 56.37 | 120 10.32 | 610 |
| SBCD | 34 22.12 | 119 20.62 | 213 |
| SBLC | 34 29.78 | 119 42.81 | 1190 |
| SBLG | 34 6.87 | 119 3.85 | 415 |
| SBLP | 34 33.56 | 120 24.01 | 134 |
| SBSC | 33 59.67 | 119 37.98 | 457 |
| SBSM | 34 2.24 | 120 21.01 | 172 |
| SBSN | 33 14.68 | 119 30.37 | 259 |
| SCI | 32 58.79 | 118 32.79 | 219 |
| SCY | 34 6.37 | 118 27.25 | 287 |
| SDW | 34 36.54 | 117 4.45 | 1184 |
| SGL | 32 38.95 | 115 43.51 | 110 |
| SHH | 34 11.26 | 115 39.26 | 1122 |
| SIL | 34 20.87 | 116 49.59 | 1730 |
| SIP | 34 12.24 | 118 47.93 | 700 |
| SJQ | 33 37.20 | 117 50.70 | 165 |
| SLU | 32 30.09 | 114 46.64 | 41 |
| SME | 33 49.35 | 117 21.31 | 494 |
| SMO | 33 32.15 | 116 27.70 | 0 |
| SNS | 33 25.90 | 117 32.90 | 190 |

Table 3.1 Station location data (continued).

| STATION | LATITUDE | LONGITUDE | HEIGHT |
|---|---|---|---|
| SNR | 32 51.70 | 115 26.20 | -30 |
| SPM | 34 28.31 | 115 24.15 | 915 |
| SSK | 34 12.97 | 117 41.31 | 1765 |
| SSV | 34 12.46 | 117 29.98 | 1609 |
| STP | 34 34.26 | 114 50.87 | 628 |
| SUP | 32 57.31 | 115 49.42 | 219 |
| SWM | 34 43.00 | 118 35.00 | 1220 |
| SYBT | 33 9.50 | 116 40.53 | 1080 |
| SYP | 34 31.62 | 119 58.67 | 1305 |
| TBLT | 34 22.92 | 117 41.06 | 2270 |
| TCC | 33 59.67 | 118 0.77 | 299 |
| TMB | 35 5.24 | 119 32.07 | 1021 |
| TPC | 34 6.35 | 116 2.91 | 761 |
| TPO | 34 52.73 | 118 13.66 | 799 |
| TTM | 34 20.12 | 114 49.65 | 1098 |
| TWL | 34 16.70 | 118 35.67 | 381 |
| VAL | 34 26.26 | 117 51.51 | 1177 |
| VCR | 33 49.90 | 116 48.54 | 1484 |
| VPD | 33 48.90 | 117 45.70 | 183 |
| VST | 33 9.40 | 117 13.90 | 112 |
| WHP | 34 18.42 | 114 29.75 | 606 |
| WH2 | 34 18.87 | 114 24.54 | 1245 |
| WIS | 33 16.56 | 115 35.57 | -68 |
| WKR | 35 48.87 | 120 30.67 | 503 |
| WLK | 33 3.08 | 115 29.43 | -48 |
| WML | 33 0.91 | 115 37.34 | -44 |
| WWR | 33 59.51 | 116 39.35 | 702 |
| YEC | 35 26.17 | 119 57.56 | 939 |
| YMD | 32 33.28 | 114 32.67 | 76 |
| | 0 0.00 | 0 0.00 | 0 |

As discussed in Chapter 2, the surface 5.5 km/sec layer is not resolvable unless several stations along a profile are within 40 km of the blast. Earthquakes in general are not adequate for studies of this shallow layer, as the hypocentral depths are usually greater than the layer is thick. As a result, this layer is not investigated. Although there is some evidence for regional variations in the thickness of the 5.5 km/sec layer, dip on the bottom of this layer is unresolved. However, variations of several km in the thickness of this layer will not significantly change our results.

The dominant crustal phase recorded as the first arrival over most of the array, for the distance range 20 to 160 km, is termed $P_g$. The apparent phase velocity ranges from 6.1 to 6.4 km/sec. Because of the large amplitude and slow decay with distance of this phase, it is frequently read, incorrectly, as the first arrival at distances well beyond the cross-over to $P_n$. Regional variations in $P_g$ have been mapped through the study of 60 travel-time curves. In this chapter we present the results of nine typical profiles.

For the Peninsular Ranges and the western Transverse Ranges, the most frequently observed crustal arrival, termed $P^*$, has an apparent velocity of 6.5 to 6.8 km/sec. This layer is interpreted as an upward extension of the relatively thin layer inferred for the lower Mojave crust, at the expense of the 6.1 - 6.4 km/sec layer, Chapter 2. In Chapter 5, a well-reversed, east-west profile through the Transverse Ranges quantifies the westward increase in thickness of this layer. One of the principal goals of this chapter is to define both the P-wave velocities and the regional extent of the phases that dominate the

observed crustal arrivals.

The use of quarry blasts in the construction of composite profiles is relatively straightforward. Frequently the origin time is known to 10 msec, and the source location is known to within 50 m. As determined from the resulting travel-time data, the cross-over from $P_g$ to $P_n$ provides a strong constraint on crustal thickness. Earthquake sources, as with blasts, provide a good determination of $P_g$ and $P_n$ velocities. However, since the depth of the hypocenter, the crustal thickness and the cross-over distance trade off against each other, the relatively large uncertainties in source depth, typically 3 to 5 km as compared with 1 to 2 km horizontally, imply a large uncertainty in the determination of crustal thickness. For this reason, for natural sources we have used only the velocities of the travel-time curves, corresponding to $P_g$ or $P^*$ and $P_n$. Note that the uncertainties in the epicentral location and origin time shift the cross-over distance and intercept time. These effects do not degrade the velocity measurements.

One of the disadvantages of using the present array in conjunction with local events is the inability, in general, to reverse a profile. This is particularly important in studies of the dip along the Moho. In the second phase of this study, we have made a special effort to find events both large enough to be recorded well and located in approximately the correct regions, in order to reverse several $P_n$ profiles. By smoothly interpolating the $P_n$ velocities between these reversed profiles, we have interpreted the remaining $P_n$ velocities along unreversed profiles as the result of dip on the Moho.

DATA

Within this section we will discuss briefly the profiles for both $P_g$ and $P_n$. Each velocity has been determined from the data, corrected for station elevation, by least squares. For convenience of presentation, the data have been reduced by $\Delta/V$, where $\Delta$ is the distance and V is the P-wave velocity, typically 6.0 or 7.8 km/sec. The locations, magnitudes, origin times and dates of the events used in this study are listed in Table 3.2.

The following nine profiles, Figure 3.2, a-i, selected from 60 profiles studied, illustrate the apparent velocities of the observed first arrivals. The stations used in each profile, the epicentral distances, azimuths, travel-times, height corrections and plotted travel-times, are listed in Table 3.3, a-i.

3.2 a: This profile extends southeast from the Corona quarry. Most of the stations were installed specifically for the blast. With the exception of PLM and DRST, all stations were located west of the Elsinore fault. Stations beyond CHMT, not shown in this figure, recorded energy that traveled predominantly within the Perris block, east of the Elsinore fault. These stations are delayed by approximately 1 sec relative to the profile shown here. This indicates a significantly slower crustal velocity ($\sim$ 6.3 km/sec) east of the fault than the 6.67 km/sec found from this profile. Cross-over from a 6.0 km/sec layer to the 6.67 km/sec branch occurs at about 40 km.

3.2 b: This profile extends north from the Corona quarry, across the central Transverse Ranges and the western Mojave. As in profile 3.2 a, all stations with four-letter names were installed for the blast. The

TABLE 3.2 Earthquake and Blast Location Data used in Travel-Time Studies.

| DATE | TIME(GMT) | $M_L$ | LAT | LONG | DEPTH | BLAST |
|---|---|---|---|---|---|---|
| 1/10/75 | 19:30:12.72 | 3.5 | 33 50.55 | 117 30.35 | 0 | X |
| 1/14/75 | 09:34:24.72 | 2.0 | 33 35.82 | 117 36.32 | 0 | X |
| 5/2/75 | 18:03:22.74 | 4.2 | 35 13/75 | 117 36.18 | 3.1 | |
| 11/15/75 | 06:13:27.65 | 4.6 | 34 18.12 | 116 20.09 | 5.1 | |
| 12/14/75 | 18:16:20.14 | 4.7 | 34 16.56 | 116 19.69 | 3.3 | |
| 1/1/76 | 17:20:12.94 | 4.3 | 33 58.00 | 117 53.24 | 8.0 | |
| 1/8/76 | 23:26:24.63 | 3.0 | 34 37.75 | 117 06.68 | 0 | X |
| 2/4/76 | 00:04:58.1 | 5.2 | 34 40.00 | 112 30.00 | 12 | |
| 3/22/76 | 05:48:12.45 | 2.5 | 33 05.28 | 115 37.90 | 0 | X |
| 4/8/76 | 15:21:38.18 | 4.5 | 34 20.81 | 118 39.74 | 12.0 | |
| 10/17/76 | 05:38:11.69 | 3.9 | 34 27.56 | 118 25.22 | 12.3 | |
| 10/18/76 | 17:26:53.0 | 4.2 | 32 45.58 | 117 55.07 | 1 | ? |
| 11/4/76 | 10:41:37.5 | 4.9 | 33 07.16 | 115 35.67 | 5.0 | |
| 11/22/76 | 17:54:57.56 | 3.8 | 33 57.20 | 118 38.53 | 3.4 | |
| 1/13/77 | 07:19:00.16 | 3.3 | 35 02.66 | 119 03.39 | 3.4 | |
| 1/17/77 | 11:13:19.24 | 4.2 | 32 27.73 | 115 11.34 | 8 | |
| 3/31/77 | 13:30:29.22 | 3.3 | 33 24.58 | 116 58.27 | 8 | |
| 4/6/77 | 06:01:02.69 | 3.5 | 33 27.66 | 116 28.45 | 12.4 | |
| 5/25/77 | 17:00:00 | 5.4 | 37 10.00 | 116 05.00 | 0 | X |
| 7/26/77 | 21:42:18.54 | 3.7 | 35 50.53 | 120 12.53 | 5 | |
| 8/12/77 | 02:19:26.04 | 4.4 | 34 23.22 | 118 26.61 | 8.8 | |
| 8/12/77 | 02:51:40.69 | 2.7 | 34 22.95 | 118 27.19 | 8.5 | |
| 8/12/77 | 04:41:38.56 | 3.3 | 34 23.19 | 118 26.34 | 8.1 | |
| 9/21/77 | 06:27:51.48 | 3.8 | 31 53.17 | 115 46.69 | 5.0 | |
| 9/22/77 | 09:41:10.51 | 3.5 | 33 58.51 | 116 35.10 | 5.0 | |
| 9/24/77 | 21:28:24.26 | 4.2 | 34 28.20 | 118 23.98 | 12.0 | |
| 9/30/77 | 15:09:52.26 | 3.4 | 34 18.82 | 116 03.19 | 5.0 | |
| 10/21/77 | 13:24:24.57 | 4.2 | 32 54.21 | 115 30.67 | 7 | |
| 10/22/77 | 04:59:17.32 | 3.7 | 34 22.83 | 117 03.15 | 1.6 | |
| 11/8/77 | 10:52:27.15 | 3.6 | 33 53.36 | 117 54.36 | 7.0 | |
| 11/10/77 | 02:35:24.13 | 3.6 | 36 05.91 | 117 54.47 | 4.7 | |
| 11/29/77 | 16:42:09.95 | 3.9 | 35 30.61 | 120 15.85 | 4.9 | |

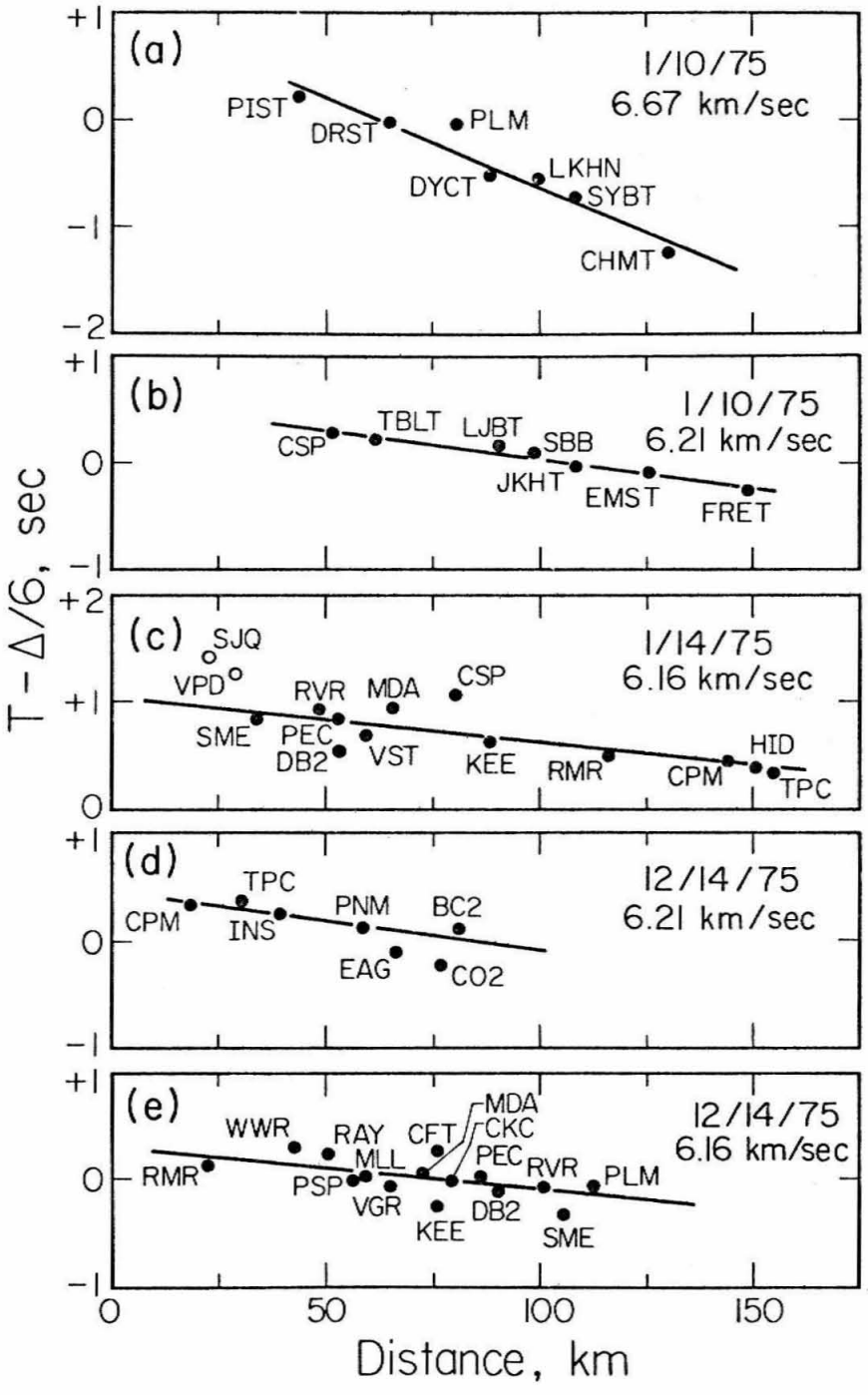


Figure 3.2 Composite profiles illustrating the regional variation in typical apparent velocities of crustal first arrivals. The location of these profiles is shown on Figure 3.2 and the travel-time data are listed in Table 3.3, a-i.

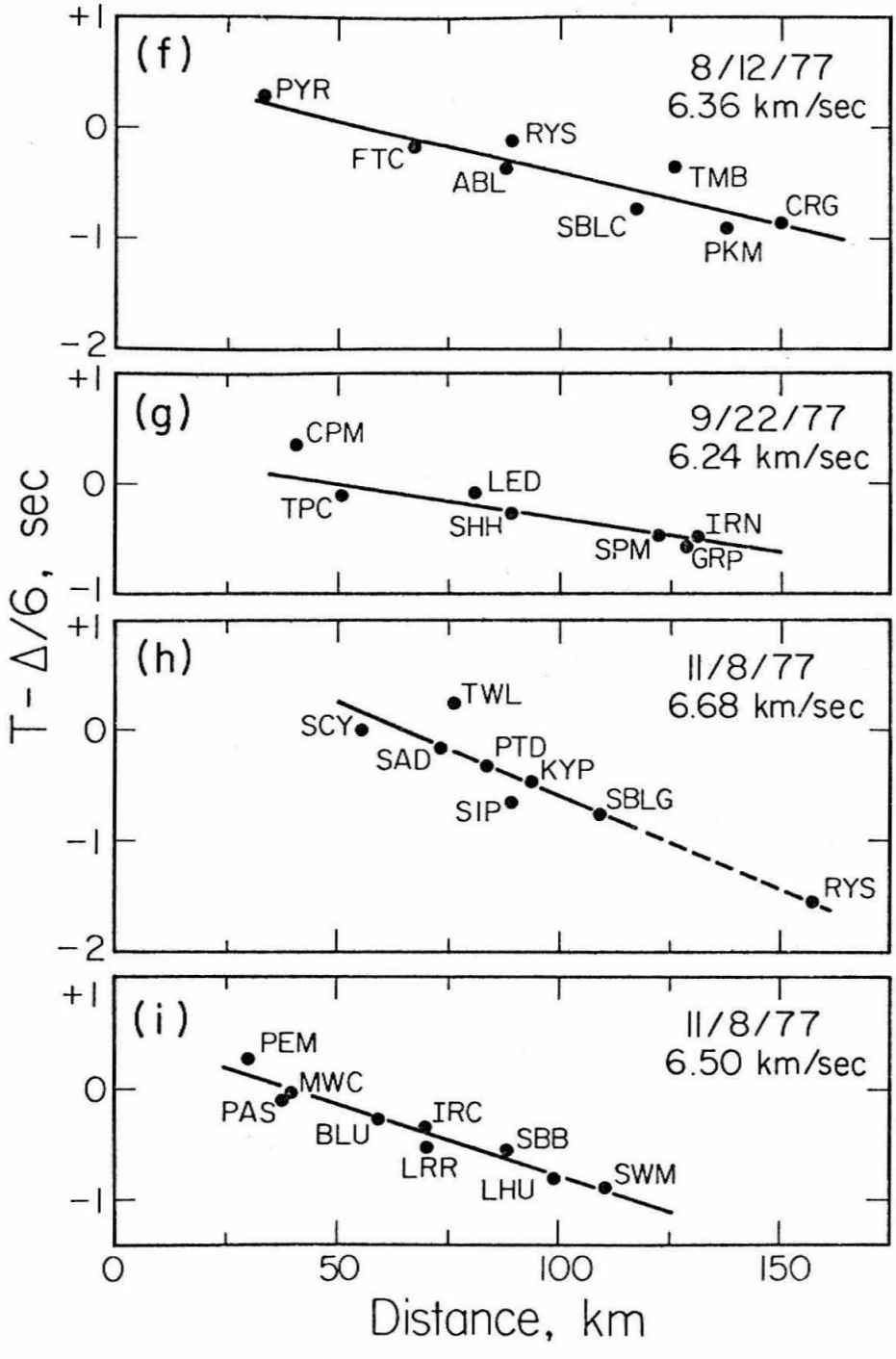


Figure 3.2 (continued)

Table 3.3 Stations and travel-time data used in the study of apparent velocities of crustal phased, plotted on Figure 3.2, a-i.

3.3a:

| STA | AZIMUTH | DISTANCE | T | T-DEL/6.0 | H*COS(I)/5 | T PLOTTED |
|---|---|---|---|---|---|---|
| PIST | 142. | 44.584 | 7.679 | 0.249 | 0.044 | 0.204 |
| DRST | 130. | 65.047 | 10.879 | 0.038 | 0.062 | -0.024 |
| PLM | 132. | 80.730 | 13.629 | 0.174 | 0.232 | -0.057 |
| DYCT | 134. | 88.576 | 14.379 | -0.382 | 0.193 | -0.576 |
| SYBT | 134. | 108.206 | 17.489 | -0.554 | 0.157 | -0.711 |
| CHMT | 135. | 130.393 | 20.679 | -1.052 | 0.174 | -1.226 |

3.3b:

| STA | AZIMUTH | DISTANCE | T | T-DEL/6.0 | H*COS(I)/5 | T PLOTTED |
|---|---|---|---|---|---|---|
| CSP | 15. | 52.372 | 9.179 | 0.451 | 0.150 | 0.300 |
| TBLT | 344. | 62.062 | 10.839 | 0.496 | 0.288 | 0.208 |
| LJBT | 338. | 90.837 | 15.409 | 0.270 | 0.124 | 0.145 |
| SBB | 342. | 98.309 | 16.609 | 0.225 | 0.121 | 0.103 |
| JKHT | 350. | 108.478 | 18.179 | 0.100 | 0.124 | -0.024 |
| EMST | 356. | 126.712 | 21.139 | 0.021 | 0.115 | -0.093 |
| FRET | 357. | 149.803 | 24.829 | -0.137 | 0.128 | -0.266 |

3.3c:

| STA | AZIMUTH | DISTANCE | T | T-DEL/6.0 | H*COS(I)/5 | T PLOTTED |
|---|---|---|---|---|---|---|
| SJQ | 276. | 22.388 | 5.149 | 1.418 | 0.012 | 1.406 |
| VPD | 329. | 28.187 | 5.980 | 1.282 | 0.015 | 1.266 |
| SME | 42. | 34.111 | 6.589 | 0.904 | 0.047 | 0.857 |
| RVR | 25. | 48.858 | 9.080 | 0.936 | 0.030 | 0.906 |
| PEC | 51. | 52.652 | 9.699 | 0.924 | 0.073 | 0.851 |
| DB2 | 72. | 52.664 | 9.429 | 0.652 | 0.074 | 0.577 |
| VST | 144. | 59.943 | 10.700 | 0.709 | 0.014 | 0.695 |
| MDA | 57. | 66.173 | 12.080 | 1.051 | 0.109 | 0.941 |
| CSP | 16. | 81.085 | 14.730 | 1.215 | 0.174 | 1.041 |
| KEE | 86. | 88.474 | 15.550 | 0.804 | 0.191 | 0.612 |
| RMR | 54. | 117.212 | 20.300 | 0.764 | 0.250 | 0.514 |
| CPM | 64. | 144.225 | 24.629 | 0.592 | 0.140 | 0.451 |
| HID | 52. | 151.451 | 25.840 | 0.598 | 0.202 | 0.395 |
| TPC | 68. | 154.715 | 26.230 | 0.444 | 0.114 | 0.329 |

3.3d:

| STA | AZIMUTH | DISTANCE | T | T-DEL/6.0 | H*COS(I)/5 | T PLOTTED |
|---|---|---|---|---|---|---|
| CPM | 138. | 18.166 | 3.479 | 0.452 | 0.076 | 0.375 |
| TPC | 126. | 31.937 | 5.789 | 0.467 | 0.071 | 0.395 |
| INS | 161. | 39.714 | 7.059 | 0.440 | 0.178 | 0.262 |
| PNM | 124. | 58.853 | 10.060 | 0.251 | 0.142 | 0.108 |
| EAC | 120. | 92.044 | 15.289 | -0.050 | 0.051 | -0.102 |
| CO2 | 117. | 102.495 | 16.909 | -0.172 | 0.039 | -0.212 |
| BC2 | 130. | 105.512 | 17.860 | 0.274 | 0.171 | 0.102 |

3.3e:

| STA | AZIMUTH | DISTANCE | T | T-DEL/6.0 | H*COS(I)/5 | T PLOTTED |
|---|---|---|---|---|---|---|
| RMR | 252. | 23.826 | 4.259 | 0.288 | 0.143 | 0.145 |
| WWR | 223. | 43.678 | 7.659 | 0.380 | 0.077 | 0.303 |
| RAY | 239. | 51.866 | 9.149 | 0.505 | 0.277 | 0.227 |
| PSP | 200. | 57.225 | 9.559 | 0.022 | 0.024 | -0.001 |
| MLL | 250. | 59.687 | 10.150 | 0.202 | 0.189 | 0.012 |
| VGR | 222. | 66.323 | 11.189 | 0.136 | 0.192 | -0.056 |
| MDA | 237. | 73.882 | 12.509 | 0.196 | 0.113 | 0.082 |
| KEE | 203. | 76.835 | 12.760 | -0.045 | 0.185 | -0.231 |
| CFT | 249. | 76.973 | 13.159 | 0.331 | 0.091 | 0.240 |
| CKC | 259. | 79.537 | 13.359 | 0.103 | 0.075 | 0.028 |
| PEC | 241. | 87.799 | 14.749 | 0.116 | 0.086 | 0.030 |
| DB2 | 228. | 90.528 | 15.069 | -0.018 | 0.088 | -0.106 |
| RVR | 252. | 101.517 | 16.909 | -0.009 | 0.037 | -0.047 |
| SME | 242. | 107.338 | 17.650 | -0.239 | 0.071 | -0.311 |
| PLM | 205. | 113.620 | 19.150 | 0.213 | 0.247 | -0.034 |



3.3f:

| STA | AZIMUTH | DISTANCE | T | T-DEL/6.0 | H*COS(I)/5 | T PLOTTED |
|---|---|---|---|---|---|---|
| PYR | 306. | 33.962 | 6.089 | 0.429 | 0.165 | 0.263 |
| FTC | 322. | 67.604 | 11.239 | -0.027 | 0.125 | -0.152 |
| ABL | 305. | 87.916 | 14.539 | -0.112 | 0.280 | -0.393 |
| RYS | 289. | 88.103 | 14.839 | 0.156 | 0.260 | -0.104 |
| SBLC | 276. | 117.346 | 18.990 | -0.567 | 0.175 | -0.743 |
| TMB | 308. | 126.569 | 20.900 | -0.194 | 0.151 | -0.346 |
| PKM | 294. | 138.151 | 22.379 | -0.645 | 0.255 | -0.900 |
| CRG | 309. | 150.696 | 24.459 | -0.656 | 0.181 | -0.837 |

3.3g:

| STA | AZIMUTH | DISTANCE | T | T-DEL/6.0 | H*COS(I)/5 | T PLOTTED |
|---|---|---|---|---|---|---|
| CPM | 60. | 40.970 | 7.069 | 0.241 | 0.103 | 0.137 |
| TPC | 73. | 51.599 | 8.569 | -0.029 | 0.091 | -0.121 |
| LED | 47. | 80.959 | 13.530 | 0.036 | 0.117 | -0.080 |
| SHH | 74. | 89.054 | 14.729 | -0.112 | 0.157 | -0.270 |
| SPM | 62. | 122.083 | 20.029 | -0.317 | 0.135 | -0.452 |
| GRP | 44. | 128.792 | 21.099 | -0.365 | 0.184 | -0.549 |
| IRN | 80. | 130.940 | 21.529 | -0.293 | 0.145 | -0.439 |

3.3h:

| STA | AZIMUTH | DISTANCE | T | T-DEL/6.0 | H*COS(I)/5 | T PLOTTED |
|---|---|---|---|---|---|---|
| SCY | 295. | 56.062 | 9.399 | 0.056 | 0.036 | 0.019 |
| SAD | 287. | 73.284 | 12.160 | -0.054 | 0.098 | -0.152 |
| TWL | 304. | 76.804 | 13.100 | 0.299 | 0.052 | 0.247 |
| PTD | 278. | 84.196 | 13.730 | -0.302 | 0.005 | -0.308 |
| SIP | 293. | 89.535 | 14.370 | -0.552 | 0.098 | -0.651 |
| KYP | 284. | 92.975 | 15.160 | -0.335 | 0.099 | -0.435 |
| SBLG | 283. | 109.868 | 17.620 | -0.691 | 0.060 | -0.751 |

3.3i:

| STA | AZIMUTH | DISTANCE | T | T-DEL/6.0 | H*COS(I)/5 | T PLOTTED |
|---|---|---|---|---|---|---|
| PEM | 6. | 31.014 | 5.529 | 0.360 | 0.059 | 0.300 |
| PAS | 319. | 37.839 | 6.319 | 0.013 | 0.036 | -0.023 |
| MWC | 339. | 39.623 | 6.699 | 0.096 | 0.206 | -0.110 |
| BLU | 16. | 59.709 | 9.929 | -0.021 | 0.241 | -0.263 |
| IRC | 320. | 71.830 | 11.709 | -0.261 | 0.077 | -0.339 |
| SBB | 4. | 88.932 | 14.429 | -0.392 | 0.119 | -0.511 |
| LHU | 331. | 98.473 | 15.760 | -0.652 | 0.148 | -0.800 |
| SWM | 325. | 110.940 | 17.789 | -0.700 | 0.178 | -0.878 |

apparent velocity of 6.2 km/sec appears well constrained and is quite similar to other measurements at different azimuths within this region.

3.2 c: This profile was constructed from seismograms from a small blast used to calibrate a six station portable array near San Juan Capistrano. The shot size was approximately 100 Kg and the depth of burial less than 30 m. In view of the shot size, the clear arrivals at distances of 150 km are surprising. As the stations SJQ and VPD are situated on deep sedimentary structures, the observed travel-times to these stations were not used in the determination of the average velocity of 6.16 km/sec. A second, short profile extended southeast from the shot, approximately parallel to the coast. Data from five stations define a 5.7 km/sec branch that extends from 10 to 40 km.

3.2 d: This profile extends southeast from an earthquake located in the eastern Transverse Ranges. The $P_g$ velocity of 6.2 km/sec measured along this profile is representative of other profiles within the region east of the Salton Sea.

3.2 e: This profile extends from the same earthquake discussed in profile 3.2 d and crosses the northeast section of the Peninsular Ranges. The profile roughly reverses profile 3.2 c discussed above. Both profiles show the same apparent velocity of 6.16 km/sec. These data require a relatively flat interface between this layer and the overlying 5.5-5.7 km/sec layer. These data also suggest that the shallow 6.7 km/sec layer found for the profile extending southeast from Corona and west of the Elsinore fault, profile 3.2 a, is not observed within the northeastern portion of the Peninsular Ranges.

3.2 f: This profile extends northwest from a San Fernando aftershock.

The $P_g$ velocity of 6.36 km/sec is slightly higher than the velocities observed in the region east of the San Andreas fault extending from Palmdale to the Imperial Valley.

3.2 g: This profile extends east from an earthquake occurring in the area of the Banning pass. These data overlap with those of profile 3.2 d. The $P_g$ velocity of 6.24 km/sec is in excellent agreement with the other profiles.

3.2 h: This profile extends northwest from an earthquake located north of the bifurcation of the Elsinore fault into the Chino and Whittier fault zones. The profile is southwest of profile 3.2 f. The observed velocity is similar to that of profile 3.2 a. The crust of the western Transverse Ranges is dominated by a thick layer with P-wave velocity of 6.7 km/sec.

3.2 i: This profile extends north from the same event studied in profile 3.2 h, and the stations are distributed between profiles 3.2 h and f. It is therefore not surprising that the observed P-wave velocity is intermediate between those two profiles: 6.5 km/sec.

The velocities defined by each travel-time curve are plotted in the center of each region studied, Figure 3.3. In addition to the profiles discussed above, for completeness the profiles from Chapter 2 have been included in this figure. It shows that the Mojave, the eastern Transverse Ranges, the Colorado desert east of the Salton Trough and the northeastern Peninsular Ranges have about the same $P_g$ velocity of $6.2 \pm 0.1$ km/sec. On the other hand, the western Transverse Ranges in the vicinity of Ventura, and the western portion of the Peninsular Ranges, are dominated by a thick layer with a velocity of

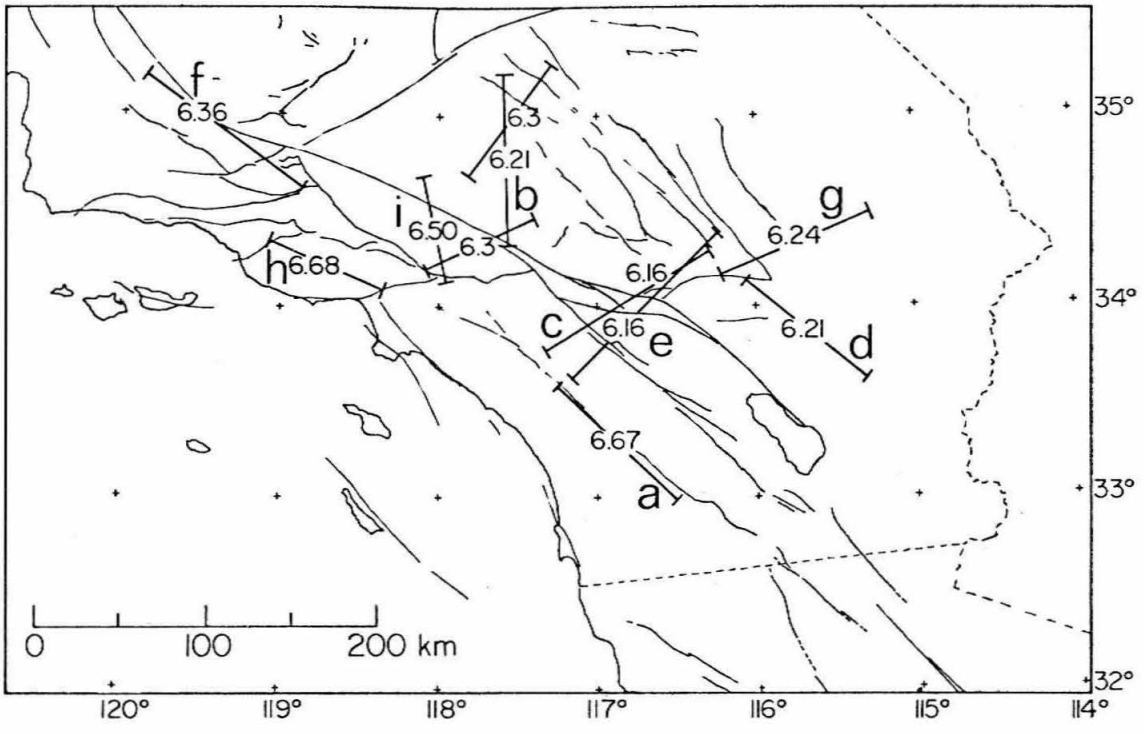


Figure 3.3 Regional variations in typical apparent velocities of crustal first arrivals. The profiles are shown on Figure 3.2. For convenience, the Randsburg and Victorville data, Chapter 2, have been added.

6.7 km/sec. The regions between these two extremes, that is, the north-central Peninsular Ranges and the west-central Transverse Ranges, form a transitional region.

The following $P_n$ profiles have been prepared in a manner similar to the $P_g$ profiles. The travel-time data are corrected to an elevation of sea level, then a least squares line is fit to the data. The section of the upper mantle studied in these profiles can be identified by tracing the rays from the station towards the source. For the crustal structure discussed in Chapter 2, these rays travel about 45 km horizontally as they propagate from the Moho to the surface. Hence the region investigated for each profile can be defined by projecting the outline of the stations composing the array about 45 km towards the source. As this study relies primarily on natural sources and a fixed array, most profiles cannot be reversed exactly. After a careful examination of the catalog of earthquakes and blasts, five independent, approximately reversed profiles were constructed. By combining these results with the reversed profiles of Roller and Healy (1963) and Healy (1963) and the results of Shor and Raitt (1956) we have been able to define regional variation in $P_n$ velocities. Over profile lengths of 100 km the data are well fit by a simple model of uniform velocity and dip. With this model, the average scatter of the data about a straight line is less than 0.2 sec, and the worst case is less than 0.4 sec. This scatter probably results from both short wavelength topographic variations along the Moho and unknown local station delays. In view of the relatively small scatter within the data, rapid deviations from the measured average Moho dip should

correspond to unresolved relief of only a few km. The reversed $P_n$ profiles are illustrated in Figure 3.4, a-e, and the associated travel-time data are listed in Table 3.4, a-e. The sections of the upper mantle studied in these profiles are shown as shaded areas in Figure 3.5. The hatched lines are approximately parallel to the direction of energy propagation. For completeness, the results of Roller and Healy (1963) and Healy (1963) are included on this summary figure. The profiles are briefly described below.

3.4 a: These two profiles sample the upper mantle beneath the region of the San Bernardino Valley. The true $P_n$ velocity of 7.7 km/sec is the lowest measured within southern California. This result is consistent with the low velocity found from the inversion of azimuthal P-delay data (Raikes, personal communication, 1978).

3.4 b: These two profiles indicate that the true $P_n$ velocity in the Colorado desert east of the Salton Sea is 7.88 km/sec. This velocity is only slightly higher than the 7.8 km/sec velocity found for the central Mojave region, Chapter 2.

3.4 c: These two profiles indicate that the $P_n$ velocity of 7.95 km/sec beneath the west-central Transverse Ranges is intermediate between the 7.7 km/sec derived in profile 3.4 a for the region around San Bernardino, and the 8.2 km/sec derived for the extreme western Transverse Ranges and the southern Coast Ranges (Healy, 1963).

3.4 d: These profiles establish a $P_n$ velocity of 8.0 km/sec for the eastern Transverse Ranges. Much like profile 3.4 c, these profiles indicate a gradation from the 7.7 km/sec velocity of the central Transverse Ranges to 8.0 km/sec in the eastern Ranges to 8.2 km/sec

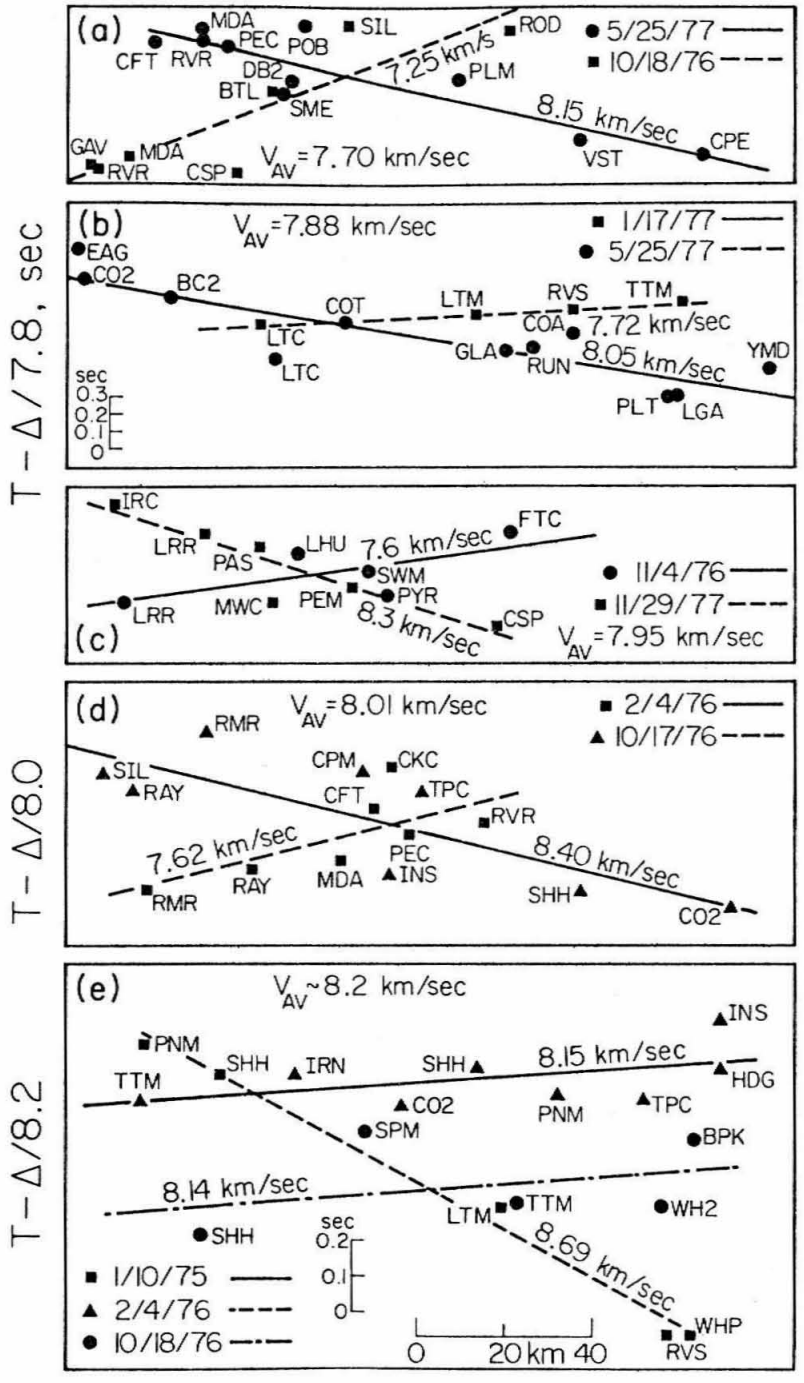


Figure 3.4 Composite reversed $P_n$ profiles. The location of these profiles is shown on Figure 3.5, and the travel-time data are listed in Table 3.4, a-e.

Table 3.4 Stations and travel-time data used in the reversed $P_n$ profiles that are plotted in Figure 3.4, a-e.

3.4a:

| STA | AZIMUTH | DISTANCE | T | T-DEL/7.8 | H*COS(I)/5 | T PLOTTED |
|---|---|---|---|---|---|---|
| CAV | 14. | 145.028 | 23.000 | 4.406 | 0.027 | 4.378 |
| RVR | 20. | 145.829 | 23.099 | 4.403 | 0.039 | 4.364 |
| MDA | 33. | 153.832 | 24.299 | 4.577 | 0.127 | 4.450 |
| CSP | 16. | 178.390 | 27.400 | 4.529 | 0.192 | 4.337 |
| BTL | 26. | 186.470 | 29.099 | 5.193 | 0.384 | 4.809 |
| SIL | 29. | 203.183 | 31.499 | 5.450 | 0.263 | 5.187 |
| ROD | 30. | 240.459 | 36.200 | 5.371 | 0.197 | 5.174 |

| STA | AZIMUTH | DISTANCE | T | T-DEL/7.8 | H*COS(I)/5 | T PLOTTED |
|---|---|---|---|---|---|---|
| CFT | 195. | 359.682 | 51.499 | 5.386 | 0.102 | 5.284 |
| MDA | 193. | 370.405 | 53.000 | 5.512 | 0.129 | 5.382 |
| RVR | 198. | 371.008 | 52.900 | 5.334 | 0.039 | 5.294 |
| PEC | 195. | 376.205 | 53.599 | 5.368 | 0.094 | 5.274 |
| SME | 197. | 388.518 | 54.900 | 5.089 | 0.075 | 5.014 |
| DB2 | 193. | 390.937 | 55.299 | 5.179 | 0.095 | 5.084 |
| POB | 191. | 393.531 | 55.849 | 5.397 | 0.000 | 5.397 |
| PLM | 189. | 428.919 | 60.349 | 5.360 | 0.259 | 5.101 |
| VST | 193. | 456.970 | 63.349 | 4.764 | 0.017 | 4.746 |
| CPE | 191. | 484.479 | 66.799 | 4.687 | 0.032 | 4.654 |

3.4b:

| STA | AZIMUTH | DISTANCE | T | T-DEL/7.8 | H*COS(I)/5 | T PLOTTED |
|---|---|---|---|---|---|---|
| EAG | 171. | 372.205 | 52.499 | 4.781 | 0.056 | 4.725 |
| CO2 | 169. | 374.317 | 52.599 | 4.610 | 0.042 | 4.568 |
| BC2 | 171. | 393.438 | 55.099 | 4.659 | 0.181 | 4.477 |
| LTC | 166. | 418.258 | 57.799 | 4.177 | 0.070 | 4.107 |
| COT | 170. | 433.532 | 59.949 | 4.368 | 0.044 | 4.324 |
| GLA | 165. | 470.628 | 64.599 | 4.263 | 0.096 | 4.166 |
| RUN | 167. | 476.104 | 65.249 | 4.210 | 0.023 | 4.187 |
| COA | 169. | 485.327 | 66.499 | 4.278 | -0.005 | 4.283 |
| PLT | 165. | 507.311 | 68.949 | 3.910 | 0.009 | 3.900 |
| LGA | 162. | 509.964 | 69.299 | 3.920 | 0.010 | 3.909 |
| YMD | 164. | 530.563 | 72.099 | 4.079 | 0.011 | 4.067 |

| STA | AZIMUTH | DISTANCE | T | T-DEL/7.8 | H*COS(I)/5 | T PLOTTED |
|---|---|---|---|---|---|---|
| LTC | 5. | 114.398 | 17.840 | 3.173 | 0.067 | 3.106 |
| LTM | 8. | 163.063 | 24.170 | 3.264 | 0.112 | 3.151 |
| RVS | 19. | 185.238 | 27.050 | 3.301 | 0.102 | 3.198 |
| TTM | 9. | 210.419 | 30.390 | 3.413 | 0.167 | 3.245 |

3.4c:

| STA | AZIMUTH | DISTANCE | T | T-DEL/7.8 | H*COS(I)/5 | T PLOTTED |
|---|---|---|---|---|---|---|
| IRC | 125. | 210.792 | 29.939 | 2.915 | 0.088 | 2.826 |
| LRR | 117. | 231.479 | 32.489 | 2.813 | 0.138 | 2.674 |
| PAS | 127. | 243.790 | 33.899 | 2.644 | 0.047 | 2.597 |
| MWC | 124. | 247.086 | 34.209 | 2.532 | 0.264 | 2.267 |
| PEM | 123. | 264.860 | 36.389 | 2.433 | 0.076 | 2.356 |
| CSP | 116. | 297.905 | 40.539 | 2.346 | 0.193 | 2.153 |

| STA | AZIMUTH | DISTANCE | T | T-DEL/7.8 | H*COS(I)/5 | T PLOTTED |
|---|---|---|---|---|---|---|
| LRR | 305. | 273.978 | 38.999 | 3.874 | 0.139 | 3.735 |
| LHU | 304. | 312.285 | 44.200 | 4.163 | 0.158 | 4.004 |
| SWM | 303. | 328.254 | 46.200 | 4.116 | 0.186 | 3.929 |
| PYR | 299. | 332.618 | 46.599 | 3.956 | 0.191 | 3.765 |
| FTC | 303. | 361.261 | 50.599 | 4.284 | 0.141 | 4.142 |

3.4d:

| STA | AZIMUTH | DISTANCE | T | T-DEL/8.0 | H*COS(I)/5 | T PLOTTED |
|---|---|---|---|---|---|---|
| RMR | 263. | 377.893 | 53.299 | 6.063 | 0.260 | 5.802 |
| RAY | 261. | 402.716 | 56.599 | 6.260 | 0.358 | 5.901 |
| MDA | 259. | 422.575 | 58.900 | 6.078 | 0.129 | 5.948 |
| CFT | 261. | 429.930 | 60.099 | 6.358 | 0.102 | 6.255 |
| CKC | 263. | 433.792 | 60.799 | 6.575 | 0.084 | 6.491 |
| PEC | 259. | 437.571 | 60.799 | 6.103 | 0.094 | 6.009 |
| RVR | 261. | 454.750 | 63.049 | 6.206 | 0.039 | 6.166 |

| STA | AZIMUTH | DISTANCE | T | T-DEL/8.0 | H*COS(I)/5 | T PLOTTED |
|---|---|---|---|---|---|---|
| SIL | 94. | 147.050 | 23.609 | 5.223 | 0.260 | 4.967 |
| RAY | 107. | 155.475 | 24.659 | 5.225 | 0.354 | 4.871 |
| RMR | 98. | 171.957 | 26.959 | 5.465 | 0.258 | 5.206 |
| CPN | 98. | 207.471 | 31.059 | 5.126 | 0.143 | 4.983 |
| INS | 105. | 213.224 | 31.310 | 4.656 | 0.259 | 4.397 |
| TPC | 99. | 221.861 | 32.709 | 4.977 | 0.116 | 4.860 |
| SHH | 95. | 256.316 | 36.510 | 4.470 | 0.171 | 4.298 |
| CO2 | 102. | 291.628 | 40.709 | 4.256 | 0.042 | 4.214 |

3.4e:

| STA | AZIMUTH | DISTANCE | T | T-DEL/8.2 | H*COS(I)/5 | T PLOTTED |
|---|---|---|---|---|---|---|
| TTM | 260. | 216.888 | 32.799 | 6.350 | 0.167 | 6.182 |
| IRN | 257. | 253.062 | 37.249 | 6.388 | 0.149 | 6.238 |
| CO2 | 251. | 277.315 | 39.999 | 6.161 | 0.042 | 6.138 |
| SHH | 260. | 294.775 | 42.399 | 6.451 | 0.171 | 6.279 |
| PNM | 256. | 313.246 | 44.549 | 6.349 | 0.175 | 6.173 |
| TPC | 260. | 332.209 | 46.799 | 6.286 | 0.116 | 6.170 |
| INS | 257. | 349.599 | 49.299 | 6.665 | 0.260 | 6.405 |
| HDG | 266. | 350.230 | 49.199 | 6.489 | 0.206 | 6.282 |

| STA | AZIMUTH | DISTANCE | T | T-DEL/8.2 | H*COS(I)/5 | T PLOTTED |
|---|---|---|---|---|---|---|
| SHH | 52. | 263.317 | 38.349 | 6.238 | 0.171 | 6.066 |
| SPM | 50. | 300.889 | 43.200 | 6.506 | 0.140 | 6.366 |
| TTM | 57. | 335.993 | 47.299 | 6.325 | 0.168 | 6.157 |
| WH2 | 61. | 368.668 | 51.299 | 6.340 | 0.190 | 6.149 |
| BPK | 65. | 376.530 | 52.349 | 6.431 | 0.077 | 6.354 |

| STA | AZIMUTH | DISTANCE | T | T-DEL/8.2 | H*COS(I)/5 | T PLOTTED |
|---|---|---|---|---|---|---|
| PNM | 84. | 158.386 | 26.209 | 6.894 | 0.173 | 6.721 |
| SHH | 76. | 175.233 | 28.179 | 6.810 | 0.170 | 6.639 |
| LTM | 87. | 239.511 | 35.579 | 6.371 | 0.113 | 6.257 |
| RVS | 84. | 277.034 | 39.779 | 5.995 | 0.103 | 5.891 |
| WHP | 78. | 282.556 | 40.449 | 5.991 | 0.092 | 5.899 |

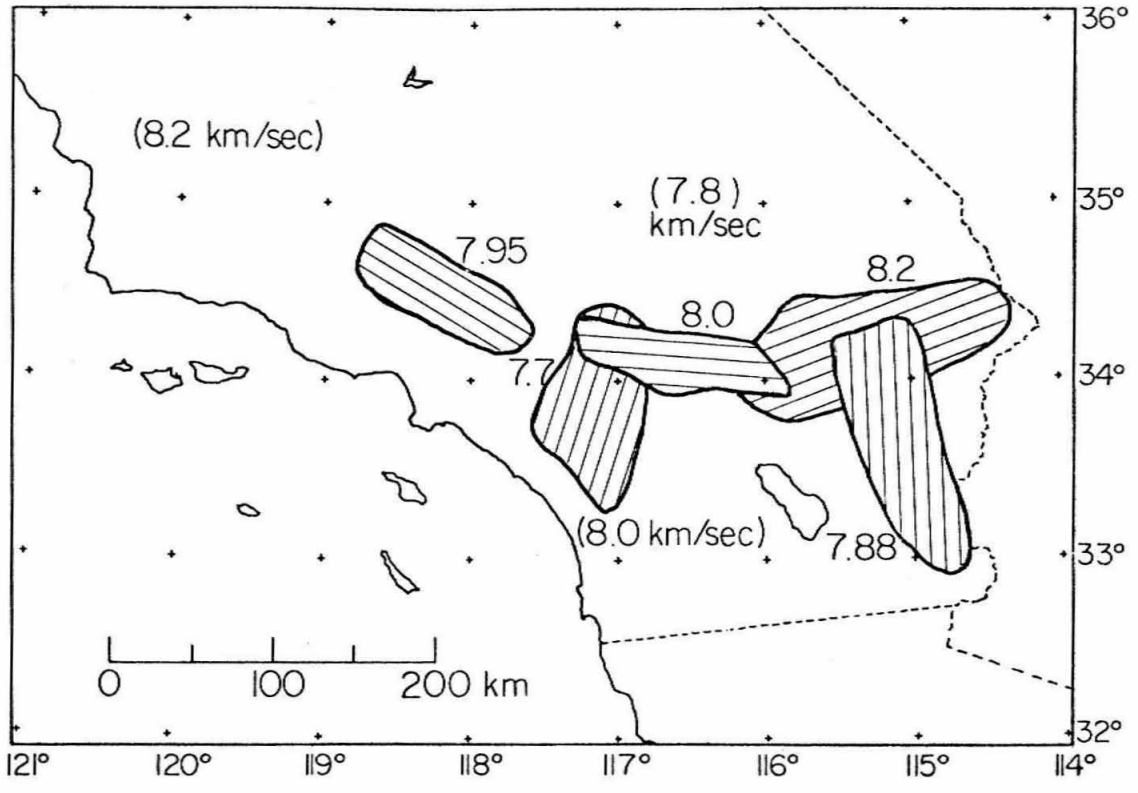


Figure 3.5 Regional variations in $P_n$ velocities. The data of Roller and Healy (1963), Healy (1963), and Simons (1977) have been included in parentheses. The hatched regions indicate the section of upper mantle sampled, and the lines are approximately parallel to the profile direction.

in the extreme eastern Mojave, profile 3.4 e.

3.4 e: The two profiles from events dated 2/4/76 and 10/18/76 indicate a true upper mantle velocity of 8.15 km/sec. A third profile, 1/10/75, is similar in azimuth to the 10/18/76 profile. However, the apparent velocity is exceptionally high: 8.64 km/sec. This profile crosses the Salton Trough slightly north of the 10/18/76 profile. Because of the presence of many profiles within the eastern Mojave, most with apparent velocities of 8.25 km/sec, we feel that this third profile is anomalous and tentatively assign a $P_n$ velocity of 8.2 km/sec to the region of the eastern Mojave.

We have been unable to reverse adequately a $P_n$ profile that extends from the northern Peninsular Ranges to the international border. The few available profiles that extend southeast from the San Fernando aftershock zone define an apparent velocity of 8.0 km/sec. This is slightly slower than the 8.2 km/sec $P_n$ velocity suggested by Shor and Raitt (1956) for the northern portion of the ranges. However, this apparent velocity is identical to that found by Simons (1977) for the San Diego area. Until additional profiles can be established within the sparsely instrumented Peninsular Ranges, we suggest a $P_n$ velocity of 8.0 km/sec.

A second, unreversed composite profile, Figure 3.6, extends north from a calibration blast located south of the Salton Sea, dated 3/22/76. The stations used in the profile and the travel-time data are listed in Table 3.5. The $P_n$ velocity of 7.8 km/sec, observed from 95 to 190 km, is compatible with the high heat flow and recent volcanism of the Salton Trough. If we adopt a $P_n$ velocity of 7.8 km/sec for the Imperial

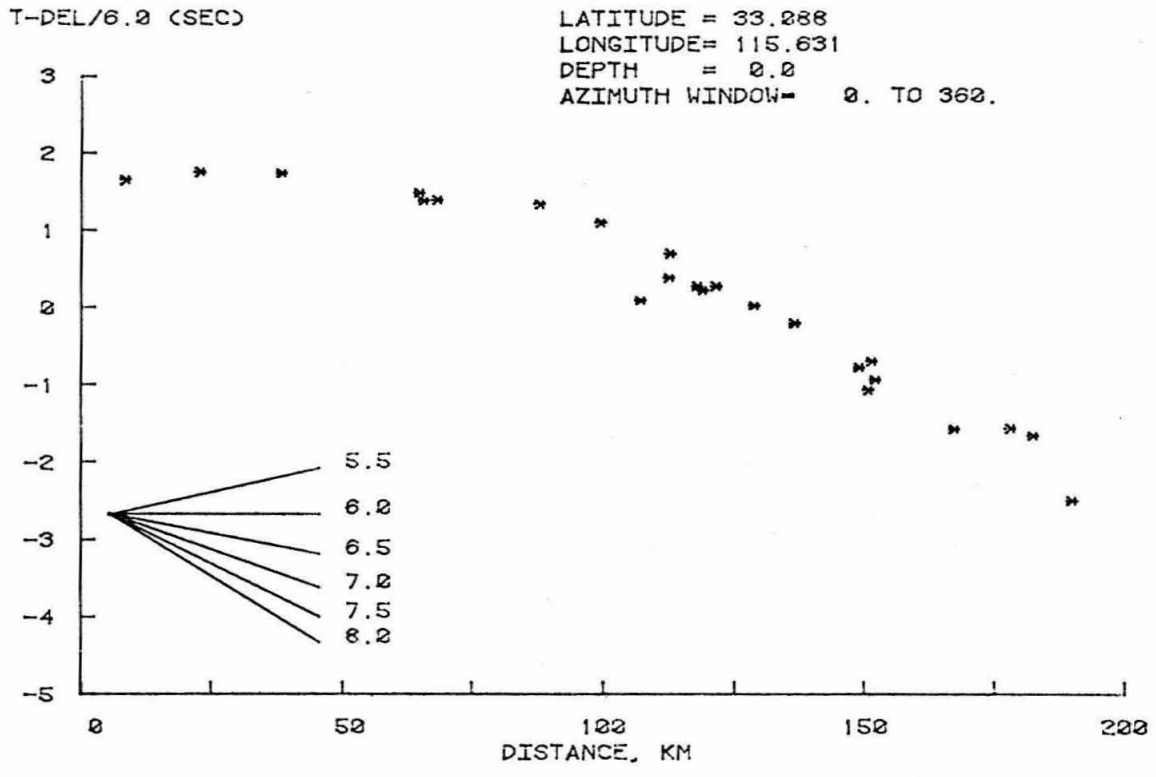


Figure 3.6 Composite profile extending north from the southern end of the Salton Sea. The cross-over from 6.2 km/sec to 7.8 km/sec occurs at 95 km. This suggests that the crustal thickness in the Coachella Valley region is less than 20 km. The travel-time data are listed in Table 3.5.

Table 3.5 Station and travel-time data used in the composite profile that extends north from the calibration blast located south of the Salton Sea, 3/22/76. The data are plotted in Figure 3.6.

| STA | AZIMUTH | DISTANCE | T | T-DEL/6.0 | H*COS(I)/5 | T PLOTTED |
|---|---|---|---|---|---|---|
| OBB | 356. | 8.814 | 3.150 | 1.680 | -0.002 | 1.683 |
| SUP | 230. | 23.271 | 5.679 | 1.801 | 0.016 | 1.784 |
| CRR | 234. | 38.655 | 8.229 | 1.787 | 0.010 | 1.777 |
| BC2 | 14. | 65.046 | 12.519 | 1.678 | 0.152 | 1.526 |
| IKP | 222. | 66.062 | 12.550 | 1.539 | 0.124 | 1.415 |
| LTC | 49. | 68.612 | 12.919 | 1.484 | 0.060 | 1.424 |
| CO2 | 17. | 88.291 | 16.129 | 1.414 | 0.038 | 1.376 |
| PNM | 350. | 99.874 | 17.949 | 1.304 | 0.164 | 1.139 |
| INS | 331. | 107.588 | 18.299 | 0.368 | 0.247 | 0.121 |
| KEE | 302. | 113.018 | 19.449 | 0.613 | 0.199 | 0.413 |
| LTM | 35. | 113.116 | 19.699 | 0.847 | 0.108 | 0.738 |
| PLM | 284. | 118.429 | 20.299 | 0.561 | 0.249 | 0.312 |
| TPC | 341. | 119.343 | 20.249 | 0.359 | 0.112 | 0.247 |
| SHH | 358. | 121.967 | 20.799 | 0.472 | 0.165 | 0.306 |
| CPM | 336. | 129.341 | 21.749 | 0.193 | 0.139 | 0.053 |
| VGR | 307. | 137.109 | 22.899 | 0.048 | 0.221 | -0.173 |
| VST | 273. | 149.563 | 24.199 | -0.727 | 0.016 | -0.744 |
| DB2 | 298. | 151.203 | 24.249 | -0.950 | 0.094 | -1.044 |
| RAY | 314. | 151.877 | 24.999 | -0.312 | 0.352 | -0.665 |
| RMR | 325. | 152.423 | 24.749 | -0.653 | 0.256 | -0.910 |
| PEC | 302. | 167.729 | 26.499 | -1.454 | 0.093 | -1.548 |
| SIL | 321. | 178.324 | 28.449 | -1.270 | 0.262 | -1.533 |
| SNS | 282. | 182.657 | 28.849 | -1.592 | 0.028 | -1.621 |
| GRP | 0. | 190.362 | 29.449 | -2.277 | 0.188 | -2.465 |

Valley, then this profile requires a crustal thickness of 16-19 km for the Coachella Valley region.

In addition to the profiles described above, we have compiled a large number of unreversed $P_n$ velocity profiles for the southern California region. Figure 3.7 shows the location of these additional profiles. The arrows represent the lengths of the profiles and also indicate the sections of upper mantle investigated. The arrows point in the direction of energy propagation. In order to convert the apparent velocity measurements into dip, we have smoothly interpolated to the center of each arrow the $P_n$ velocities shown on Figure 3.5. The apparent dip angle along the seismic profile is a simple function of the apparent velocity. Because the dip on intermediate crustal layers, such as the 6.2 to 6.7 km/sec interface, is not well known, we have not made any crustal corrections to the Moho dip. For much of southern California the assumption of a relatively uniform crust appears to be valid. However, as shown by the nine crustal profiles discussed in this chapter, the northern Peninsular Ranges and the western Transverse Ranges are regions of rapid change. Within the Mojave, the eastern Transverse Ranges and the Colorado desert, the 6.2 km/sec layer dominates the crust. The 6.7 km/sec layer thickens substantially in the western Transverse Ranges and the Peninsular Ranges. On the basis of these observations we anticipate that the uncorrected Moho dips in the region of the northwestern Peninsular Ranges and the western Transverse Ranges should be inaccurate. As shown in Figure 3.8, the largest apparent dips on the Moho occur in this transition zone. We feel that these large apparent dips are

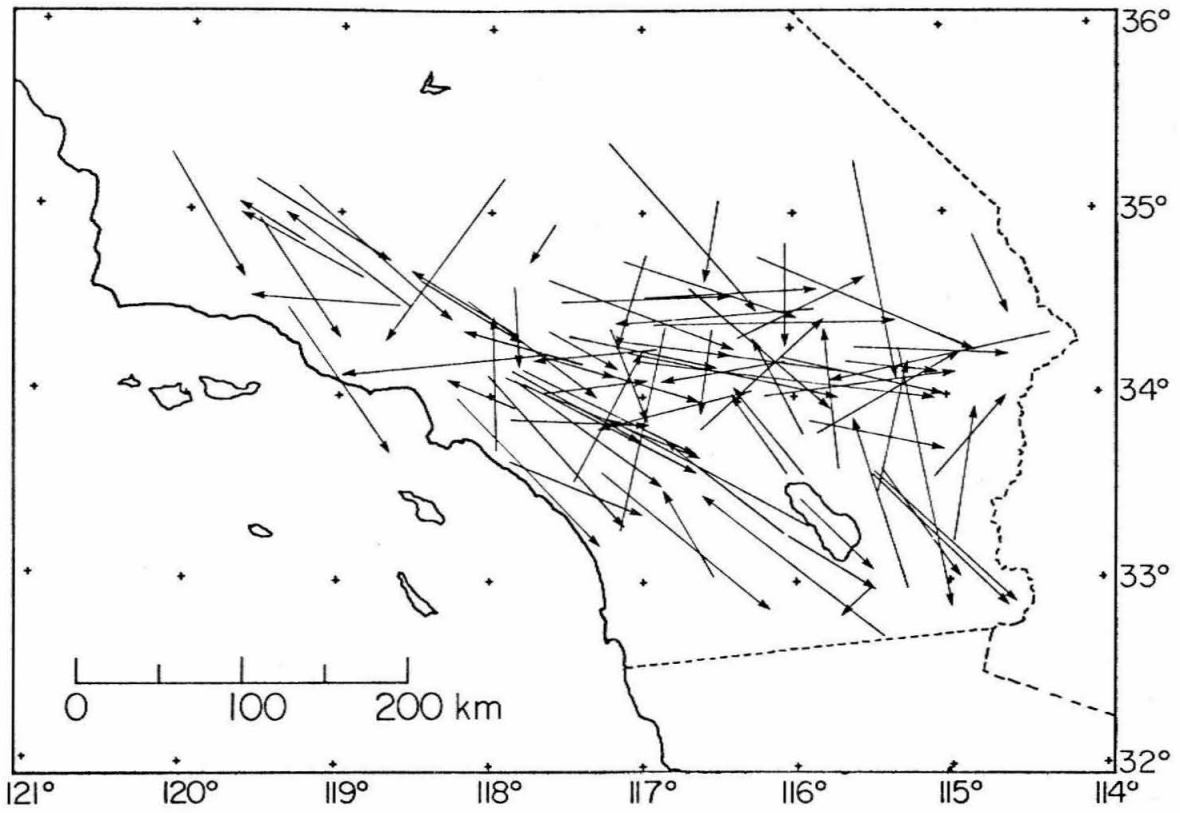


Figure 3.7 Location of the upper mantle sampled in the $P_n$ studies. Each arrow indicates the distance over which the refractor was observed and the direction energy was propagating.

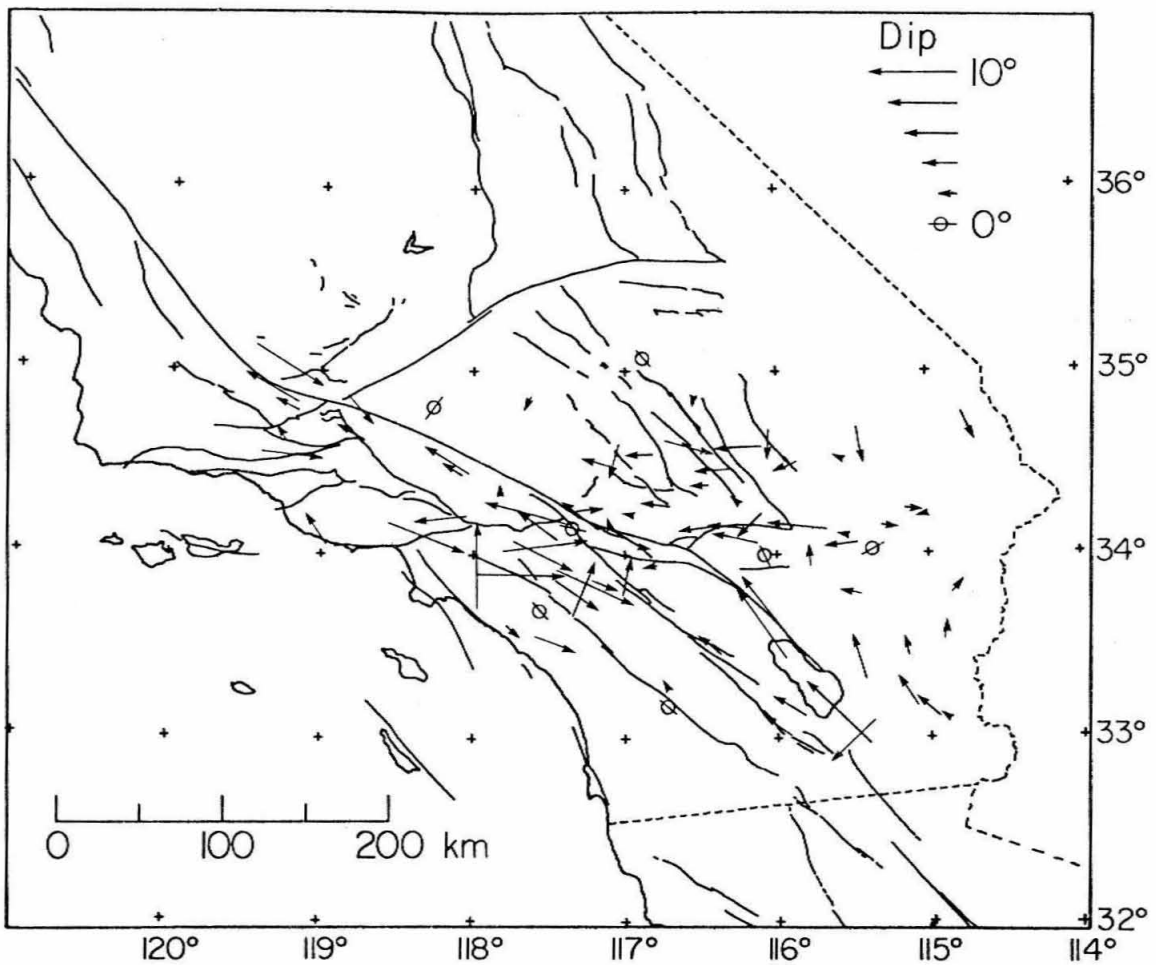


Figure 3.8 Regional Moho dip. The apparent dips have been calculated from the observed velocities and the smoothly interpolated true velocities shown in Figure 3.5.

unreliable.

# CONCLUSIONS

Through the study of 60 travel-time curves for crustal first arrivals within southern California, we have found that the commonly observed first arrival east of the San Andreas fault is 6.2 ± 0.1 km/sec. This velocity is also observed for profiles that extend across the northeast end of the Peninsular Ranges. Limited data suggest that within the Peninsular Ranges, the region between the crustal sections dominated by a velocity of 6.2 vs the 6.7 km/sec is in the vicinity of the Elsinore fault. A similar transition from 6.2 to 6.7 km/sec occurs between the San Gabriel mountains and the western Transverse Ranges.

The $P_n$ profiles show that subcrustal velocities vary from 7.7 to 8.2 km/sec. It is interesting to note that the low $P_n$ velocity of 7.8 km/sec extends northwest from the Salton Trough, through the region of San Bernardino, and fans out across the central Mojave. This geometry is quite similar to that of the horizontal decoupling zone that we propose in later chapters to account for the apparent offset between the plate boundaries in the crust and the upper mantle. Moho dips calculated from unreversed profiles by smoothly interpolating known $P_n$ velocities indicate a relatively uniform westward dip in the region of the eastern Transverse Ranges and the Mojave.

A composite profile composed of stations of the southern California array extends north from a calibration blast located at the south end of the Salton Sea. This travel-time curve is the first long refraction profile that defines the crustal thickness of the northern Salton Trough. The depth to Moho of 16-19 km for the Coachella Valley is

consistent with the estimates derived from regional gravity studies (Biehler, personal communication).

REFERENCES

Healy, J. H. (1963). Crustal structure along the coast of California from seismic-refraction measurements, J. Geoph. Res., 68, 5777.

Johnson, C. (1978). Cedar, An approach to the computer automation of short Period local seismic networks, EOS, 59, 316.

Roller, J. C., and Healy, J. H. (1963). Seismic-refraction measurements of crustal structure between Santa Monica Bay and Lake Mead, J. Geophys. Res., 68, 5837-5848.

Shor, G. G. and Raitt, R. W. (1956). Seismic studies in southern California continental borderlands, International Geological Congress, 20th, Mexico, Trabajos Seccion 9, t. 2, p. 243-359.

Simons, R. (1977). Seismicity of San Diego, 1934-1974, Bull. Seism. Soc. Am., 67, 809-826.

# CHAPTER 4

## Regional S-Wave Structure for Southern California from the Analysis of Teleseismic Rayleigh Waves

ABSTRACT

Teleseismic Rayleigh waves, $M_s > 7.0$, in the period range 14 to 28 sec, are well recorded by the short period Benioff array within southern California. Multiple arrivals that hamper local dispersion analysis within this period range are detected by narrow band-pass filtering. The records are then windowed on distinct, coherent peaks that move uniformly across the array. Four to seven stations are included in the determination of both the phase velocity across the array and the incidence azimuth. For earthquakes in the western Pacific, the derived incidence azimuths are systematically rotated counterclockwise by $2 - 16^{\circ}$. Most of the rotation results from refraction at the continental shelf. However, for events in the southern Pacific, the corrected azimuths for the first arrivals deviate several degrees from the great circle path. Phase velocity data for both the southern Mojave-central Transverse Ranges and the Peninsular Ranges are inverted to obtain regional S-wave velocity models. The starting models are constructed from travel-time studies of local, natural and artificial sources as described in Chapters 2 and 3. Poisson's ratio as a function of depth is calculated for these two regions. The comparison with laboratory ultrasonic studies requires a quartz-rich crust within the southern Mojave-central Transverse Ranges and a mafic crust within the Peninsular Ranges.

## INTRODUCTION

Many investigators are currently pursuing research on such diverse topics as visco-elastic models of the great bend in the San Andreas and the possibly related mechanisms of uplift and deformation; propagation of energy from the seismic source to the free surface; and the quantification and description of the ongoing seismicity. These examples and many others all have in common the requirement of an accurate description of the structure of the crust and upper mantle. As discussed in Chapter 2 and 3, P-wave travel-time studies from both natural and artificial, local and teleseismic, sources have provided significant data on the regional average structure (Gutenberg, 1944, 1951, 1952, 1955; Richter, 1950; Shor, 1955; Press, 1956, 1960; Roller and Healy, 1963; Kanamori and Hadley, 1975). With the rapid growth of the short-period vertical seismic array within southern California, recorded at Caltech in conjunction with the USGS, average P-wave models for individual geologic provinces are available, Chapters 3 and 5. The relatively coarse nature of these models reflects the averaging effects of refraction profiles that extend over pathlengths of several hundred kilometers. Teleseismic P-delay studies, with somewhat better local resolution, have mapped local velocity anomalies within the upper mantle beneath southern California (Raikes, 1976; Raikes and Hadley, 1978). These studies have demonstrated a remarkable continuity of a mantle P-wave velocity anomaly across the San Andreas fault. Observations such as these have major implications for the lateral and vertical position of the boundary between the North American and the Pacific plates.

Although the P-wave velocity model for southern California is slowly becoming more detailed and precise, the S-wave structure has been virtually ignored. There are several obvious reasons for this: first, good S-wave travel-times are difficult to measure as the initial S-wave is often obscured by the P-wave coda. This is particularly true for the phase that refracts along the top of the mantle, $S_n$. The arrival most often timed as S, even beyond the crossover to $S_n$, is the phase that propagates at approximately midcrustal velocities, $S_g$. Second, about 95% of the southern California array is devoted to short-period vertical instruments and no SH energy is observed. If SH energy were observable, the first problem would not be quite as acute. Third, S-waves are not well excited by artificial sources. The S energy observed at stations must typically result from a strong P-S conversion at some unknown velocity gradient. This uncertainty adds an ambiguity to the origin point and time for the S-wave. If the first difficulty were not so severe, this complication would be acceptable. We would anticipate mapping at least three branches of the travel-time curve corresponding to the average P-wave branches of 5.5, 6.1-6.3 and 7.8 km/sec.

As suitable refraction data are not readily available, we have designed a technique for deriving local crustal structure that utilizes the dispersion characteristics of fundamental mode Rayleigh waves from distant teleseisms. Our period range of interest is from 10 to approximately 50 sec. However, the band-pass of the presently available data recorded by short period Benioff instruments limits the data set to periods shorter than 30 sec. As we will show later, even this

limited band can provide important constraints on the local S-wave structure.

The use of the Rayleigh waves in the period range 10 - 30 sec is severely complicated by the effects of multipathing. Unless the inherent effects of this interference can be removed, the data are most often unusable. Capon (1970) has introduced a high-resolution frequency wave-number method for handling the problem. This technique requires "approximately one hour ...(of)... IBM 360/65" computer time for the analysis of about four periods from one event. Within this study we present a somewhat simpler, and hence less expensive, technique for separating Rayleigh waves that have traveled along multiple paths. The method relies on a careful windowing of the recorded Rayleigh wave. The window characteristics are chosen by first narrow band-pass filtering the records and then processing distinct peaks in the amplitude envelope that propagate uniformly across the array. The technique is unable to unambiguously separate two arrivals of the same period that arrive simultaneously at the array from two distinct paths. This occurrence is manifest in the analysis by large error bars in the estimated azimuth and phase velocity. However, if the phase velocity were known in advance, good estimates of the azimuths of the two interferring groups could be estimated. Fortunately, at any particular period, multiple arrivals usually are separated in time by several multiples of that period.

The method of using phase velocity as determined from a local array for the investigation of local structure was discussed and used by Press (1956) and Alexander (1963). In these studies three stations

and the crest and trough method were employed to define both the azimuth and the phase velocity. The resulting data were compared with a set of standard curves of phase velocity vs. crustal thickness. From this relatively simple analysis, good estimates of crustal thickness for various sub-regions of southern California were obtained. In the present study, we utilize data from 4 to 7 stations, constrain the crustal thickness from previous P-wave studies, and then derive regional S-wave models. The resolution of this technique is controlled by both the available Rayleigh wave period range and the physical dimensions of the array. In future studies, with instrumentation designed for this task and with array dimensions of about 30 km, the resolution of local crustal structure will substantially surpass that which is currently available from crustal refraction studies. The method has the additional advantage of being applicable to structures with velocity reversals.

## DATA ANALYSIS

The fundamental problem in utilizing short-period Rayleigh waves results from multipathing. In the frequency domain, this interference produces scalloping of the amplitude spectrum. The periodicity of the scallops is controlled by the time separation of the multiple arrivals. The amplitude spectrum suggested to us that a signal processing technique could possibly make use of this periodicity in order to separate the interfering arrivals. Good separation of interfering Rayleigh waves from multiple, closely spaced events has been achieved with the complex cepstrum technique (Oppenheim and Schafer, 1975; Tsai, 1972). Although this method is most effective when the interfering signals have the same wave shape, tests with chirped sinusoids with slightly different dispersion were quite promising (Linville, 1971). Simple linear filtering of the cepstrum reproduced both input records. However, tests with real data were rather disappointing. The failure of this technique can be attributed to at least two problems: 1) For the events studied ($M_s$ > 7.0), short period Rayleigh waves arrived at the stations for about one hour. Clearly the later phases represent energy that has traversed paths differing substantially from the initial arrivals. These later phases strongly violate the assumption of an approximately stable waveform. Truncation of the data is required, but the location and the manner of this truncation are quite ambiguous. If the truncation is done incorrectly, spurious energy is convolved with that portion of the record which is of most interest. 2) Although the linear filtering of the complex cepstrum for the synthetic data was rather obvious and could have been automated, filtering of the

real data verged on an art form. Because of these complications we have abandoned the technique for the present problem.

Our present approach for identifying and separating multiple arrivals relies on narrow band filtering of the data. Figure 4.1, lower left, shows a good example of the original Rayleigh waves recorded by six stations. The records on the lower right show the same data after processing with a narrow band-pass, zero phase shift filter centered at a period of 25 sec. The second arrival, marked "B", is clearly visible. The window location for processing the original data is selected by band-pass filtering the data with filters that span the range of observable periods and are spaced by about 4 sec. The dashed lines in Figure 4.1, labeled "B", indicate a fairly typical window selection. As the determination of the phase velocity uses the Fourier transform of the windowed data, the shape of the window is also of some interest. Figure 4.2 shows a suite of phase velocity curves derived from data selected in a manner identical to that shown in Figure 4.1. Before processing, the amplitude of the front and back portions of the record are smoothly decreased to zero by multiplying by a cosine term. The percentages shown on the curves of Figure 4.2 indicate the portion of the processed record modified by the window. The vertical lines indicate the range of expected energy as determined from the previous narrow bandpass filtering. Within the range of expected energy, the derived phase velocity is relatively insensitive to the window. Outside of this range, the window has the effect of smoothing the data. For this study, the phase velocity curves have been constructed in sections by overlapping windows. All selected

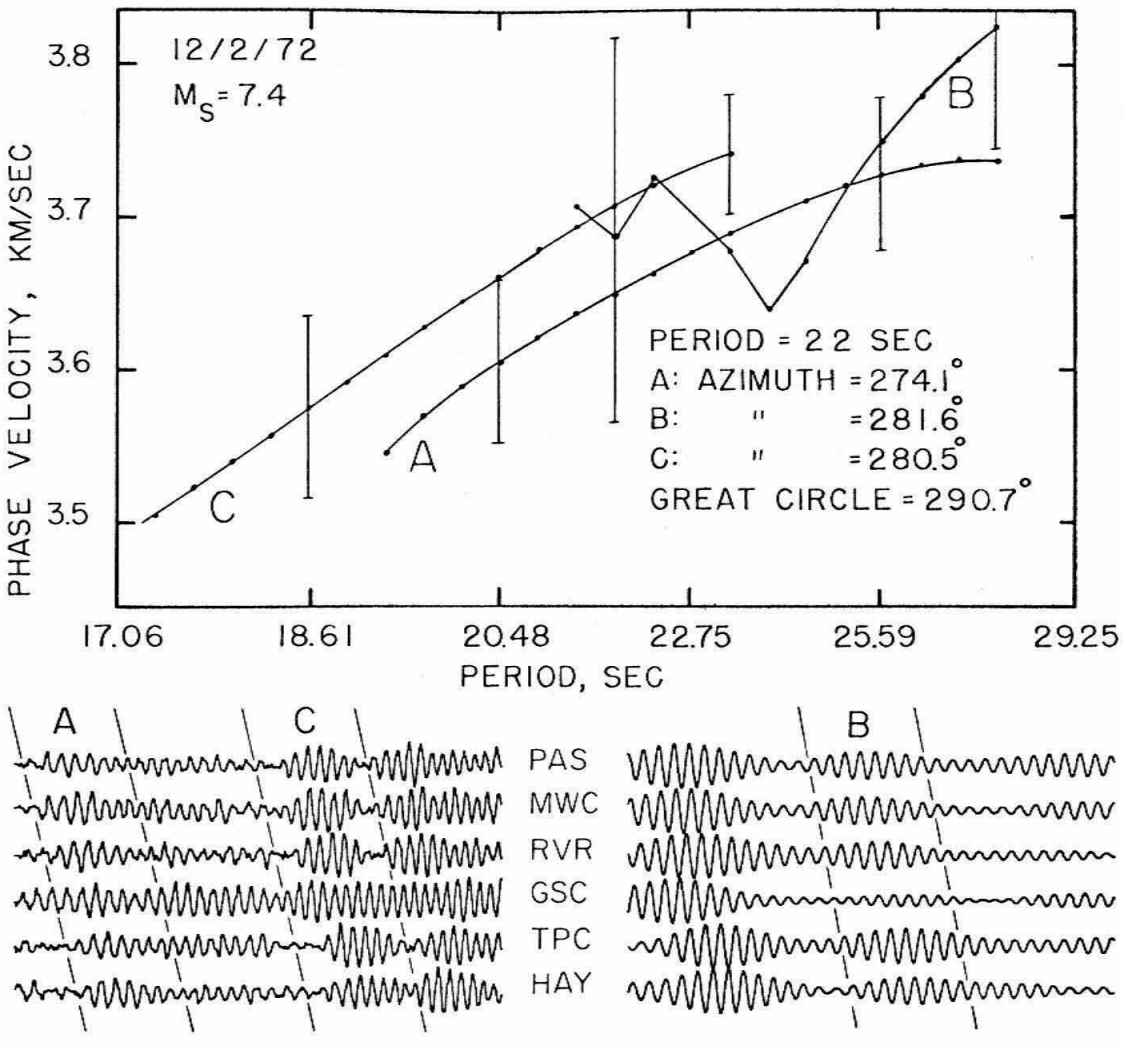


Figure 4.1 Rayleigh waves recorded across the southern California array for a magnitude 7.4 event in the Philippines. The records at the lower right are narrow band-passed filtered for a period of 25 sec. Note the second multipathed arrival. The phase velocity curves derived from the windowed data as shown, and the calculated incidence azimuths, illustrate the extensive multipathing. The duration of the record sections is 12 min.

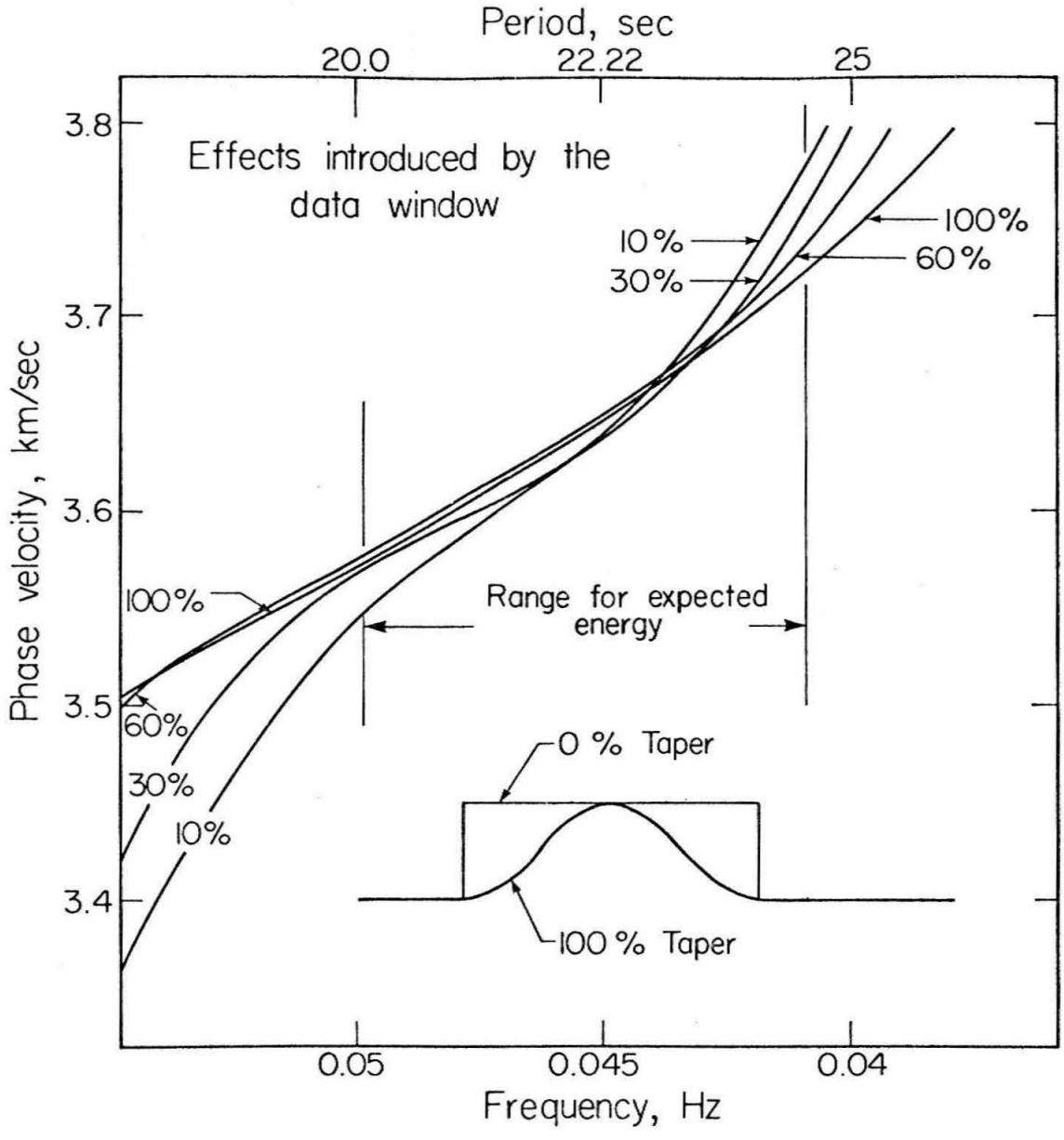


Figure 4.2 The averaging effect of the cosine taper used to window the data. The percentages shown on the curves indicate the portion of the processed record modified by the window. The vertical lines indicate the range of expected energy as determined from the previous narrow band-pass filtering.

data have been smoothed with a 100% cosine taper. Figure 4.1 shows a fairly typical example of the phase velocity curves derived by this overlap processing technique. The phase velocity curves presented later represent maximum likelihood estimates constructed from overlapping determinations.

The phase velocity curves are obtained by first Fourier transforming the windowed data. The phase data that result from this transform are simply related to the phase velocity of the propagating Rayleigh wave. The derived phase angles range between 0 and $2\pi$ . For the general case of an array several wavelengths in dimension, an appropriate multiple of $2\pi$ must be added to the phase angles to restore the true absolute angles. The expected phase difference between two stations separated by D km (measured along the wave path), for a wave with period T and phase velocity C, is $2\pi$ (D/CT). For a wide range of C, such as $3.7 \pm 0.4$ km/sec, and an average station spacing of about one wavelength or less, the appropriate number of multiples of $2\pi$ are easily restored to the phase data. Finally, the phase velocity across the array and the azimuth of approach at each frequency step are simple functions of the strike and dip of the plane fit by least squares to the phase angles from all of the stations (Press, 1956, Aki, 1961). By using more than three stations, the regression also provides error estimates on the phase velocity and azimuth. We typically use from 4 to 7 stations in the analysis.

Figure 4.1 lists the derived incidence angles for the windowed data. It is interesting to note that at the same period, T = 22 sec, the incidence paths for the three distinct windows are all rotated

counterclockwise from the great circle path. For the first arrival, "A", the rotation is in excess of $16^{o}$. These large variations in incidence angles pose a minor problem in regard to the restoration of the $2\pi$ multiples to the phase. If the phase is incorrectly restored, the phase velocities and azimuths typically show erratic behavior between adjacent periods. We have found that a simple search over a range of azimuths, each separated by about $15^{o}$, rapidly recovers the true phase.

Figure 4.3 illustrates the systematic variation in the observed incidence angles for events around the Pacific. The dark lines represent the great circle azimuths and the light the derived azimuths for the period T = 20 sec. The systematic counterclockwise deflection is largely controlled by refraction at the continental shelf. The upper part of Figure 4.3 plots the calculated phase velocity within the Pacific plate as a function of incidence angle at the Patton escarpment. At large incidence angles the calculated velocity is similar to the measured velocity of 4.0 km/sec (Kausel and others, 1974; Forsyth, 1975). This suggests that the initial Rayleigh waves detected in southern California traverse the northern Pacific along the great circle path. The calculated high phase velocities for the small incidence angles indicate that energy crossing the south Pacific deviates from the great circle path by several degrees.

The phase velocity curves from the seven teleseisms are plotted in Figure 4.4. The inset map shows the station distribution and the measured incident azimuths. The average probable error, weighted by the inverse of the standard deviations of the individual determinations,

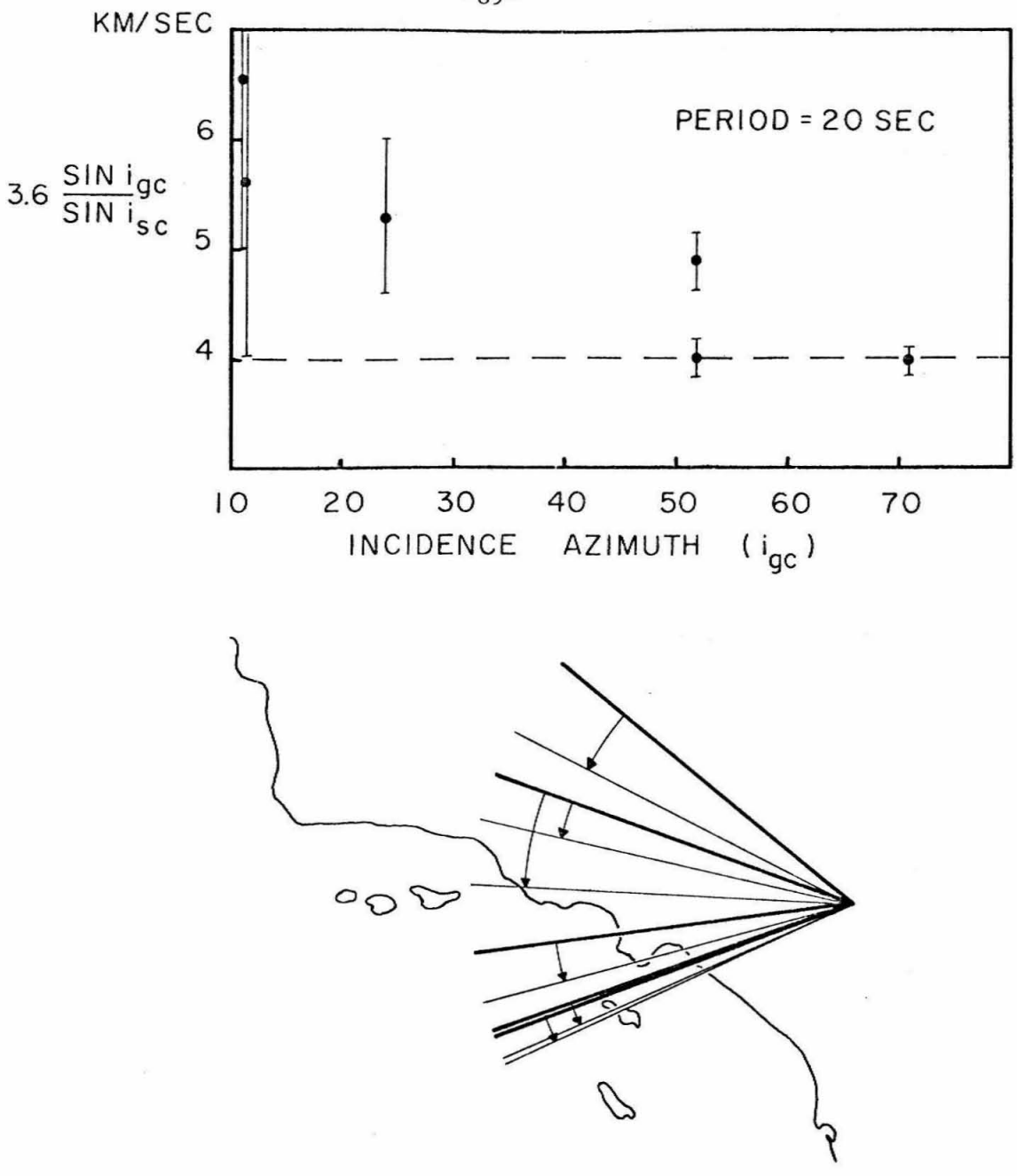


Figure 4.3 The systematic counterclockwise rotation of the incidence azimuth for earthquakes located around the Pacific. The incidence azimuths were determined from the data recorded by the array shown in Figure 4.4. If the deflection is entirely controlled by the continental shelf, the calculated phase velocity for the oceanic crust, T = 20 sec, computed from the observed phase velocity, azimuth and expected incidence azimuth at the shelf, should be 4.0 km/sec. The deviation from this value for waves crossing the south Pacific suggests a deviation from the great circle path.

is approximately 0.05 km/sec. For an array with smaller physical dimensions, the assumption of lateral homogeneity should be improved and the scatter in the velocity curves significantly reduced. The phase velocity data used in the inversion described below were calculated from an average of the individual curves, weighted by the inverse of the standard deviations. Data for the inversion were then sampled at a period spacing of 2 sec. For the present study these phase velocities provide a good constraint on the regional average S-wave velocities.

The phase velocity curves are inverted with a damped generalized inverse technique (e.g., Franklin, 1970; Wiggins, 1972). We assume the data and the model are related by:

$$AM = D \tag{4.1}$$

where M and D are vectors representing, respectively, the desired perturbation to the starting model and the difference between the real and the model data. A is the matrix of partial derivatives that maps M into D. The model is then calculated using:

$$M = A^T(AA^T + (r/(1-r))V)^{-1}D \tag{4.2}$$

The range of r extends from 0 to 1. This variable controls the stability of the solution. Clearly, as r tends to zero, the solution moves smoothly to the undamped inverse. The matrix V is the data variance matrix. The diagonal elements are the variance of each determination of the phase velocity. The off-diagonal terms describe the covariance between different frequencies. Because of the window

characteristics used in the data processing, the covariance terms are not all zero. However, the covariance between periods at opposite ends of the frequency band is near zero. We therefore have tapered the covariance matrix with a Gaussian function to approximate the data smoothing inherent in the processing. Finally, the average kernel for layer i is given by:

$$F_i = A^T(AA^T + (r/(1-r))V)^{-1}AE_i \qquad (4.3)$$

where $E_i$ is the unit vector in the ith direction. The averaging kernel describes the resolution of the derived model.

The geographical region shown in Figure 4.4 is essentially the same as that previously discussed in Chapter 2. For the inversion of the data shown in Figure 4.4, the starting model was modified from the earlier study. The 6 km thick upper layer was divided into a 1 km low velocity surface layer, $V_p$ = 3.5 km/sec, and a second layer with $V_p$ = 5.5 km/sec. The 21 km thick, $V_p$ = 6.3 km/sec layer was subdivided into four layers. The rest of the model was unchanged. The S-wave velocity for the starting model was calculated from the P-wave model with the assumption of Poisson's ratio of 0.25.

An examination of the layer partials in the A matrix indicates that except for the shallow crustal layers the S-wave partials are several times larger than those for P-waves. This means that perturbations to the model occur primarily in the S-wave structure. Because of this insensitivity to P-wave structure, we have inverted the phase velocity data with several different P-wave starting models. The range of P-wave models employed in the inversion actually extend beyond

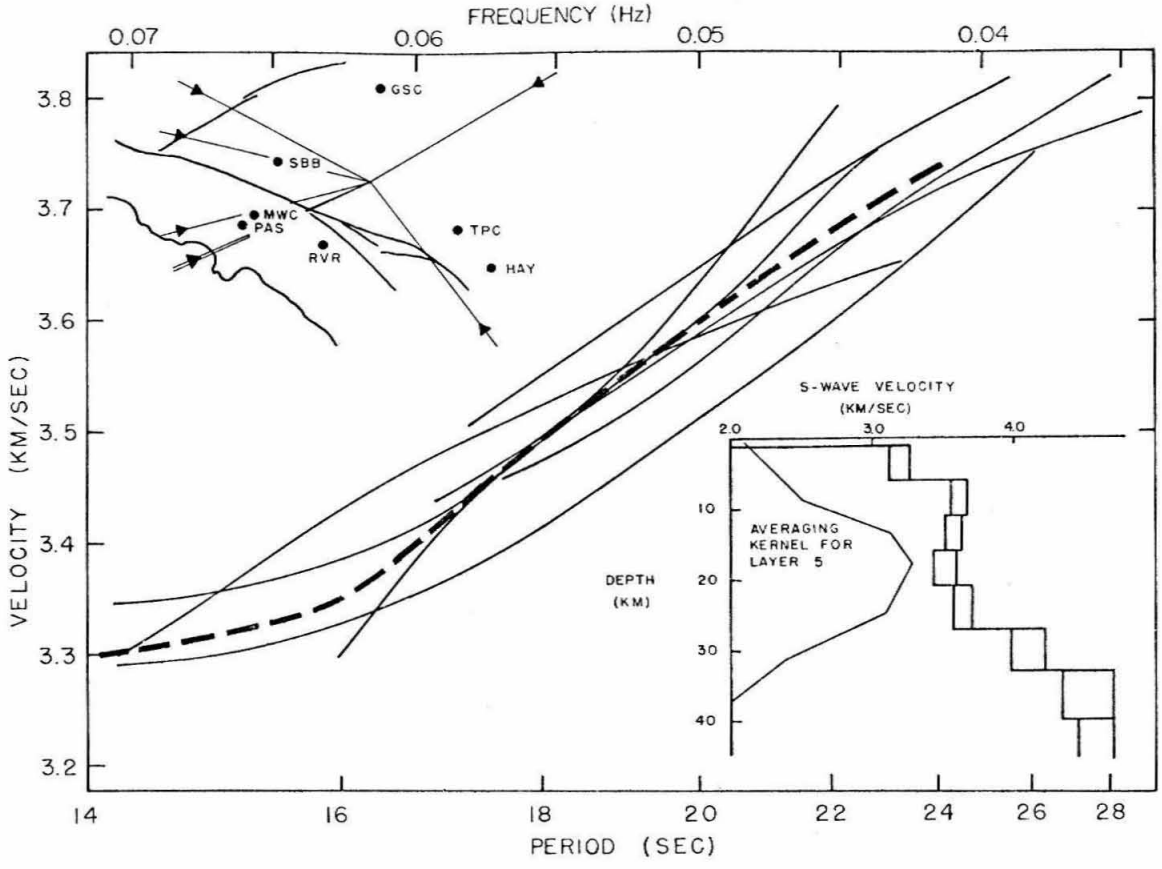


Figure 4.4 Phase velocity dispersion curves for the Mojave region, the stations used, azimuth of approach for the seven events analyzed, and the S-wave crustal model derived from the inversion of the dispersion curves. The bounds on the model are maximum and minimum models derived from a wide range of starting models. A mid-crust low velocity zone is suggested by all inversions; however, the resolution is not sufficient to require this feature. The averaging kernal for layer 5 is inset with the model. The broken curve represents the weighted average of the phase velocity data.

the limits imposed by the quarry blast travel-time data. The velocity limits shown in Figure 4.4 bound all S-wave models that resulted from the various inversions. The averaging kernels indicate that the derived layer velocities actually represent weighted averages of the adjacent model layers, the weighting function being the averaging kernel. The combination of the P-wave data from the quarry blasts and the phase velocity data requires a model at least as complex as that shown in Figure 4.4.

Through all the inversions an average high velocity layer was required at the base of the crust, $V_s$ = 4.1 km/sec. This result is similar to that derived from the previous P-wave velocity studies for this region, but not dependent upon them. The Moho reflection, $P_MP$, was observed to reach critical at a distance, $\Delta_c$, of 90 to 98 km. Combined with good data for the upper crust and the $P_n$ velocity of 7.8 km/sec, the observed $\Delta_c$ required a high velocity layer at the base of the crust (Chapter 2).

The inversion of the phase velocity data suggested an additional interesting complication. All S-wave models, originating from rather diverse starting models, have a mid-crustal, layer 5, low velocity zone. The velocity contrast between layer 3, typically the fastest overlying layer, and layer 5, ranges from .1 to 3%. The depth to this possible velocity reversal is similar to the thickness of the seismic zone within southern California. These results are very similar to those of Keller and others (1975) and Bache and others (1978) for profiles in the adjacent Basin and Range province. Unfortunately, the limited frequency band of the phase velocity data does not provide

sufficient information to resolve this feature. The resolution and possible lateral variation of a crustal low velocity zone, and its influence, if any, on the depth of the seismic zone within southern California, will require studies that employ small, dense arrays of broad-band instruments.

The previously discussed, averaged model for the southern Mojave and the central and eastern Transverse Ranges has been a useful model for location and focal mechanism studies of earthquakes recorded by the regional array. A similar, average model appears useful for ongoing studies within the Peninsular Ranges of southern California. Toward this goal, we have collected travel time data from several natural and artificial sources, determined the Rayleigh wave phase velocity curves as discussed above, and surveyed previous geophysical studies of the province. The first and most obvious conclusion of this study is that most physical parameters of the province have large lateral variations. An east-west profile of the depth to the Moho through the latitude of the Salton Sea would show a crustal thickness of 20-25 km in the adjacent continental borderlands (Shor, 1956), a relatively smooth increase to 30-35 km beneath the center of the range, and a rapid decrease to possibly less than 20 km beneath the Salton Sea. The P-wave velocities in general show similar variations. The shallow upper crust varies from 5.8 km/sec in the north to 6.4 km/sec (Simons, 1977) in the south. The east-west lateral changes are equally severe, with velocities increasing to the west. The details of the multiple profiles crossing this province and of other profiles within southern California are discussed in Chapter 3. A simple, regionally

averaged model based on the compilation of these profiles is presented in Figure 4.5. The velocity profile presented by Shor and Raitt (1956) for the north-central portion of the province is shown for comparison. The slightly higher velocities are the result of the southern high velocity crust.

We have attempted to derive an average Rayleigh wave phase velocity curve for the province, period range of 14 to 26 sec. The available stations are shown in Figure 4.6. The station distribution, the lateral heterogeneity and the timing resolution prevent the utilization of the teleseisms that arrive at an incidence angle normal to the northwest structural grain of the province. Unfortunately this means that surface waves appropriate for studying the province propagate along paths parallel to the continental shelf. The resulting records are severely multipathed and difficult to use.

Figure 4.6 shows the station distribution, incidence azimuths and phase curves derived from four teleseisms. Because of the unfavorable geometry of the array and the lateral heterogeneity, the probable error for the weighted average phase velocity curve is 0.08 km/sec. The inversion of the phase velocity data, starting from a range of P-wave models as discussed above, results in a fairly simple regionally averaged S-wave model, Figure 4.6 As in the Mojave region, the various inversions suggested a mid-crustal S-wave low velocity zone. However, within the uncertainty in the data, the phase velocities can be matched without this feature. Unlike that from the Mojave, these data do not require a thin, high velocity, 4.1 km/sec layer or transition zone at the base of the crust.

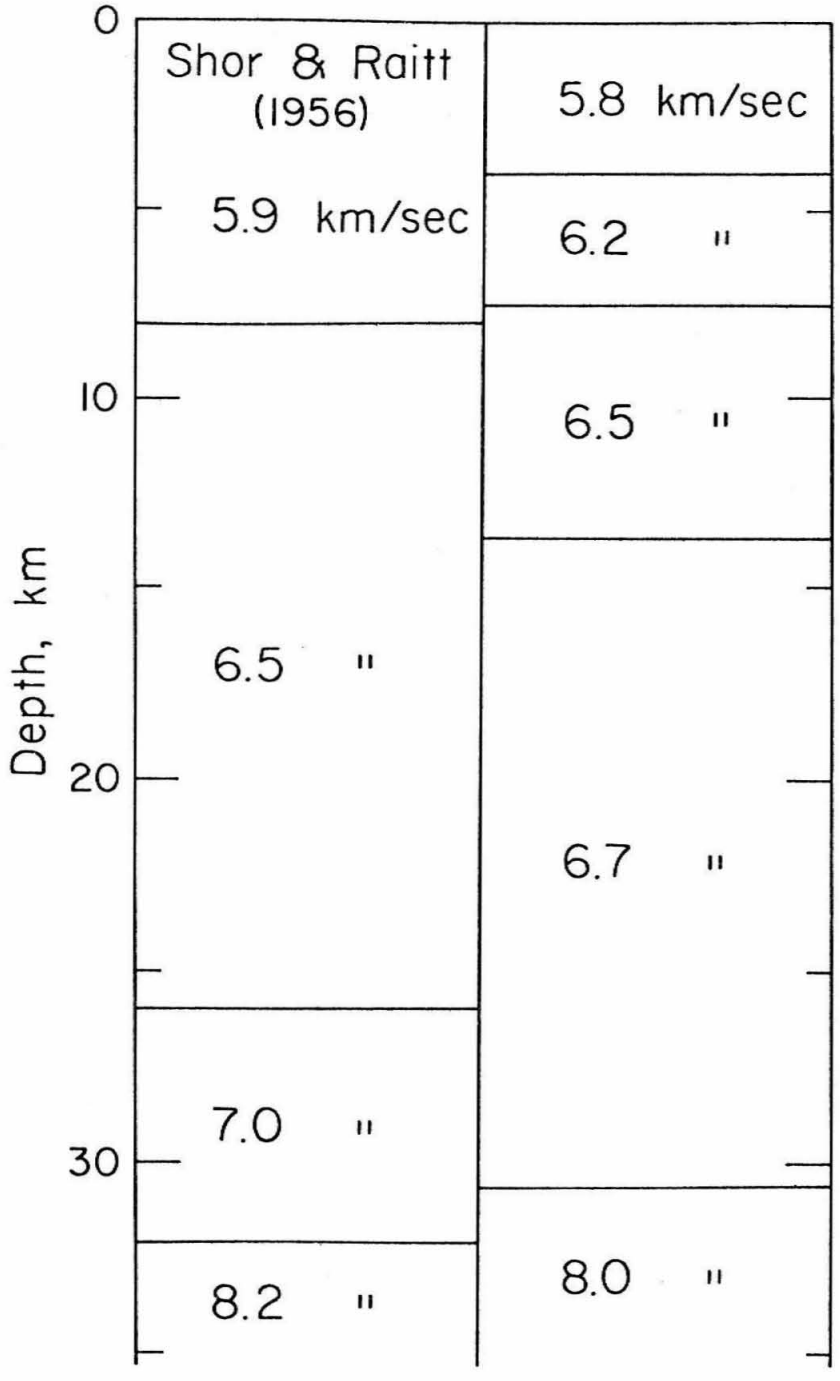


Figure 4.5 Regionally averaged P-wave model for the Peninsular Ranges north of the international border. The model of Shor and Raitt (1956) for the northern portion of the province is shown for comparison. The slightly higher velocities in the average model reflect contributions from the southern high velocity crust.

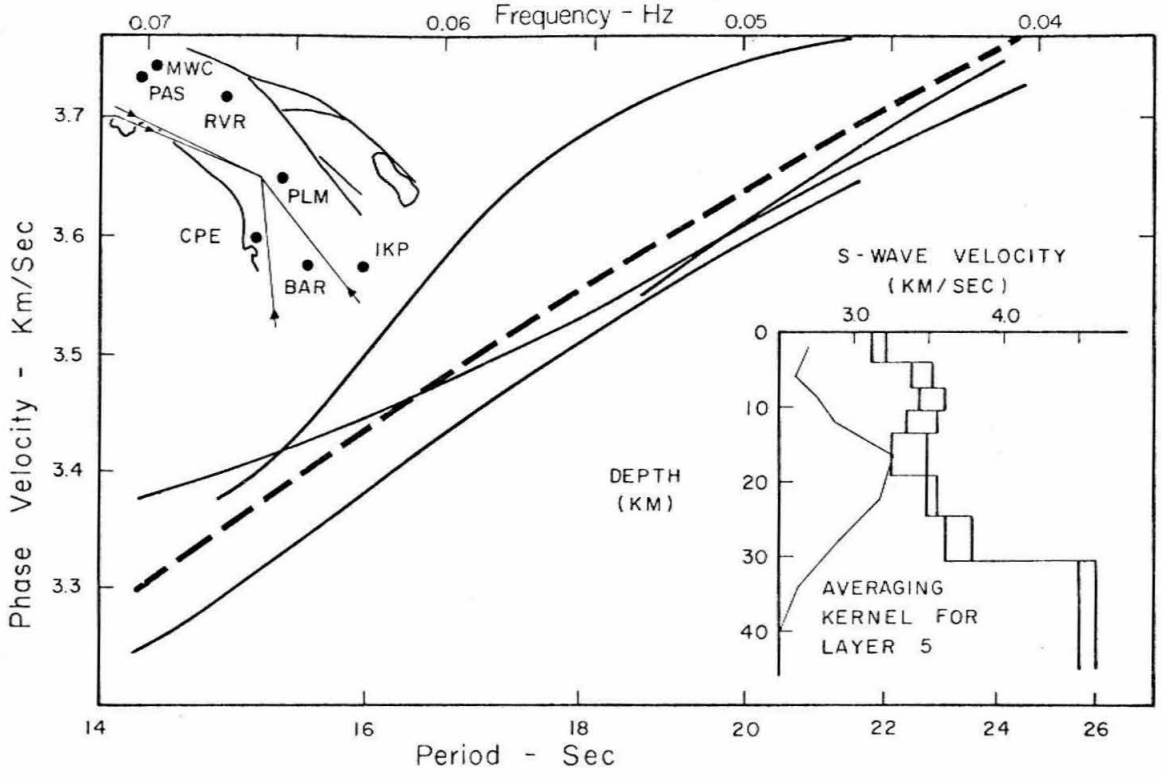


Figure 4.6 Phase velocity dispersion curves for the Peninsular Ranges, the stations used, azimuth of approach for four events analyzed, and the S-wave crustal model derived from the inversion of the dispersion curves. The bounds on the model are maximum and minimum models derived from a wide range of starting models. The broken curve represents the weighted average of the phase velocity data.

The P-wave models for the mid and upper crust for the Mojave and the Peninsular Ranges are quite distinct, in contrast to the S-wave models, which are all remarkably similar. This regional variation in the ratio $V_p/V_s$ requires a major change in lithology between the two provinces. The P-wave upper crustal velocities in the Mojave, 6.1 to 6.3 km/sec, are comparable with those from ultrasonic laboratory measurements on granites, Table 4.1. The average P-wave velocities within the Peninsular Ranges, 6.5 to 6.7 km/sec, are indicative of more mafic rocks such as gabbro and diorite. This is consistent with the known surface geology. The Mojave region contains many plutons of quartz monzonite. Plutons within the Peninsular Ranges grade from granodiorite to gabbro. Additional support for the continuation of the surface geology to the mid and lower crust is provided by Poisson's ratio, which is sensitive to composition of the crustal rocks. Table 4.2 shows values of Poisson's ratio derived from both the P- and S-wave velocities for several depths. A comparison of these values with measured ratios, Table 4.2, is consistent with major crustal compositional differences between the two provinces. The observed Poisson's ratio requires a mafic crust for the Peninsular Ranges and a more quartz-rich crust for the southern Mojave and the central Transverse Ranges.

Table 4.1 $V_p$, $V_s$ and Poisson's ratio as a function of rock type, confining pressure = 4 KB. The last column contains values of σ corrected to a temperature of 290°C.

| Rock | Density | $V_p$ | $V_s$ | σ | | σ(T = 290°C) | Ref. |
|---|---|---|---|---|---|---|---|
| Stirling quartzite | 2.495 | 4.71 | 3.00 | .159 | | .152 | 1 |
| Granite, Stone Mt., Ga. | 2.639 | 6.27 | 3.74 | .224 | | .217 | 2 |
| Texas gray granite | 2.609 | 6.25 | 3.61 | .227 | | .227 | 3 |
| Woodbury granite | 2.634 | 6.29 | 3.67 | .236 | | .234 | 3 |
| Granite, Barre, Vt. | 2.655 | 6.25 | 3.64 | .243 | | .236 | 2 |
| Granite, Rockport, Mass. | 2.638 | 6.39 | 3.68 | .252 | | .245 | 2 |
| Westerly granite | 2.63 | 6.09 | 3.50 | .254 | | .247 | 1 |
| Climax stock granodiorite | 2.665 | 6.31 | 3.53 | .273 | | .266 | 1 |
| Basalt | 2.586 | 5.80 | 3.27 | .274 | | .274 | 3 |
| Hornblend gabbro | 2.933 | 6.86 | 3.71 | .289 | | .289 | 3 |
| Bytownite gabbro | 2.885 | 6.81 | 3.53 | .309 | | .309 | 3 |
| San Marcos gabbro | 2.993 | 7.01 | 3.52 | .329 | | .329 | 3 |
| Eclogite, Headlsburg, Ca. | 3.444 | 8.01 | 4.58 | .257 | (10 KB) | | 2 |
| Periodtite, Hawaii | | | | | | | |
| #1 | 3.29 | 8.21 | 4.49 | .287 | " | | 4 |
| #2 | 3.29 | 8.36 | 4.68 | .272 | " | | 4 |

Ref.


1 Shock, Bonner & Louis 1974.
2 Press 1966.
3 Hughes & Maurette 1956.
4 Christensen 1966.

Table 4.2. Poisson's ratio for the southern Mojave and Peninsular Ranges.

| Depth | Peninsular Ranges | Mojave |
|---|---|---|
| 5 | .287 ± .024 | .244 ± .031 |
| 10 | .295 ± .028 | .246 ± .027 |
| 28 | .280 ± .028 | .220 ± .040 |
| 35 | .269 ± .020 | .251 ± .025 |

## CONCLUSIONS AND RESULTS

1) Narrow band filtering can identify multiple Rayleigh wave arrivals from teleseisms. Careful windowing of the data, from four or more stations, can provide good estimates of the phase velocity, the incidence azimuth and the respective error estimates.

2) Incidence azimuths for the first arrival, T = 20 sec, for events located in the western Pacific, are systematically rotated counterclockwise from the great circle path. A large part of the rotation results from refraction at the continental margin. After correcting for the refraction, the incidence azimuths for Rayleigh waves crossing the south Pacific deviate from the great circle path by a few degrees ($1 - 4^{\circ}$).

3) Fundamental mode Rayleigh wave phase velocity curves, T = 14 to 28 sec, have been measured for both the southern Mojave-central Transverse Ranges and the Peninsular Ranges.

4) The phase velocity data have been inverted with a damped generalized inverse. The P-wave starting models span and extend slightly beyond the limits imposed by quarry blast data. The resulting range of S-wave models, Figures 4.4 and 4.6, represents the simplest models consistent with the data. All inversions suggest a mid-crustal low velocity zone that is comparable in depth with the bottom of the seismic zone. However, the accuracy of the present data does not require this feature.

5) The P-wave velocities determined from natural and artificial sources, and Poisson's ratio derived from both the P- and S-wave velocities, Table 4.2, require a quartz-rich crust within the southern

Mojave-central Transverse Ranges and a mafic crust within the Peninsular Ranges. Both observations are consistent with the surface geology.

REFERENCES

Aki, K. (1961). Crustal structure of Japan from the phase velocity of Rayleigh waves, Bull. Earthquake Res. Inst., Tokyo, 39, 249-277.

Alexander, S. S. (1963). Surface wave propagation in the western United States, Ph.D. Thesis, California Institute of Technology.

Bache, T. C., Rodi, W. and D. Harkrider (1978). Crustal structure inferred from Rayleigh wave signatures from NTS explosions, Bull. Seism. Soc. Am., submitted.

Capon, J. (1970). Analysis of Rayleigh wave multipath propagation at LASA, Bull. Seism. Soc. Am., 60, 1701-1731.

Christensen, N. I. (1966). Elasticity of ultrabasic rocks, J. Geophys. Res., 71, 5921-5931.

Forsyth, D. W. (1975). The early structural evolution and anisotropy of the oceanic upper mantle, Geophys. J. R. Astr. Soc., 43, 103-162.

Franklin, J. N. (1970). Well-posed stochastic extension of ill-posed linear problems, J. Math. Anal. Appl., 31, 682-716.

Gutenberg, B. (1944). Travel times of principal P and S waves over small distances in southern California, Bull. Seism. Soc. Am., 34, 13-32.

Gutenberg, B. (1951). Revised travel times in southern California, Bull. Seism. Soc. Am., 62, 427-439.

Gutenberg, B. (1952). Waves from blasts recorded in southern California, Trans. Am. Geophys. Union, 33, 427-431.

Gutenberg, B. (1955). Wave velocities in the earth's crust, Geol. Soc. Am. Special Paper, 62, 19-34.

Hadley, D. and H. Kanamori (1977). Seismic structure of the Transverse Ranges, California, Geol. Soc. of Am., 88, 1469-1478.

Hughes, D. S. and C. Maurette (1956). Variation of elastic wave velocities in granites with pressure and temperature, Geophysics, 21, 277-284.

Hughes, D. S. and C. Maurette (1957). Variation of elastic wave velocities in basic igneous rocks with pressure and temperature, Geophysics, 22, 23-31.

Kanamori, H. and D. Hadley (1975). Crustal structure and temporal velocity change in southern California, Pageoph, 113, 257-280.

Kausel, E. G., Leeds, A. R. and L. Knopoff (1974). Variations of Rayleigh wave phase velocities across the Pacific Ocean, Science, 186, 139-140.

Keller, G. R., Smith, R. B. and L. W. Braile (1975). Crustal structure along the Great Basin - Colorado plateau transition from seismic refraction studies, J. Geophys. Res., 80, 1093.

Linville, A. (1971). Rayleigh-wave multipath analysis using a complex cepstrum technique, Texas Instruments Incorporated, 66 p.

Oppenheim, A. V. and R. W. Schafer (1975). Digital signal processing, Prentice-Hall, Inc., Englewood Cliffs, New Jersey, 585 p.

Press, F. (1956). Determination of crustal structure from phase velocity of Rayleigh waves, Part I: Southern California, Bull. Geol. Soc. Am., 67, 1647-1658.

Press, F. (1960). Crustal structure in the California-Nevada region, J. Geophys. Res., 65, 1039-1051.

Press, F. (1966). Seismic velocities, in Handbook of physical constants, ed. S. P. Clar, Geol. Soc. of America Memoir 97, pp. 195-218.

Raikes, S. (1976). The azimuthal variations of teleseismic P-wave residuals for stations in southern California, Earth and Planetary Sci. Letters, 29, 367-372.

Raikes, S. and D. Hadley (1978). The azimuthal variation of teleseismic P-residuals in southern California: Implications for upper mantle structure, submitted to Tectonophysics.

Richter, C. F. (1950). Velocities of P at short distances, Bull. Seism. Soc. Am., 40, 281-289.

Roller, J. C. and J. H. Healey (1963). Seismic-refraction measurements of crustal structure between Santa Monica Bay and Lake Mead, J. Geophys. Res., 68, no. 29, 5837-5848.

Shock, R. N., Bonner, B. P. and H. Louis (1974). Collection of ultrasonic velocity data as a function of pressure for polycrystalline solids, Lawrence Livermore Laboratory.

Shor, G. G. (1955). Deep reflections from southern California blasts, Trans. Am. Geophys. Union, 36, 133-138.

Shor, G. G. and R. W. Raitt (1956). Seismic studies in the southern California continental borderlands, International Geological Congress, 20th, Mexico, Trabajos section 9, t. 2, pp. 243-259.

Simons, R. (1977). Seismicity of San Diego, 1934-1974, Bull. Seism. Soc. Am., 67, 809-826.

Tsai, Yi-Ben (1972). Use of LP surface waves for source characterizations, Geophys. J. R. Astr. Soc., 31, 111-130.

Wiggins, R. A. (1972). The general linear inverse problem: Implication of surface waves and free oscillations for earth structure, Rev. of Geophys. and Space Phys., 10, 251-285.

# CHAPTER 5

## Seismic Structure of the Upper Mantle Beneath Southern California: Implications for Plate Tectonics

ABSTRACT

Travel-time data obtained from both natural and artificial events occurring in southern California indicate a major, lateral crustal transition within the Transverse Range Province. The eastern crust is very similar to the adjacent Mojave region, where a crustal velocity of 6.2 km/sec is typically observed. The western ranges are dominated by an extensive 6.7 km/sec layer. $P_n$ velocity beneath the western Mojave, Transverse Ranges and northern Peninsular Ranges is 7.8 km/sec. The crustal thickness of these provinces is 30-35 km. The Transverse Ranges do not have a distinct crustal root. Unlike other provinces within southern California, the Transverse Ranges are underlain at a depth of about 40 km by a refractor with a P-velocity of 8.3 km/sec. P-delays from a vertically incident, well-recorded teleseism suggest that this velocity anomaly extends to a depth of 100 km. These data indicate that this high velocity, ridge-like structure is coincident with much of the areal extent of the geomorphic Transverse Ranges and is not offset by the San Andreas fault. Four hypotheses are advanced to explain the continuity of this feature across the plate boundary: 1) Dynamic phase change, 2) A coincidental alignment of crust or mantle anomalies, 3) The lithosphere is restricted to the crust, 4) The plate boundary at depth is displaced from the San Andreas fault at the surface. Within the context of the last model, we suggest the plate boundary at depth is at the eastern end of the velocity anomaly, in the vicinity of the active Helendale-Lenwood-Camprock faults. The regionally observed 7.8 km/sec layer is suggested as a zone of decoupling necessary to accommodate the horizontal shear that

results from the divergence of the crust and upper mantle plate boundaries. We suggest that the geomorphic Transverse Ranges may be, in part, the result of coupling between the crust and upper mantle which is suggested by the locally thin 7.8 km/sec layer.

## INTRODUCTION

The Transverse Ranges have long been an enigma in both the seismological and the geological understanding of the structure of southern California. These east-west trending ranges clearly transverse the tectonic grain not only of southern California, but also of the entire east Pacific coast from the Andes to the Aleutians. Passing obliquely between the San Gabriel and San Bernardino Mountain Ranges and yet not significantly offsetting the east-west topography is the active San Andreas fault system with a horizontal dislocation of 250 km (Crowell, 1973).

The present style of faulting within this area is predominantly east-west, left lateral, strike slip and thrust faulting as typified by the San Fernando and Point Mugu earthquakes (Division of Geological and Planetary Sciences, Caltech, 1971, Ellsworth, et al., 1973). However, the structural geology of the region is extremely complex. The Transverse Ranges east of Cajon Pass are bound on the south by the Banning fault system (Allen, 1957), where crystalline rocks are thrust to the south over very young gravels. North of the Banning system, in the region of Lucerne Valley, Figure 5.1, crystalline and metamorphic rocks are thrust to the north over young alluvium (Dibblee, 1964). Passing through and associated with these two systems is the San Andreas fault system. Thrust faulting in the western Transverse Ranges is similar to that in the eastern Ranges. Crystalline rocks again are thrust south over valley alluvium (Wentworth, et al., 1971). However the general style of tectonic deformation is somewhat different from that within the eastern portions of the range. Large, deep,

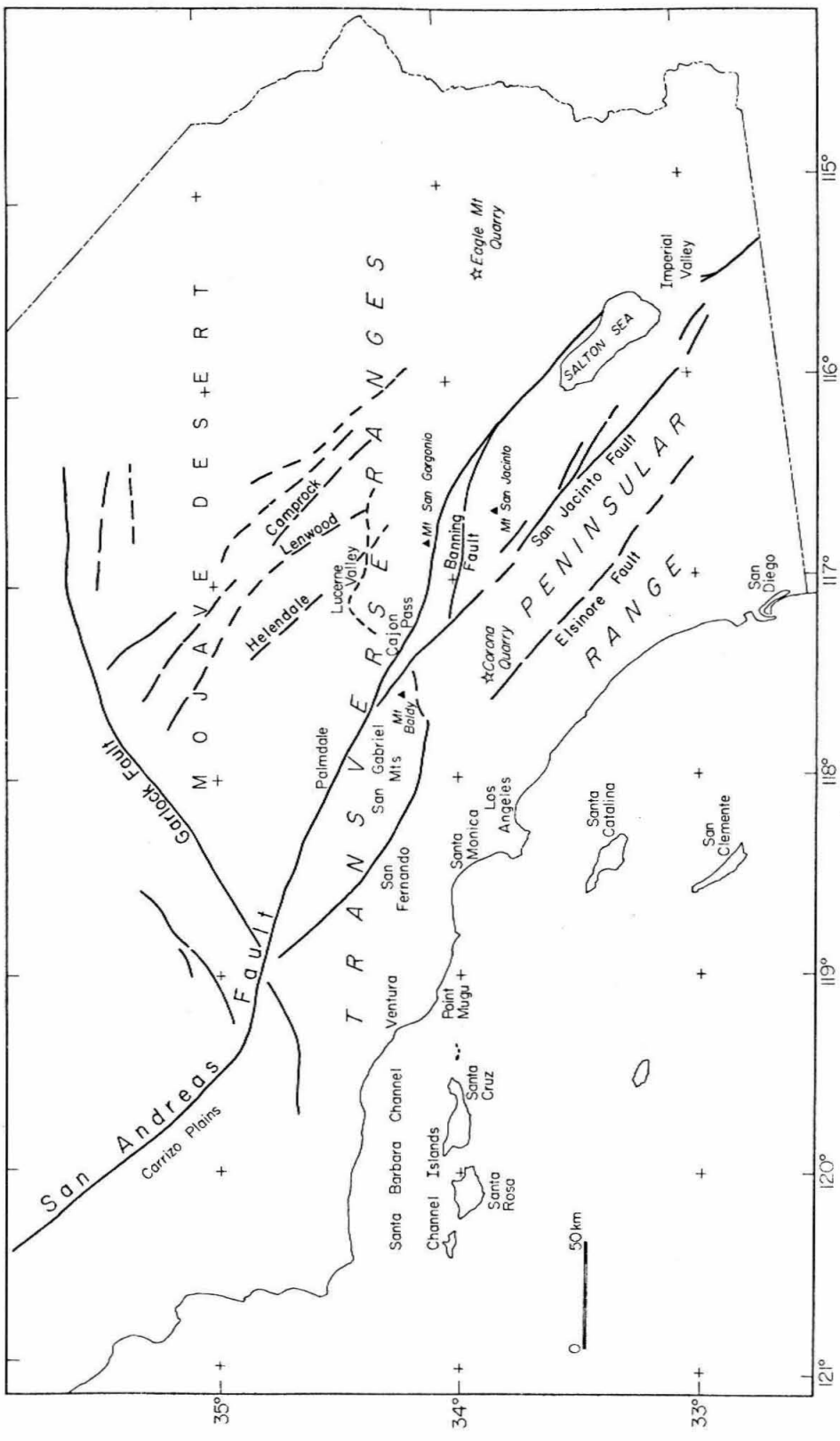


Figure 5.1 Index Map

actively subsiding basins such as the Ventura-Santa Barbara channel and the Los Angeles basin (Vedder, et al., 1969; Yerkes et al., 1965) suggest a mode of vertical tectonics with great uplift and subsidence occurring within the same geologic province. In apparent conflict with this mode of vertical deformation within the Transverse Ranges is the available gravity data (McCulloh, 1960). A warp in the Moho corresponding to the 10 km subsidence within the Los Angeles basin and the great uplift within the San Gabriel mountains is not indicated by the Bouguer gravity data. Instead the data suggest a gentle thinning of the crust towards the offshore borderlands and an essentially uniform crustal thickness beneath the Transverse Ranges (Biehler, personal communication).

Although many investigators have used extensive seismic data in the past to discern crustal structure within southern California, i.e.: Gutenberg (1944, 1951, 1952, 1955), Richter (1950), Shor (1955), Press (1956, 1960), Roller and Healy (1963), Kanamori and Hadley (1975), the great number of seismic stations necessary to delineate structure within a single province is only recently available.

## DATA

The southern California array operated by the California Institute of Technology since the early thirties has experienced of late a nearly exponential growth. The few critical stations initially installed were increased several fold in the early sixties. More recently, in cooperation with the U.S. Geological Survey, the number of stations has been increased to approximately 120. Most of these stations are within the Transverse Ranges, the eastern Mojave and the Imperial Valley.

The present study was initially motivated by the need to interrelate many seismic refraction profiles from different provinces of southern California (Chapter 3). Recent testing at the Nevada Test Site (NTS) provided an ideal source for three distinct seismic refraction profiles that extend to Santa Monica, Corona, and Eagle Mountain, Figure 5.1. An upper crustal velocity of 6.2 km/sec was observed between the distances of 40 and 150 km. Consistent with the northeast trending, reversed refraction profile of Roller and Healy (1963), an intermediate crustal branch with a velocity of 6.7-7.0 km/sec was not observed as a first arrival. $P_n$ velocities appear to increase from 7.8 km/sec for the western profile to about 8.0 km/sec for the eastern. The crustal thickness of about 32 km derived from these profiles is similar to that derived in earlier work (Kanamori and Hadley, 1975). A Corona quarry blast in January, 1975, was used to reverse the center profile. This reversed profile indicates that the Moho is essentially flat. Furthermore, even though the profile passed obliquely through the Transverse Ranges, the travel-time curves

are identical. If the Ranges have a significant crustal root structure, then some shift in the reversed travel-time curve should have been observed. A minimum thickness of the 7.8 km/sec layer is estimated to be about 20 km from the large distance over which this branch is observed.

The same Corona shot was used to establish travel-time curves northwest to the Carrizo Plain, east across the northern end of the Salton Trough and southeast down the Peninsular Ranges, Figure 5.1. $P_n$ data obtained from these profiles are consistent with the earlier interpretation of Kanamori and Hadley,(1975): the western Mojave, central Transverse Ranges and northern Peninsular Ranges are underlain by a relatively uniform 7.8 km/sec layer. Crustal velocities and crossover distances are 6.2 km/sec and 155 km for the Carrizo Plain and 6.2 km/sec and 130 km for the northern end of the Salton Trough. Unlike those obtained for other profiles to date, a crustal velocity of 6.7 km/sec was obtained for the profile down the Peninsular Ranges. The crossover to $P_n$ is 165 km. Finally, a small blast located just south of the Salton Sea was detonated to calibrate the Imperial Valley array. $P_n$ velocity along a composite profile striking approximately N30W was 7.8 km/sec, crustal velocity was 6.2 km/sec and the crossover distance was 100 km. The details of these results are discussed in Chapter 3.

The uniform 7.8 km/sec $P_n$ velocity observed over much of southern California is similar to that typically observed for the tectonically active Basin and Range Province (Pakiser, 1963, Pakiser and Hill, 1963, Keller et al., 1975). The inversion of both Rayleigh wave (Biswas

and Knopoff, 1974) and body wave (Archambeau et al., 1969) data for the Basin and Range indicates that the relatively low $P_n$ velocity extends to depths of at least 150 km. This zone is interpreted as the low velocity zone (LVZ). The base of the crust is viewed as the top of the LVZ. The inferred minimum thickness of 20 km for the uppermost layer of the mantle and the low velocity of 7.8 km/sec suggest, by analogy, that much of the crust of southern California is riding directly upon the LVZ.

In attempting to relate differing crustal thicknesses and velocity profiles derived from these data, an impulsive, distant teleseism was studied. The initial hope was to map the changing crustal sections by observing subtle changes in the observe P-delay times throughout southern California. The teleseism chosen for this purpose was a deep earthquake occurring within the Java Trench. The U.S. Geological Survey hypocentral data are: $7.5^{o}$S, $119.9^{o}$E, depth = 620 km, origin time = 5:45:30.7 GMT, January 23, 1976, $m_b$ = 6.4. The source station separation is approximately $120^{o}$. At this distance the direct P-wave is not well observed, owing to the shadow zone of the earth's core. However, a particularly strong PKP phase, emerging through the crust at an incidence angle of $4^{o}$, was well recorded. The curvature of the wavefront for this phase is extremely slight, $dt/d\Delta$ is constant, and the relative theoretical arrival times at all southern California stations are easily computed. All stations used recorded on 16 mm film that is viewed at a scale of 1 sec/cm. All P-arrival times were read twice and the average time used. Fifty msec was typical of the difference between the two readings.

The theoretical travel times from the source to the stations were calculated by interpolating the Jeffreys-Bullen (J-B) tables over the appropriate depth and distance range. A simple correction for the earth's ellipticity was calculated, although over the area of southern California the relative variation of this correction is negligible. Finally, a height correction was introduced to reduce all stations to a common elevation, sea level. This correction was simply the height of the station divided by the average velocity of the uppermost layer of the crust, 5.0 km/sec. In the worst case, for the highest station, if the velocity is locally as low as 3 km/sec, then this correction is too small by 0.3 sec. More typically, the height correction is probably in error by less than about 0.1 sec. Hence the average error of the relative arrival times across southern California, incorporating both uncertainties in the height correction and reading errors, is of the order of 0.1 sec for low elevation stations and 0.2 sec for the few stations with large height corrections. Table 5.1 lists the stations, distances, arrival times, calculated J-B times, height corrections and final P-delay residuals. Travel-time corrections for stations in the Los Angeles basin situated on deep accumulations of sediments were made on the basis of past refraction data. Similar corrections for the suite of stations north of the Santa Barbara channel have not been included, as our present seismic data do not provide a good estimate of these delays. However, from geologic considerations, these stations are probably delayed by 0.1 to 0.3 sec.

The consistency of the observed residuals, Figure 5.2, attests to the quality of both the timing system and the impulsive, unambiguous

TABLE 5.1 Observed PKP Arrival Times, Epicentral Distances, Jeffreys-Bullen Calculated Travel Times, Station Corrections for Elevation and Sediments and Final P-Delay Times.

Event: Date: January 23, 1976
Origin Time: 5:45:30.7 GMT
Location: 119.9°E, 7.5°S
Depth: 620 km

| Station | Δ(DEG) | T(6:03) | $T_{JB}$ | $T_{HTCR}$ | $T_{SED}$ | $T_{FINAL}$ |
|---|---|---|---|---|---|---|
| CKC | 121.296 | 17.02 | 15.08 | 0.11 | | 1.83 |
| MDA | 121.488 | 17.67 | 15.45 | 0.17 | | 2.07 |
| RAY | 121.613 | 18.12 | 15.69 | 0.47 | | 1.96 |
| WWR | 121.748 | 18.12 | 15.94 | 0.14 | | 2.04 |
| VGR | 121.660 | 18.17 | 15.78 | 0.3 | | 2.09 |
| DB2 | 121.478 | 17.42 | 15.43 | 0.12 | | 1.87 |
| PSP | 121.881 | 18.16 | 16.20 | 0.04 | | 1.92 |
| KEE | 121.832 | 18.39 | 16.11 | 0.27 | | 2.01 |
| CHM | 123.284 | 21.32 | 18.87 | 0.19 | | 2.26 |
| TTM | 123.136 | 21.30 | 18.58 | 0.22 | | 2.50 |
| WH2 | 123.476 | 21.66 | 19.26 | 0.25 | | 2.15 |
| BPK | 123.685 | 21.98 | 19.68 | 0.10 | | 2.20 |
| RVS | 123.461 | 21.69 | 19.24 | 0.14 | | 2.31 |
| LTM | 123.169 | 20.91 | 18.66 | 0.15 | | 2.10 |
| BMM | 123.477 | 21.56 | 19.28 | 0.11 | | 2.17 |
| LGA | 123.798 | 22.17 | 19.94 | 0.01 | | 2.22 |
| FTM | 123.978 | 22.49 | 20.31 | 0.05 | | 2.13 |
| YMD | 123.805 | 22.41 | 19.96 | 0.02 | | 2.43 |
| COT | 122.966 | 20.41 | 18.26 | 0.0 | | 2.15 |
| OBB | 122.767 | 20.45 | 17.89 | 0.0 | | 2.56 |
| SUP | 122.664 | 20.11 | 17.70 | 0.0 | | 2.41 |
| SGL | 122.814 | 20.21 | 17.99 | 0.00 | | 2.22 |
| ING | 123.076 | 20.96 | 18.49 | 0.0 | | 2.47 |
| SNR | 123.002 | 21.27 | 18.35 | 0.0 | | 2.92 |
| COA | 123.258 | 21.51 | 18.86 | 0.0 | | 2.65 |
| THR | 120.764 | 16.11 | 14.04 | 0.21 | | 1.86 |
| BLU | 120.792 | 16.44 | 14.09 | 0.38 | | 1.97 |
| ADL | 121.006 | 16.73 | 14.51 | 0.18 | 0.40 | 1.64 |
| SDW | 121.269 | 16.91 | 15.01 | 0.24 | | 1.66 |
| SIL | 121.529 | 17.72 | 15.52 | 0.35 | | 1.85 |
| SSK | 120.863 | 16.19 | 14.24 | 0.35 | | 1.60 |
| SSV | 121.024 | 16.45 | 14.56 | 0.32 | | 1.57 |
| SYP | 118.947 | 13.01 | 10.50 | 0.26 | | 2.25 |
| ISA | 119.912 | 14.32 | 12.32 | 0.17 | | 1.83 |
| CLC | 120.570 | 15.96 | 13.62 | 0.15 | | 2.19 |
| GSC | 121.320 | 17.60 | 15.10 | 0.20 | | 2.30 |
| SBB | 120.648 | 16.12 | 13.80 | 0.17 | | 2.15 |
| CSP | 121.114 | 16.47 | 14.73 | 0.25 | | 1.49 |
| RVR | 121.116 | 16.61 | 14.84 | 0.05 | | 1.72 |
| PEC | 121.363 | 17.29 | 15.22 | 0.12 | | 1.95 |
| TPC | 122.212 | 19.10 | 16.82 | 0.15 | | 2.13 |
| PLM | 121.726 | 18.19 | 15.92 | 0.34 | | 1.93 |

TABLE 5.1 (continued)

| Station | Δ(DEG) | T(6:03) | $T_{JB}$ | $T_{HTCR}$ | $T_{SED}$ | $T_{FINAL}$ |
|---|---|---|---|---|---|---|
| VST | 121.466 | 17.46 | 15.43 | 0.02 | | 2.01 |
| CPE | 121.633 | 17.88 | 15.76 | 0.04 | | 2.08 |
| SCI | 120.423 | 15.28 | 13.39 | 0.04 | | 1.85 |
| IKP | 122.499 | 19.95 | 17.41 | 0.19 | | 2.35 |
| GLA | 123.455 | 21.67 | 19.25 | 0.13 | | 2.29 |
| RMR | 121.762 | 18.26 | 15.97 | 0.34 | | 1.95 |
| HDG | 121.929 | 18.48 | 16.28 | 0.27 | | 1.93 |
| CPM | 122.081 | 18.90 | 16.57 | 0.19 | | 2.14 |
| INS | 122.135 | 19.09 | 16.68 | 0.34 | | 2.07 |
| PNM | 122.442 | 19.71 | 17.26 | 0.23 | | 2.22 |
| LED | 122.215 | 19.06 | 16.82 | 0.17 | | 2.07 |
| SHH | 122.509 | 19.75 | 17.38 | 0.22 | | 2.15 |
| GRP | 122.397 | 19.98 | 17.15 | 0.25 | | 2.58 |
| SPM | 122.641 | 20.38 | 17.63 | 0.18 | | 2.57 |
| PIU | 122.820 | 20.59 | 17.96 | 0.24 | | 2.39 |
| IRN | 122.894 | 20.60 | 18.12 | 0.20 | | 2.28 |
| CO2 | 122.842 | 20.44 | 18.03 | 0.05 | | 2.36 |
| BC2 | 122.794 | 20.49 | 17.94 | 0.24 | | 2.31 |
| LTC | 123.151 | 20.73 | 18.64 | 0.09 | | 2.00 |
| SBLP | 118.598 | 11.84 | 9.81 | 0.03 | | 2.00 |
| SBSM | 118.739 | 12.18 | 10.10 | 0.03 | | 2.05 |
| SBLC | 119.167 | 13.32 | 10.92 | 0.24 | | 2.16 |
| SBSC | 119.332 | 13.19 | 11.25 | 0.09 | | 1.85 |
| SBSN | 119.581 | 13.79 | 11.74 | 0.05 | | 2.0 |
| SBCD | 119.492 | 13.80 | 11.55 | 0.04 | | 2.21 |
| SBLG | 119.770 | 13.68 | 12.09 | 0.08 | | 1.52 |
| SNS | 121.148 | 17.22 | 14.81 | 0.04 | | 2.37 |
| SJQ | 120.866 | 16.52 | 14.26 | 0.03 | 0.40 | 1.83 |
| CIS | 120.454 | 15.42 | 13.44 | 0.10 | | 1.88 |
| VPD | 120.892 | 16.60 | 14.31 | 0.04 | 0.40 | 1.85 |
| TCC | 120.649 | 15.97 | 13.82 | 0.06 | 0.34 | 1.75 |
| MWC | 120.563 | 15.84 | 13.64 | 0.35 | | 1.85 |
| PAS | 120.487 | 15.50 | 13.49 | 0.06 | | 1.95 |
| SCY | 120.267 | 14.79 | 13.06 | 0.06 | | 1.67 |
| TWL | 120.117 | 14.93 | 12.74 | 0.08 | 0.40 | 1.71 |
| IRC | 120.251 | 14.85 | 13.01 | 0.12 | | 1.72 |
| PYR | 119.937 | 14.90 | 12.38 | 0.25 | | 2.27 |

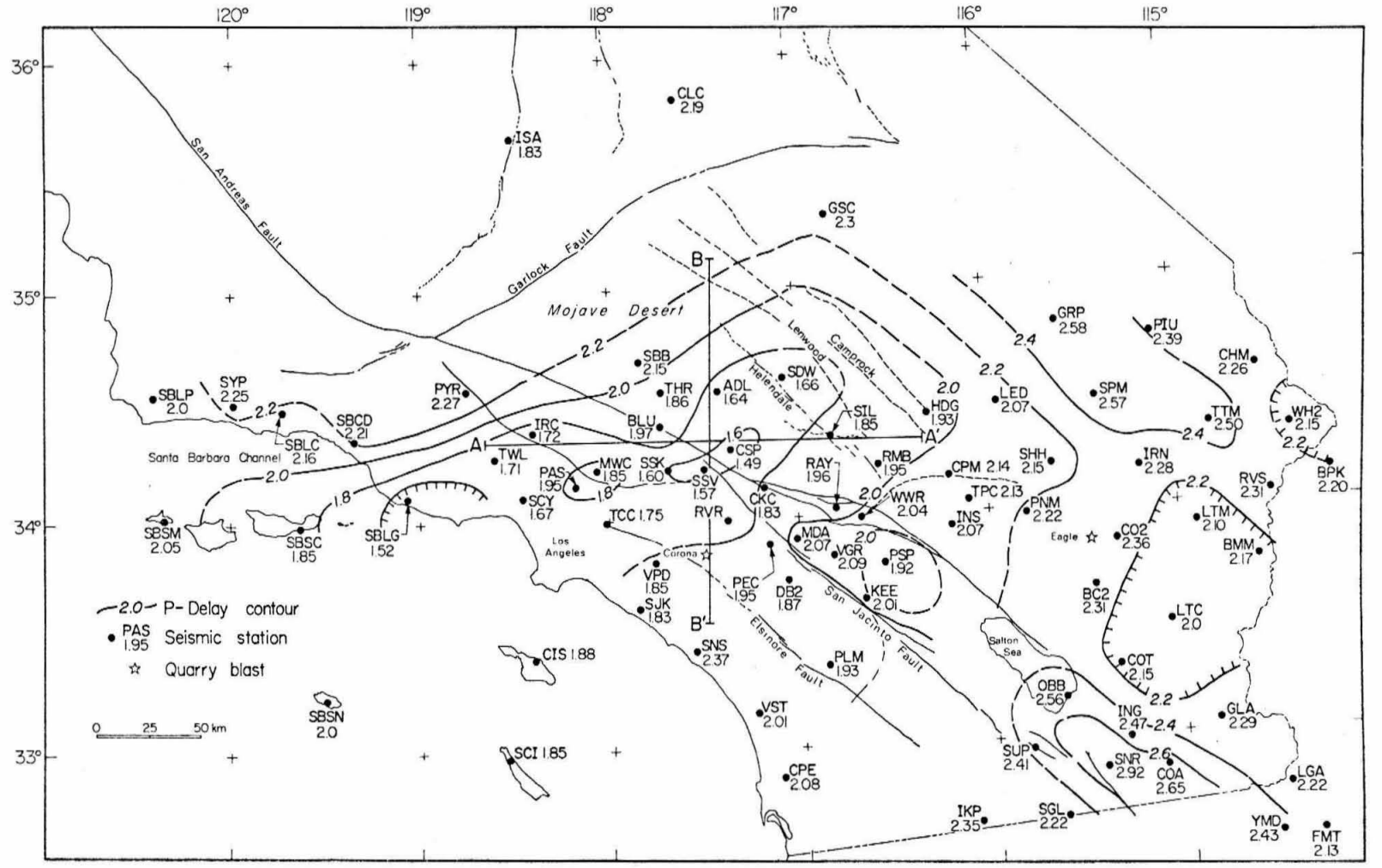


Figure 5.2 P-delay contours. The data for the reduction of the raw arrival time to the final station P-delay residual are listed in Table 5.1. As compared to the Jeffreys-Bullen travel time tables, all stations are late by 1.5 to 2.9 seconds. Station corrections for the sediment delay for the Santa Barbara and for the Imperial Valley stations have not been included.

arrival of this phase. The most striking feature seen in the pattern of P-delays is the very early arrivals recorded throughout most of the Transverse Ranges. The three earliest arrivals, stations SSK, SSV, and CSP straddle the surface expression of the San Andreas fault and arrive 0.7 sec earlier than GSC, a northern Mojave station. This band of advanced arrivals includes the Los Angeles basin and part of the Santa Barbara channel. Corrections for sediment delay north of the Santa Barbara channel would probably broaden the band of early arrivals to include stations SBCD, SBLC, SYP, and SBLP. A second feature is the abrupt transition of delays in the eastern Mojave. Delays range from 2.07 to 2.15 sec at LED and SHH to 2.57 and 2.58 sec for SPM and GRP respectively. Another region of large delays is within the Imperial Valley. The relative P-arrivals for stations within the valley, not corrected for the low-velocity sediments, are 2.5 to 2.9 sec, whereas stations on bedrock and on the periphery of the valley are about 2.3 sec.

The variation in P-delay residuals within southern California is greater than one second. However, the delay from varying crustal structures was expected to be about 0.2 sec. As a large contribution to this variation is associated with the Tranverse Ranges, additional seismic refraction data were collected for paths solely within this region. Two earthquakes with local magnitude of about 4.5 have occurred at opposite ends of the Transverse Ranges since the most recent augmentation of the array, Figure 5.2, Profile A-A. The large number of stations that recorded both events provide excellent hypocenter locations and define several branches of the travel time

curves, Figure 5.3. Epicentral distances to the stations used to locate both events were less than 120 km. More than 20 stations were used for both locations. The crustal velocity model used for the hypocentral determinations was quite similar to that shown at point A', Figure 5.3. The epicentral uncertainty for both events is estimated to be less than 1 km. However, the determined depth for these earthquakes is dependent on the crustal velocity model. On the basis of previous studies, Chapter 2 and 3, the model used to locate the eastern event is probably quite realistic and the hypocentral depth is not likely to be seriously in error. The depth of the western event is somewhat less certain. The calculated depth for this event is 12 km. However, uncertainty in the model suggests 3 km error bars on the location. This results in an uncertainty in the crustal model determination, since the source depth, crustal thickness and crossover distance from $P_g$ to $P_n$ all trade off. Given a crossover distance, the derived crustal thickness and the depth of the event are directly related. In the model presented, the event was located as deep as possible and the resulting crustal thickness represents a maximum. The dissimilarity between the two curves is the result both of differing source depths and of dip on the top of the 6.7 km/sec layer. The solid lines are calculated from the velocity model shown. The thickness and velocity of the topmost layer, although not constrained by the present data, are very typical of many regions in southern California. The eastern end of this structure is similar to that derived in Chapter 2. The western section has a very thick 6.7 km/sec layer. The shallow depth to this interface and the thickness of this

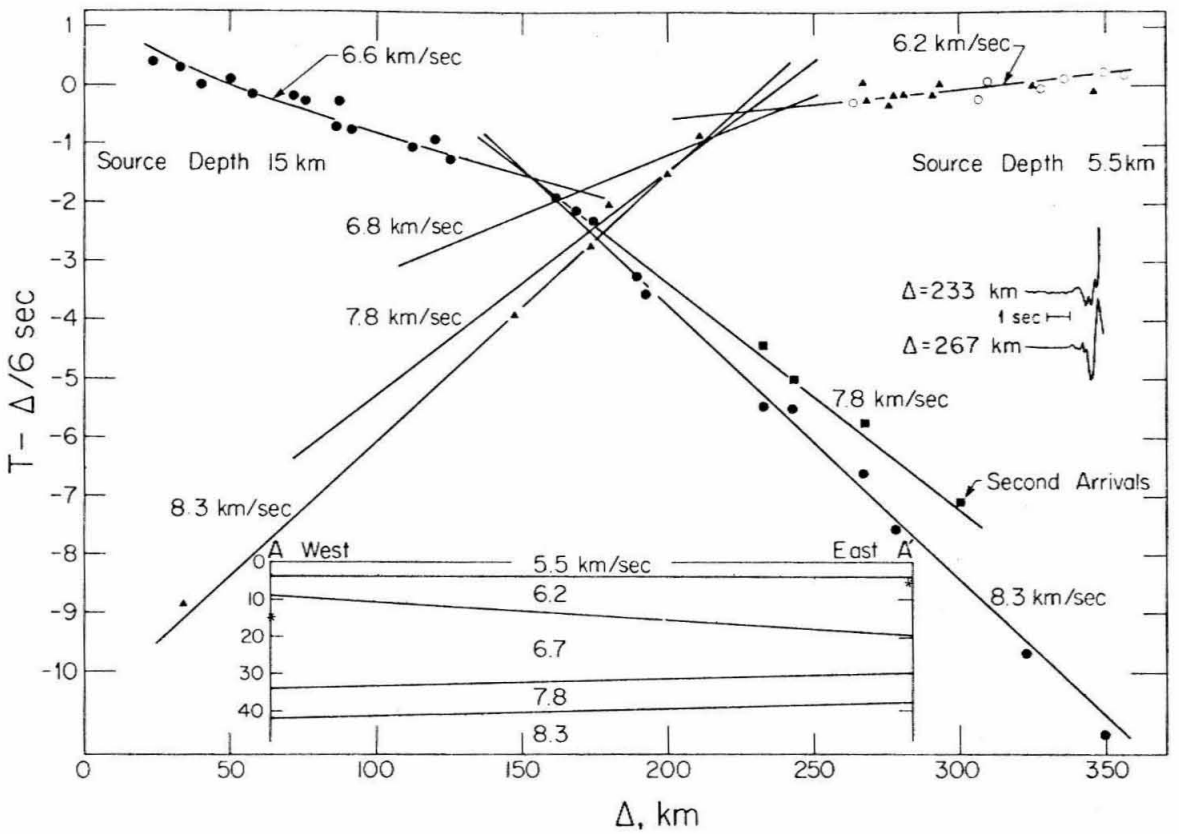


Figure 5.3 Travel-time data from two magnitude 4.5 earthquakes which occurred and were recorded within the Transverse Range Province. Open circle data points are from stations east of the profile. Solid lines are calculated from the inset model. Waveforms show the relative amplitudes of the initial and secondary arrivals. The location of this profile is shown on Figure 5.2.

unit are consistent with the crustal model derived by Stierman and Ellsworth (1976), for the Point Mugu region. Although a large secondary arrival with an apparent velocity of 7.8 km/sec was observed in the distance range 230-300 km for the western, deeper event, the apparent velocity of the first arrival from both earthquakes was 8.3 - 8.4 km/sec. The thickness of the 7.8 km/sec layer is about 8 km, and the top of the 8.3 km/sec layer is approximately 40 km.

## INTERPRETATIONS

The observed P-delay times recorded both within and around the Transverse Ranges cannot be explained as differences arising from dissimilar crustal structure. The expected time difference for a ray passing vertically through the eastern or western ranges, or even through the Mojave crust, is about 0.1 sec. The remaining travel-time advance within this province of about 0.5 sec must then result from an upper mantle, high-velocity structure. The observation of a shallow, high-velocity, 8.3 km/sec structure beneath the Transverse Ranges is consistent with the P-wave advance. The observed velocity difference of 0.5 km/sec between the 8.3 km/sec and the more typical $P_n$ velocity in southern California, 7.8 km/sec, suggests that the high-velocity structure beneath the region of greatest teleseismic P-wave advance must exist over a vertical distance of about 60 km. Figure 5.4 shows a north-south profile through the Cajon Pass area, Profile B-B, Figure 5.2, based on this interpretation. The lateral extent of this high-velocity body must coincide with the region of P-wave advance, the vertical thickness or velocity contrast decreasing to zero beneath regions reporting a more intermediate P-delay of about 2.2 sec. The cross-sectional shape of the body is not well constrained by the present data. An equally acceptable model is a lens-shaped body. The refraction data from both NTS and Corona suggest the 8.3 km/sec body is not at a shallow depth beneath either the southern Mojave or the northern Peninsular Range. This observation precludes a distribution of higher velocity material in a form with the upper and lower boundaries flat and concave upwards respectively. Extending from 40

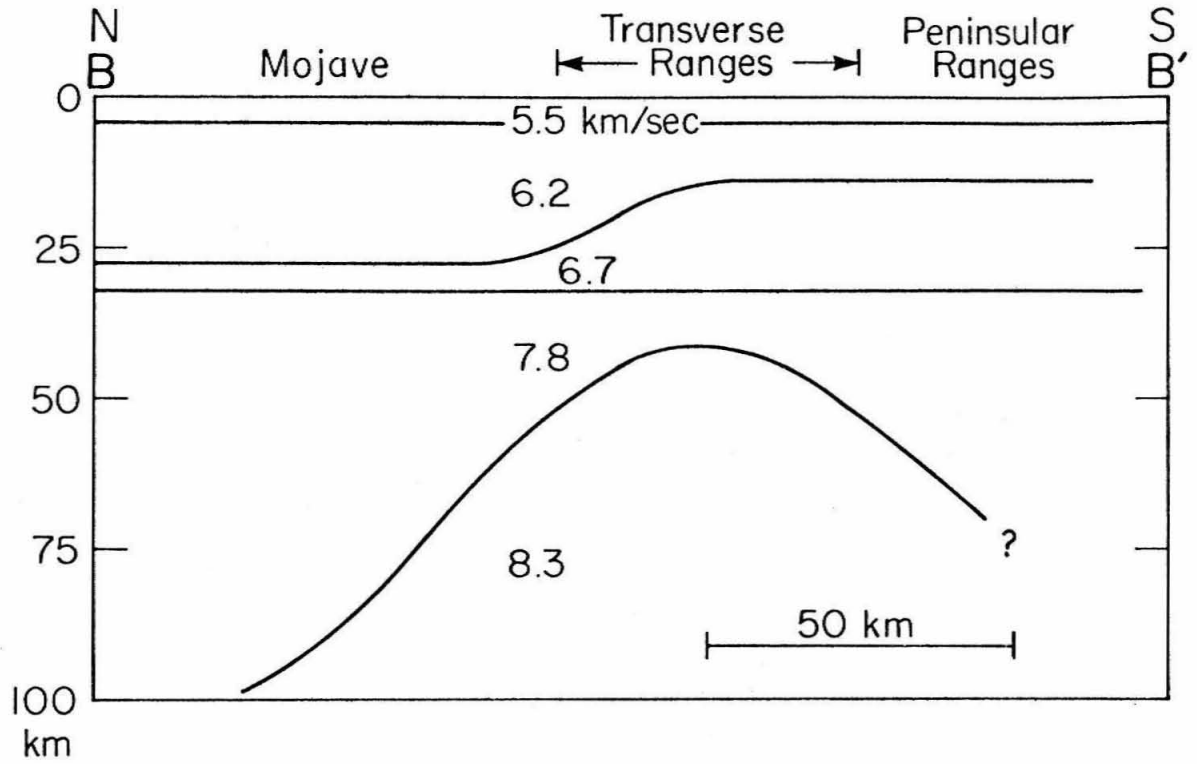


Figure 5.4 North-south cross-section through the Transverse Ranges in the vicinity of Cajon Pass. Seismic sections for the crust from the Mojave, Transverse Ranges and Peninsular Ranges have been smoothly connected in constructing this model. The thickness of the high-velocity upper mantle anomaly is constrained by the vertical travel-time of a well recorded PKP phase.

to 100 km in depth at the point of greatest thickness, this body forms a high-velocity ridge beneath much of the area of the Transverse Ranges.

An alternative contouring of the vertically incident P-delay data in the region bounded by stations SBB, PYR, ISA and GSC would extend the high velocity upper mantle anomaly as far north as ISA. However, the teleseismic data of Raikes (1975), indicates that arrivals from the northeast at PYR, northwest at SBB and southeast at ISA are all delayed relative to other azimuths. This suggests that the upper mantle in the PYR-SBB-ISA region is slow compared with the mantle southeast of SBB and PYR, as indicated by relatively early arrivals. In addition, stations TPC and PEC show early arrivals for northwest azimuths. The lateral extent and the travel-time advance of this anomaly are consistent with the azimuthal P-delay data presented by Raikes (1975).

The surface expression of the San Andreas fault traverses this high-velocity ridge at the pointof greatest inferred thickness, Figure 5.2. If the San Andreas fault represents the plate boundary between the Pacific and the North American plates, then one would normally expect to find this feature truncated by the fault. One of several hypotheses may explain the observed lateral continuity: 1) The anomaly is the result of a phase change that continuously adjusts to maintain this feature across the plate boundary, 2) The apparent continuity is simply the result of a coincidental alignment of crust or upper mantle anomalies, 3) The plate or lithosphere is restricted to the crust, 4) The plate boundary extends to the upper mantle but is

displaced at depth from the San Andreas fault at the surface.

Either temperature or pressure could drive the phase change (Ringwood, 1975). However, changing phases with variable temperature appears difficult. An ad hoc mechanism that could alternately cool and reheat large sections of the upper mantle in the required geometry would be necessary. In addition, the time constant for changing temperatures by diffusion in a body with the observed physical dimensions is several million years; this time constant would be too long to maintain the continuity of the upper mantle feature which is continuously offset by the fault. Although temperature perturbations seem inadequate, stress deviations within the upper mantle could serve to drive the phase change. The lack of earthquakes at depths greater than 20 km implies that if such a stress deviation exists, its magnitude is not large. These arguments suggest that maintaining the continuity of the anomaly, a phenomenon that must continually readjust as the plates move, via a dynamic phase change driven either by the temperature or pressure fields, is unlikely.

Without additional data on the frequency of occurrence of anomalous upper mantle structures elsewhere along the present plate boundary, the probability of a coincidental alignment is difficult to evaluate. The possibility that the anomalous body results from a phase change resulting from a relatively long-lived lithostatic load is worthy of mention. In this model the mantle anomaly is controlled simply by the crust. Indeed, much of the anomaly lies beneath a region of substantial relief, Figure 5.5. Perhaps the continuity of the anomaly across the San Andreas fault is as coincidental as the continuity of

Figure 5.5 Relief map and P-delay contours. Note that much of the relief associated with the Transverse Ranges, including a broad uplift within the south-central Mojave, is underlain by the mantle anomaly. However, the anomaly is present beneath the relatively flat Los Angeles Basin and absent beneath adjacent Mt. San Jacinto. This suggests the crust, via a crustal loading, pressure induced phase change, is not controlling the anomaly.

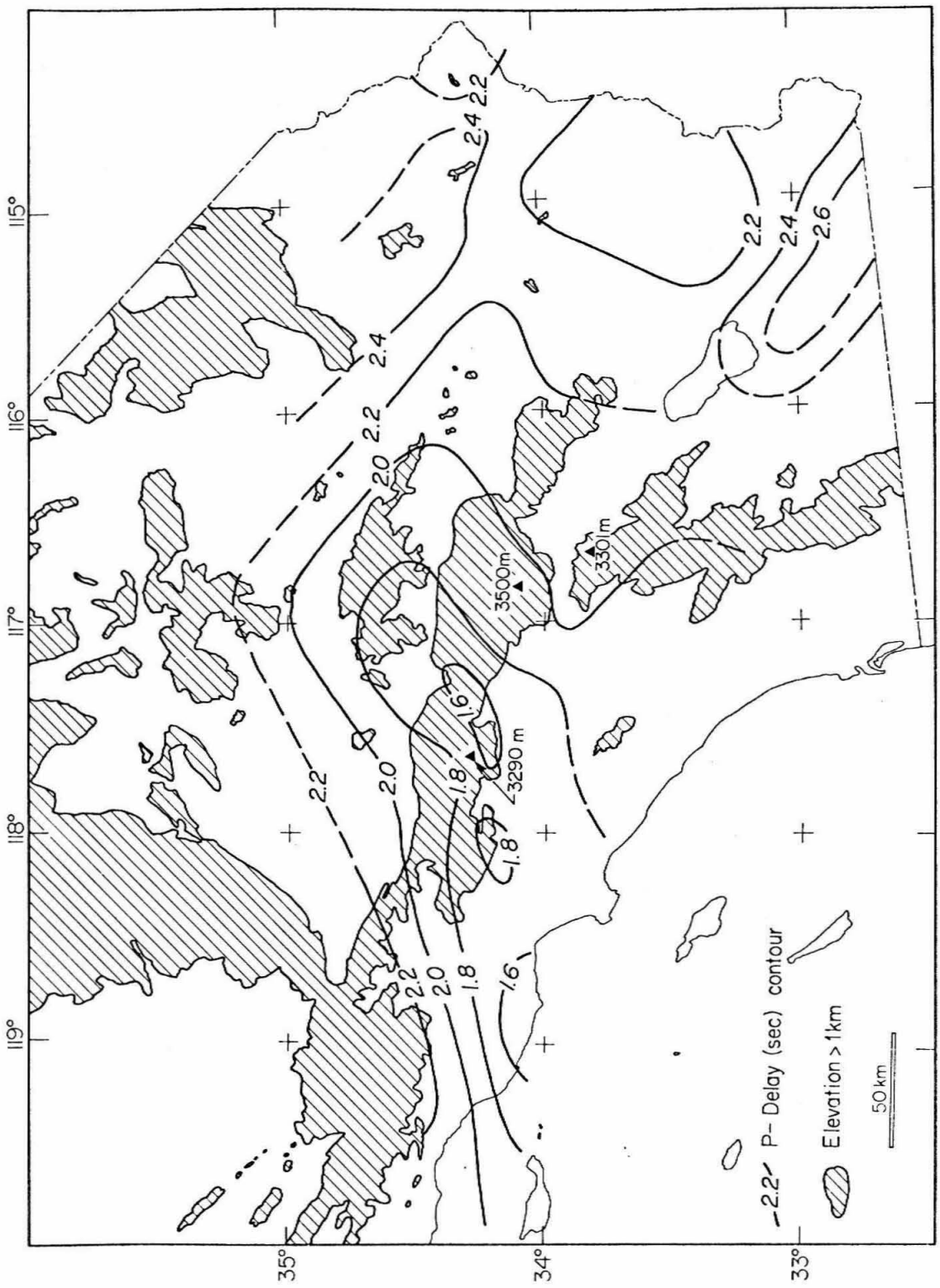
115°
116°
117°
118°
119°
35°
34°
33°
2.2
2.4
2.6
2.0
1.8
1.6
3500m
3290 m
330m
-2.2- P- Delay (sec) contour
Elevation > 1km
50 km

the geomorphic Transverse Ranges. However, the absence of an anomaly beneath Mt. San Jacinto, the second highest peak in southern California and adjacent to the anomalous area, and the presence of the anomaly beneath the low-lying Los Angeles basin, suggests that the lithostatic load is not controlling the anomaly.

The third hypothesis shares an important implication with the fourth. The regionally observed 7.8 km/sec $P_n$ layer, by analogy with the adjacent Basin and Range province as discussed above, suggests the low-velocity zone extends up to the base of the crust. If the low-velocity zone serves as a complete decoupling layer and plate motion is confined to the crust, then most of southern California is underlain by a major zone of horizontal shear at a depth of approximately 30-35 km. The San Andreas fault need not extend beyond the Moho; most of the southern California crust simply moves over a relatively stationary upper mantle. This consequence excludes the possibility that the local plate driving force arises from a viscous drag on the base of the crust from sympathetic motion in the upper mantle. The tractions necessary to move the plate must be applied to the lithosphere in regions exterior to southern California. If this is the present mechanism, then the concentration of strain release along the San Andreas fault, in contrast with the many other faults that could participate, is quite remarkable. One might more reasonably expect the horizontal shear between the North American and the Pacific plates to be manifested in a number of faults within the thin lithosphere.

If the upper mantle participates in the plate motion, then the following question arises: Where is the plate boundary at depth?

The continuity of the high-velocity ridge suggests that the boundary, at depth, is removed either east or west from the San Andreas by at least the amount represented by the lateral extent of the early P-wave arrivals. As in the third hypothesis, this requires a zone of horizontal shear or decoupling within the upper mantle between the surface trace of the plate boundary and that at depth. Unlike the third hypothesis, the decoupling is largely limited to the region between the boundaries at the surface and at depth. Outside of this area, in the general region of the great bend in the San Andreas, minor decoupling must also occur in order to accommodate the variations in slip directions between the crust and upper mantle. The observed low $P_n$ velocity of 7.8 km/sec, substantially lower than $P_n$ velocities of 8.1 to 8.3 km/sec obtained in tectonically stable regions, suggests shear may be occurring within this layer. The structural rifting of the Gulf of California (Henyey and Bischoff, 1973) and the Salton Trough (Biehler et al., 1964) requires a plate boundary extending at least as far north as the Salton Sea. Rather than inferring that the plate boundary at depth strikes west from the Imperial Valley to the Channel Islands, a trend contrary to all of the recent tectonics, we propose the boundary extends northwest along the strike of the structural elements of the trough and passes through the eastern end of the anomaly in the vicinity of the active Helendale-Lenwood-Camprock faults, Figure 5.2. Figure 5.6 is a schematic representation of the proposed model. The plate boundary beneath the Mojave desert is probably not a simple planar structure, but rather a broad zone of shear.

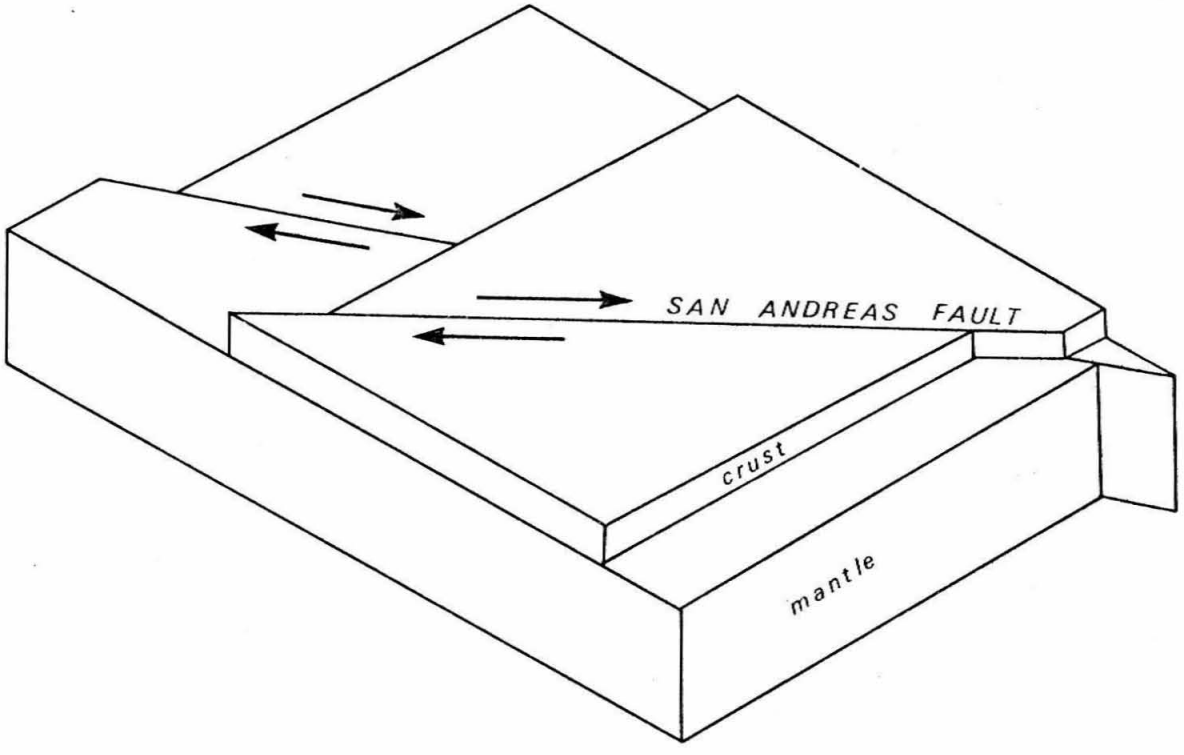


Figure 5.6 Block diagram of the proposed divergence of the crust and mantle plate boundaries: Hypothesis 4. The crust and mantle boundaries are assumed to be coincident within the Salton Trough. The location of the mantle boundary in the Mojave region is inferred from the P-delay data to be in the vicinity of the active Helendale-Lenwood-Camprock Faults.

The present data do not answer the question of the northern continuation of this proposed plate boundary. The great crustal extension seen in the Basin and Range Province must affect the trend of any plate boundary within southern California. However the nature of this interaction, particularly at subcrustal depths, is not yet understood.

The observed thinning of this proposed decoupling layer beneath most of the Transverse Ranges suggests that this region may result simply from greater local coupling between the mantle and the crust than occurs elsewhere. The differential motions between the crust and the upper mantle, which must occur under southern California if the crust and mantle plate boundaries diverge, would have a profound effect upon the crust in this region of greater drag. Within model 4 the morphologic Transverse Ranges, extending across the San Andreas fault, should appear as a constant phenomenon associated with the high velocity upper mantle structure and the thin decoupling layer. As the Pacific plate moves northwest, the Ranges should likewise migrate. Fault systems that penetrate only the crust should have only minor effects on the geomorphology of the range. The Transverse Ranges are viewed as a ripple in the crust that reflects a major upper mantle structure. Both great uplift, such as the San Gabriel Mountains and relatively minor, recent uplift, such as that at Palmdale (Castle, et al., 1975), within the Transverse Ranges, may be reconcilable with a mode of crustal buckling associated with a subcrustal viscous drag.

Ignoring the possibility that the high-velocity structure results from a dynamic, recent process, the maximum emplacement age of the

anomaly should coincide with the cessation of subduction, 15-20 my ago (Atwater, 1970). If this structure were the remnant of subduction, one of two possible mechanisms might control its history: 1) A long lived thermal perturbation or 2) An inherent change in petrology. As a rough estimate of the thermal time constants of this body, consider a slab 100 km thick with initial temperature $T_o$ welded between two half-spaces. After 10 million years the temperature 10 km from the boundaries has changed by only 25 percent. Although the anomaly is clearly not a slab, the time necessary to alter significantly by diffusion the thermal field of a body with dimensions approaching 100 km suggests that an emplacement temperature field is relatively stable over the time bracket of millions of years. This suggests that if an anomalous temperature field were present in the subducted slab, a major portion of that field would still remain today. If the temperature field controls a phase change, such as from garnet-granulite to eclogite, or from a partial melt to the solidus, then the heat of the phase change further stabilizes the field. Although a major, localized change in upper mantle petrology beneath southern California seems unlikely, the phase transition boundary for garnet-granulite to eclogite can be significantly modified by small variations in chemistry (Ringwood, 1975). These considerations suggest that the anomalous mantle structure could result from either an initial thermal field or minor petrologic differences. The regionally averaged Bouguer gravity data might allow a distinction between these two phase change models. Less than one percent melt can reduce the P-velocity from 8.3 to 7.8 km/sec (Anderson and Spetzler, 1970). The associated density change

is less than 0.03 $g/cm^3$. The minimum density change for an equivalent velocity reduction via an eclogite to garnet granulite transition is 0.15 $g/cm^3$ (Ringwood, 1975). For the assumption of a buried horizontal cylinder with the appropriate physical dimensions, the expected maximum Bouguer anomaly is 30 and 150 mgal respectively. The available data (Biehler, personal communication) suggests the partial melt model is preferable.

Assuming that the anomaly is a relic of subduction, either of these two mechanisms implies an inherent, localized variation in the sea floor most recently subducted. The most obvious feature on strike with and approximately the same width as the anomaly is the Murray Fracture Zone, Figure 5.7. South of the Murray scarp--the solid east-trending line in the left third of Figure 5.7--is a broad zone of ridges, troughs and seamounts (Malahoff and Woolard, 1968). The juxtaposed normal and reverse magnetized bodies south of the scarp were interpreted by Malahoff and Woollard as resulting from the incorporation of new crustal material at different times. The magnetic offset around 125°W longitude indicates that about 25 my ago the ridge system of the Pacific-Farallon plates was offset 160 km (Mason, 1958; Atwater and Menard, 1970; Atwater, 1970). The rapid decay of the peak to peak magnetic field intensity from 600 to 200 gamma as the continental slope is approached, compared with a background noise of 50 gamma for any given measurement, hinders attempts to estimate the magnitude of the more recent offset. McKenzie and Parker (1967), have suggested that the Pacific and American plates shared a common pole of rotation during subduction of the

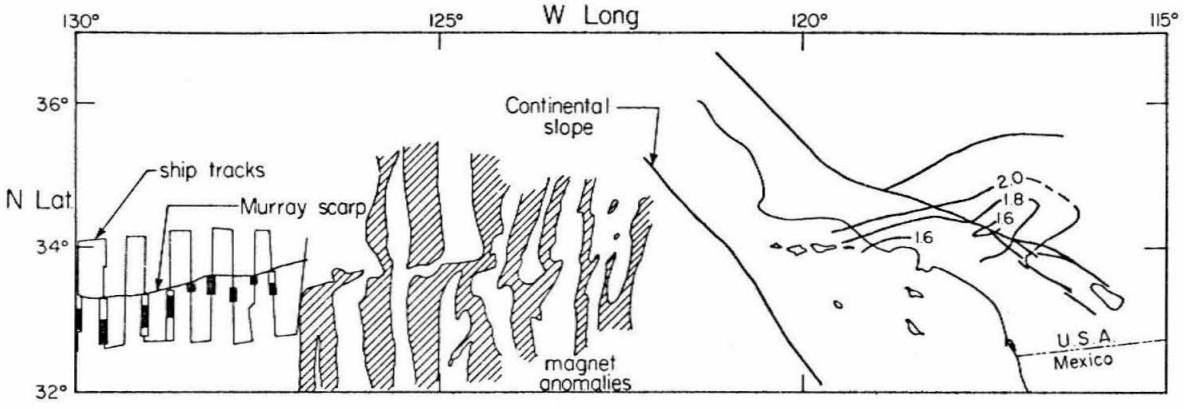


Figure 5.7 Murray Fracture Zone, magnetic anomalies and the southern California P-delay contours. Solid and open rectangles along the ship tracks are normal and reversed magnetized bodies inferred to have been emplaced along the fracture zone (Malahoff and Woollard, 1968). Crosshatched anomalies are magnetized in the normal direction. Offset at 125°W longitude is 160 km (Mason, 1958).

Farallon plate. Although the convergence rate of the Farallon-American plates has been estimated to have been 7 cm/year (Atwater, 1970), the relative motion of the Pacific-American plates, for the same time period, is not constrained. The region of the present anomalous upper mantle structure must have been the site of at least a Trench-Transform junction, or more probably a Trench-Transform-Transform triple junction, depending upon the magnitude of the relative motion between the Pacific and American plates. This junction was active for about 2 million years ($\sim$ 160 km/7 cm/year). However, because of the possibility of major, undetected right-lateral shear between the observable eastern extent of the Murray Fracture Zone and the anomalous, high-velocity structure, a clear connection between these two features cannot be made. The 60-100 km width of the subducted fracture zone (Menard, 1955), intruded by crustal material after the plate left the ridge, and the once active triple junction suggest the present anomaly is at least potentially the site of some unusual past tectonics. Menard (1955) suggested the Transverse Ranges were a direct extension of the Murray Fracture Zone. Perhaps by way of coupling with the present mantle anomaly, he was correct.

## CONCLUSIONS

The velocity structure derived in this chapter for the eastern end of the Transverse Ranges is very similar to a previously published model for the Mojave (Kanamori and Hadley, 1975). The crust beneath the western Ranges, although of similar thickness, has a greater extent of the 6.7 km/sec layer. In this region the depth to the Moho, based on reversed refraction data obtained from accurately located earthquakes, is comparable with that of both the Mojave and the Peninsular Ranges. The Transverse Ranges do not appear to have a distinct crustal root structure. A $P_n$ velocity of 7.8 km/sec has been measured over much of southern California. Refraction profiles, $\Delta > 30$ km, extending from NTS and from Corona suggest a minimum thickness of 20 km for the 7.8 km/sec layer. Beneath the Transverse Ranges this layer has been thinned to about 8 km and is underlain by a refractor with a velocity of 8.3 km/sec. Travel-time advances of a well recorded PKP phase indicate this anomalous body extends in depth from 40 to 100 km. These results suggest a high-velocity ridge in the mantle beneath much of the area of the Transverse Ranges that is not offset by the San Andreas fault. Four possible models are suggested to explain the continuity of this upper mantle anomaly across the San Andreas fault: 1) Dynamic phase change, 2) A coincidental alignment of crust or mantle anomalies, 3) The lithosphere is restricted to the crust, 4) The plate boundary at depth is displaced from the San Andreas fault at the surface. Although all hypotheses are viable, the last model would have the greatest impact upon our understanding of the past and present tectonics of this plate boundary. Within the context of this hypothese we propose

that the plate boundary within the upper mantle is at the eastern end of the anomaly, in the vicinity of the active Helendale-Lenwood-Camp-rock faults and on strike with the southern end of the San Andreas fault. The regionally observed 7.8 km/sec layer is suggested as a zone of decoupling necessary to accommodate the horizontal shear that must result from a divergence of the crust and upper mantle plate boundaries. We suggest that the geomorphic Transverse Ranges may be, in part, the result of enhanced coupling between the crust and the upper mantle as is suggested by the locally thin 7.8 km/sec layer.

REFERENCES

Allen, C. R. (1957). San Andreas Fault Zone in San Gorgonio Pass, Southern California, Bull. Geol. Soc. Am., 68, 315-350.

Anderson, D. L. and H. Spetzler (1970). Partial melting and the low-velocity zone, Phys. Earth Planet. Interiors, 4, 62-64.

Archambeau, C. B., Flinn, E. A., and D. G. Lambert (1969). Fine structure of the upper mantle, J. Geophys. Res., 74, no. 25, 5825-5865.

Atwater, T. (1970). Implications of plate tectonics for the Cenozoic Tectonic Evolution of Western North America, Bull. Geol. Soc. Am., 81, 3513-3535.

Atwater, T., and H. W. Menard (1970). Magnetic lineations in the Northeast Pacific, Earth and Planetary Sci. Letter, 7, 445-450.

Biehler, S., Kovach, R. L., and C. R. Allen (1964). Geophysical framework of the northern end of the Gulf of California Structural Province, Am. Assoc. Petroleum Geologists Mem., 3, 126-143.

Biswas, N. N., and L. Knopoff (1974). The structure of the upper mantle under the United States from the dispersion of Rayleigh Waves, Geophys. J. R. Astro. Soc., 36, 515-539.

Castle, R. O., Church, J. P., Elliott, M. R., and N.L. Morrison (1975). Vertical crustal movements preceding and accompanying the San Fernando Earthquake of February 9, 1971, Tectonophysics, 29, 127-140.

Crowell, J. C. (1973). Problems concerning the San Andreas Fault System in Southern California, Proc. Conf. Tect. Prob. San Andreas Fault System, Kovach and Nur, eds., Stanford Univ. Publ. Geol. Sci.

XII, p. 125-135.

Dibblee, T. W. (1964). Geologic map of the Lucerne Valley Quad., San Bernardino Co., California: U.S. Geol. Surv. Misc. Geol. Inv. Map I-426.

Division of Geological and Planetary Sciences, California Institute of Technology (1971). Preliminary seismological and geological studies of the San Fernando, California, Earthquake of February 9, 1971, Bull. Seism. Soc. Am., 61, no. 2, 491-495.

Ellsworth, W. L., Campbell, R. H., Hill, D. P., Page, R. A., Alewine, R. W., Hanks, T. C., Heaton , T. H., Hileman, J. A., Kanamori, H., Minster, B., and J. H. Whitcomb (1973). Point Mugu, California, Earthquake of 21 February 1973 and its aftershocks, Science, 182, 1127-1129.

Gutenberg, B. (1944). Travel times of principal P and S waves over small distances in Southern California, Bull. Seism. Soc. Am., 34, 13-32.

Gutenberg, B. (1951). Revised travel times in Southern California, Bull. Seism. Soc. Am., 62, 427-439.

Gutenberg, B. (1952). Waves from blasts recorded in Southern California, Trans. Am. Geophys. Union, 33, 427-431.

Gutenberg, B. (1955). Wave velocities in the earth's crust, Geol. Soc. Am. Special Paper 62, 19-34.

Henyey, T. L., and J. L. Bischoff (1973). Tectonic elements of the northern part of the Gulf of California, Bull. Geol. Soc. Am., 84, 315-330.

Kanamori, H. and D. Hadley (1975). Crustal structure and temporal velocity change in Southern California, Pageoph, 113, 257-280.

Keller, G. R., Smith, R. B., and L. W. Braile (1975) Crustal structure along the Great Basin - Colorado Plateau transition from seismic refraction studies, J. Geophys. Res., 80, 1093.

Malahoff, A., and G. P. Woollard (1968). Geophysical studies of the Hawaiian Ridge and Murray Fracture Zone, in: The Sea, A. E. Maxwell, Ed., v. 4, Part II, p. 73-131, John Wiley and Sons, New York, 1971.

Mason, R. G. (1958). A magnetic survey off the West Coast of the United States, Geophys. Jour., 1, 320-329.

McCulloh, T. H. (1960). Gravity variation and the geology of the Los Angeles Basin of California, U.S. Geol. Surv. Prof. Paper 400-B, p. 320-325.

McKenzie, D. P., and R. L. Parker (1967). The North Pacific: An example of tectonics on a sphere, Nature, 216, 1276-1280.

Menard, H. W. (1955). Deformation of the Northeastern Pacific Basin and the West Coast of North America, Bull. Geol. Soc. Am., 66, 1149-1198.

Pakiser, L. C. (1963). Structure of the crust and upper mantle in the Western United States, J. Geophys. Res., 68, 5747-5756.

Pakiser, L. C. and D. P. Hill (1963). Crustal structure in Nevada and Southern Idaho from nuclear explosions, J. Geophys. Res., 68, 5757-5766.

Press, F. (1956). Determination of crustal structure from phase velocity of Rayleigh waves, 1., Bull. Geol. Soc. Am., 67, 1647-1658.

Press, F. (1960). Crustal structure in the California-Nevada Region, J. Geophys. Res., 65, 1039-1051.

Raikes, S. (1975). The azimuthal variations of teleseismic P-wave residuals for stations in Southern California, Earth and Planetary Sci. Letters, 29, 367-372.

Richter, C. F. (1950). Velocities of P at short distances, Bull. Seism. Soc. Am., 40, 281-289.

Ringwood, A. E. (1975). Composition and Petrology of the Earth's Mantle, 618 p., McGraw-Hill, New York.

Roller, J. C., and J. H. Healy (1963). Seismic-refraction measurements of crustal structure between Santa Monica Bay and Lake Mead, J. Geophys. Res., 68, 5837-5848.

Shor, G. G. (1955). Deep reflections from Southern California blasts, Trans. Am. Geophys. Union, 36, 133-138.

Stierman, D. J., and W. L. Ellsworth (1976). Aftershocks of the February 21, 1973 Point Mugu, California Earthquake, Bull. Seism. Soc. Am., 66, 1931-1952.

Vedder, J. G., Wagner, H. C., and J. E. Schoellhammer (1969). Geological framework of the Santa Barbara Channel Region, U.S. Geol. Survey Prof. Paper 679, p. 1-12.

Wentworth, C. M., Yerkes, R. F., and C. R. Allen (1971). Geologic setting and activity of faults in the San Fernando Area, California, U. S. Geol. Survey Prof. Paper 733, p. 6-16.

Yerkes, R. F., McCulloh, T. H., Schoellhammer, J. E., and J. G. Vedder (1965). Geology of the Los Angeles Basin, California - An introduction, U. S. Geol. Survey Prof. Paper 420-A.

# CHAPTER 6

## Recent Seismicity in the San Fernando Region and Tectonics in the West-Central Transverse Ranges, California

ABSTRACT

Since the San Fernando earthquake, February 1971, the density of the southern California seismic array has increased by an order of magnitude. The enhanced coverage provides an ideal setting for the study of the long-term seismicity of the San Fernando aftershock zone and adjacent regions. Most of the recent activity within the San Fernando zone has been thrust faulting at depths shallower than and south of the mainshock. One event located slighly deeper than and several km north of the main event suggests shear along a flat plane. Transport of the upper block is south. This event is very similar to another deep, $M_L$ = 4.5, earthquake 30 km west of San Fernando. If these events are typical of midcrustal deformation, the west-central Transverse Ranges may be a form of decollement. A rapid increase in seismicity ($M_L \geq 3.0$) in the region south of San Fernando suggests an increase in regional strain that either was contemporaneous with or immediately followed the San Fernando earthquake.

## INTRODUCTION

The San Fernando earthquake of February 9, 1971, $M_L$ = 6.4, and the first three months of aftershock activity have been described in detail by a number of authors (Allen et al., 1971; Hanks et al., 1971; Whitcomb, 1973). The purpose of this paper is to investigate and document the ongoing, long-term nature of this aftershock sequence. The relatively shallow location of this event ($h \sim 13$ km) and the high station density provide an ideal setting to monitor the spatial, temporal and mechanical variations in strain release within both the aftershock zone and the region.

The tectonic setting of the aftershock region is quite complex. The northwest trending grain of much of southern California is disrupted by the east-west trending Transverse Ranges. At this time it is not clear if these ranges result from the structurally intimate great bend in the San Andreas or if both features are the response to a deeper structural complexity (Chapter 5). The southern boundary of the western Transverse Ranges is marked by a gently to steeply north dipping thrust fault system. The dip-slip offset has been estimated to be as large as 1 to 3 km (Oakeshott, 1952; Bailey and Jahns, 1954). Recent activity along this fault system is demonstrated by faulted crystalline rocks that rest on Quaternary conglomerates. In addition to the obvious thrust faulting, two other major lineations pass through the aftershock zone. The first lineation is defined by a northeast trending belt of earthquakes that extends from Point Dume to Palmdale. This zone has been described by Whitcomb (1973) and by Hileman (1977). Earthquakes within this zone are interpreted as

northeast trending, left-lateral strike-slip events. Seismic activity along the western limb of the San Fernando aftershock area is associated with this belt. The second lineation is the northwest trending, right-lateral San Gabriel fault. Undisturbed sediments northwest of San Fernando cover this fault and indicate that the structure has not experienced significant movement since the Pliocene (Crowell, 1954).

The hypocentral location of the main shock, $34^{o}$ 24.7' N, $118^{o}$ 24.0' W, h $\sim$ 8.4 km, (Allen et al., 1972) has been problematic. The mechanical instrumentation at Pasadena recording the signals telemetered from stations of the regional seismic array was subjected to strong ground shaking. This disruption obscured the true arrival at the stations telemetered to Pasadena. The subsequent errors in timing and uncertainty in the crustal velocity model used in the location resulted in standard errors of several km. Teleseismic waveform studies (Langston, 1978) are very sensitive to converted phases reflected from the free surface. Langston's study provides a better constraint on the depth of the initiation of the rupture and added insight into variations in the slip parameters during the event. The waveforms confirm Whitcomb's focal mechanism for the mainshock and indicate that rupture started at approximately 13 km depth on a plane dipping $54^{o}$ to the northeast and propagated towards the surface. At a depth of approximately 5 km, the dip of the fault plane shallowed to $30^{o}$. The immediate aftershocks studied by Whitcomb suggest a similar shallowing of the fault dip. The seismic moment for the event, from a number of observers (Aki, 1971; Alewine, 1974; Langston, 1978), is $1 - 2 \times 10^{26}$ dyne-cm.

Previous aftershock studies of this event have been limited to the three months following the main event. As aftershocks are still occurring, this chapter seeks to relate systematically present and past seismic activity. We have chosen to exclude from the study events with magnitudes less than $M_L = 3.5$. This reduces the potential data set from 750 detected events to 125. Since larger events are better recorded by the regional array, this cutoff effectively limits the study to events that potentially can be accurately located. In addition, the tectonic energy release is controlled by the larger events, and hence the conclusions reached from this subset of events should reflect the ongoing tectonics.

In order to compare the hypocentral locations of past and present earthquakes, all events were systematically relocated. Station delays used in this relocation were primarily determined using the station residuals from a carefully timed and relocated recent event that occurred on October 10, 1976, $M_L = 3.9$. This earthquake was well recorded by a dense array and the calculated standard errors for the location are 1 km horizontally and 2.2 km vertically. This master event technique minimizes the effects of lateral velocity variations external to the source region (Johnson and Hadley, 1976). The final absolute locations are a function of the master event. The relative spatial distribution of relocated events is largely independent of minor changes in the absolute location of the master event. The velocity model used in the relocation is similar to that derived for the western Transverse Ranges in Chapter 5. The only major change in the model was the smoothing of velocity contrasts by the addition

of several thin layers. This reduces rapid variations in take-off angles for small changes in the depth of the source and tends to stabilize the determination of focal mechanisms. Mechanisms were determined with the aid of a computer program that exhaustively searches the model space (Whitcomb, 1973). This approach provides a quantitative evaluation of the fit of 80 possible slip-vectors distributed uniformly over the focal hemisphere.

## SPATIAL AND TEMPORAL LOCATION OF ACTIVITY

The relocation technique used for the main event was similar to that described above except that S-P intervals from several epicentrally close strong motion instruments (Earthquake Engineering Research Laboratory, 1976) were included in the relocation. The resulting hypocenter is slightly northeast of earlier determinations: $34^{o}$ 25.45' N and $118^{o}$ 22.63' W. The depth has increased to 11.5 km. Standard errors are 1.1 km horizontally and 2.4 km vertically. This depth is compatible with that determined from teleseismic waveforms. This location is also on the plane defined by aligning Langston's fault geometry with the observed surface faulting.

Figure 6.1a is a stereo pair showing the hypocenters of all accurately located events. Standard location errors are typically less than 3 km. The following descriptions of the aftershock activity have been divided into four intervals of approximately logarithmically increasing duration:

First Day. The well-located events, Figure 6.1b, outline a triangular region. Unfortunately, many events that occurred during the first day were recorded within the coda of previous events. This resulted in large timing errors and excessively large standard errors. The locations of these events are compatible with aftershock activity over the entire triangular region. The fault plane area defined by surface faulting and the wedge-shaped activity during this interval is 200 $km^2$.

Next 10 Days. The area of the aftershock zone has expanded to 300 $km^2$ (Figure 6.1c). The events locate predominately outside of

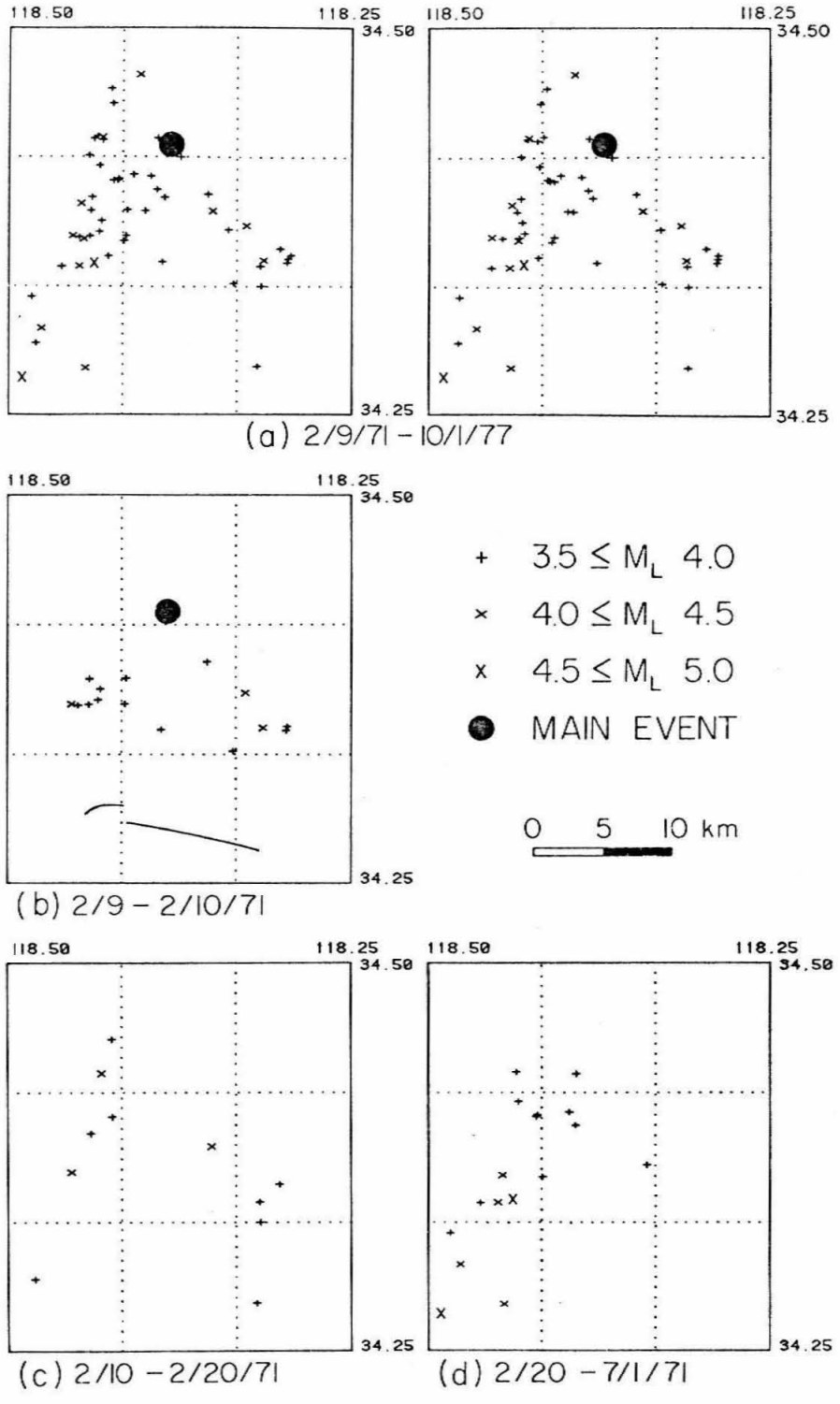


Figure 6.1 Epicenters of well-located events for the time periods: A) 2/9/71 - 10/1/77, B) 2/9 - 2/10/71, C) 2/10 - 2/20/71, D) 2/20 - 10/1/71. The east-west lines in B) are the approximate locations of surface faulting. The first plot is a stereo pair. Average standard errors of the events plotted are 2 km and 3 km for the horizontal and vertical directions respectively.

the region defined by the first day of activity and are north of the surface faulting.

Next 130 Days. There is substantial activity along the west limb of the aftershock zone (Figure 6.1d). This activity includes nine events with magnitudes greater than 4.0 and extends several km south of the surface faulting. Unlike the thrust mechanisms found for most of the events in other parts of the aftershock zone, these events are left-lateral strike-slip along a plane parallel to the lineation of events (Whitcomb, 1973). The absence of surface faulting suggests that the lateral displacement did not extend to the surface. Furthermore, if the seismicity represents reactivation of an old structure, movement on that fault never has reached the surface, since the San Gabriel fault, passing at a right angle through this zone, is not offset (L. Silver, personal communication).

Using a relationship between seismic moment, M, and local magnitude, $M_L$, of the form $\text{Log}(M) = 15 + 1.7\ M_L$ (Hartzell and Brune, 1978), we have computed the cumulative seismic moment for the aftershocks located within the San Fernando region, Figure 6.2. During the interval .1 to 10 days the cumulative moment approaches an asymptote. The subsequent burst of activity along the western limb and migration of activity south of the surface rupture are reflected in the moment sum as a break in slope. This rapid increase in strain release and subsequent return to a slowly decaying rate of release, and the change in style of deformation, suggest that this sequence is distinct from the San Fernando earthquake.

Next 2300 Days. The seismicity is concentrated in a relatively

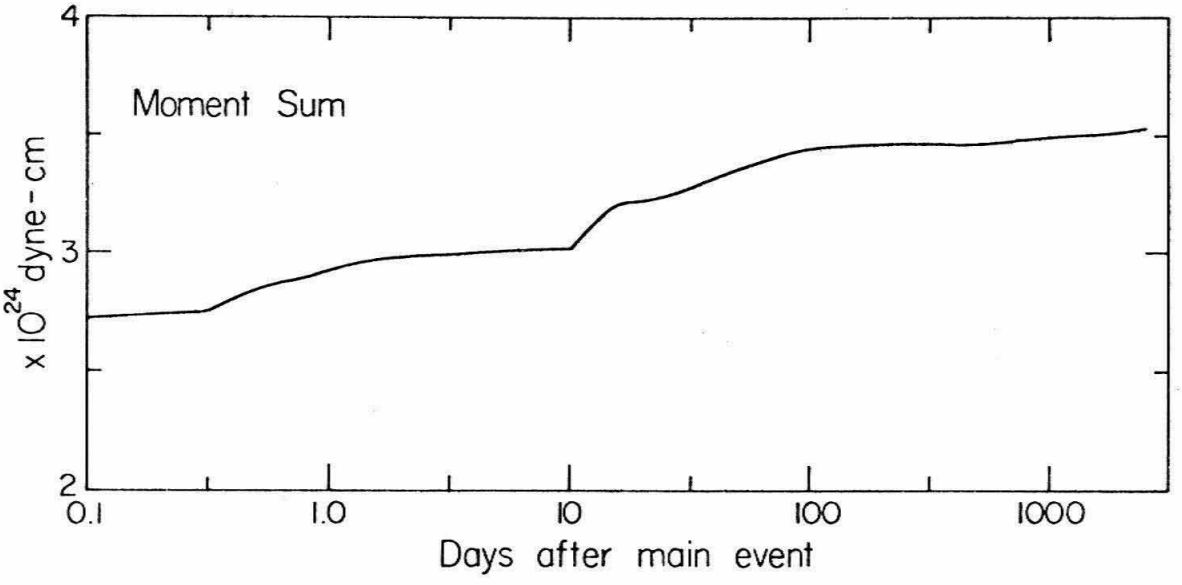


Figure 6.2 Cumulative moment sum as a function of logarithmic time for the entire aftershock sequence. The sharp break in slope at 10 days corresponds to the initiation of the predominately left-lateral strike-slip events plotted in Figure 6.1c.

small subregion southwest of the mainshock (Figure 6.3). Focal mechanisms show considerable variation in the sense of motion. This diversity probably reflects movement on pre-existing planes of weakness, such as older faults, which are geometrically favorable for slip but not necessarily aligned with the planes of maximum shear (McKenzie, 1969). Even allowing for such diversity, the region is presently dominated by thrust events. Figure 6.4 is a north-south cross-section through the main event. All earthquake hypocenters computed for this time interval and determined focal planes have been projected onto this section. Three observations are immediately apparent from this projection: (1) Most of the recent activity is shallower than the main event; (2) movement on the north dipping plane is consistent in both dip and sense of motion with the main shock; and (3) allowing for the projection of the fault plane of the main event, the shallowest earthquakes west of the mainshock are consistently 3-5 km below the inferred mainshock fault plane. This suggests either the fault surface has been downstepped to the west, or these events are occurring along deeper, subparallel fractures.

The focal mechanism of the deepest event, occurring October 17, 1976, is extremely interesting. The depth places this event at the bottom of the seismically active portion of the crust, and the focal mechanism can potentially tell us something about the tectonics at this depth. Our preferred choice of fault plane for this event, most consistent with the observed displacement for the main event, is the very shallow, almost flat fault plane (Figure 6.4). If this event is typical of deformation occurring at midcrustal depths within

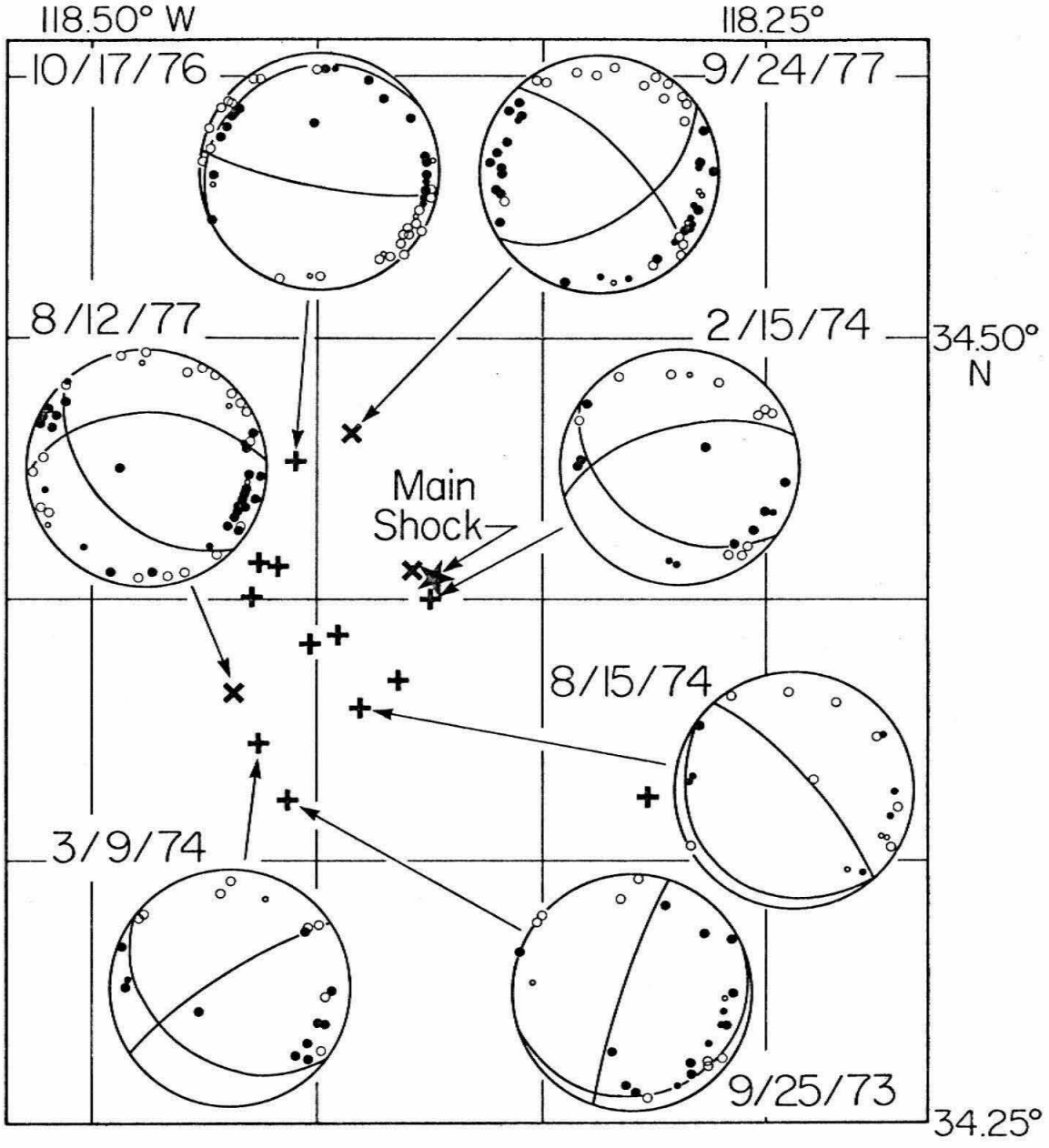


Figure 6.3 Hypocenters and local mechanisms for the period 7/1/71 - 10/1/77. The stereonet projections are lower hemisphere and the solid circles are compression. The deepest event in this sequence, occurring on 10/17/76, suggests southward movement of the upper block on a near horizontal plane.

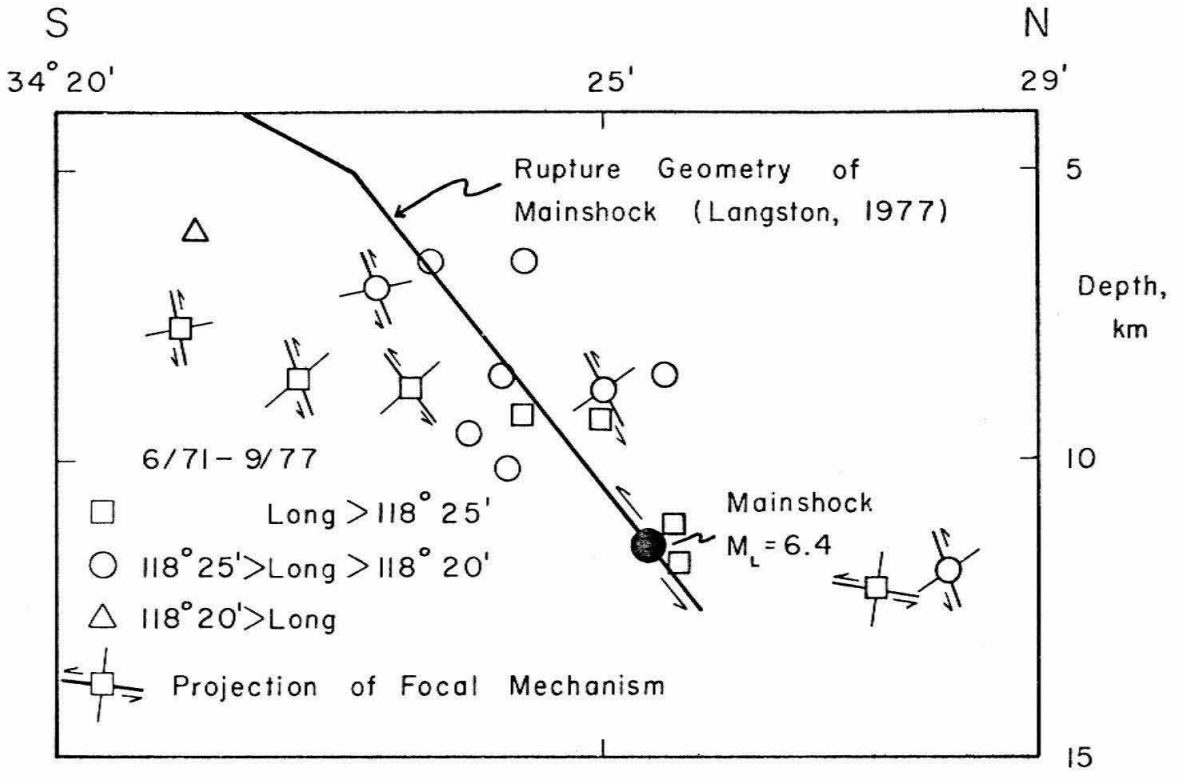


Figure 6.4 Projection of hypocenters and focal mechanisms of the recent activity, shown in plan view on Figure 6.3, onto a north-south plane passing through the main event. The focal planes that pass through the events show the apparent dip as viewed from the east. The arrows indicate the sense of motion on the preferred fault planes.

this province, then the San Gabriel Mountains would be a form of decollement. Movement of the upper block would be to the south.

## REGIONAL TECTONICS

The October 17, 1976 event suggests deformation at midcrustal depths on a very shallow, north-dipping structure. A similar model has been previously proposed to account for regional uplift within the Transverse Ranges and the southwestern Mojave (Thatcher, 1976). Although this is certainly a plausible model for the western Transverse Ranges, a single isolated event is not particularly persuasive. However, in April, 1976, a sequence of earthquakes located 30 km west of the San Fernando mainshock began with a $M_L = 4.5$ event. The location of this event is shown on Figure 6.5, and the focal mechanism data are shown in Figure 6.6. In this area, distinct from San Fernando, the current seismicity was apparently triggered by a deep ($h \sim 12$ km) event. Motion of the upper plate on another near horizontal fault plane was southwest. The similarities between this event and the October 1976 earthquake--both occurred at the bottom of the seismic zone and indicate southward transport of the upper block on a subhorizontal fault surface--suggest a regional decollement.

Within southern California, a $P_n$ velocity of 7.8 km/sec is observed over pathlengths of 400 km. This suggests a minimum thickness for this layer of 20 km. By analogy with studies of the adjacent Basin and Range province (Biswas and Knopoff, 1974; Archambeau et al., 1969), this layer is interpreted as an upward extension of the low velocity zone to the base of the crust. The low upper mantle velocity, depressed from a more typical velocity observed in stable regions of 8.3 km/sec, is interpreted as the result of partial melting. This interpretation is supported by the observation of a substantial velocity anomaly

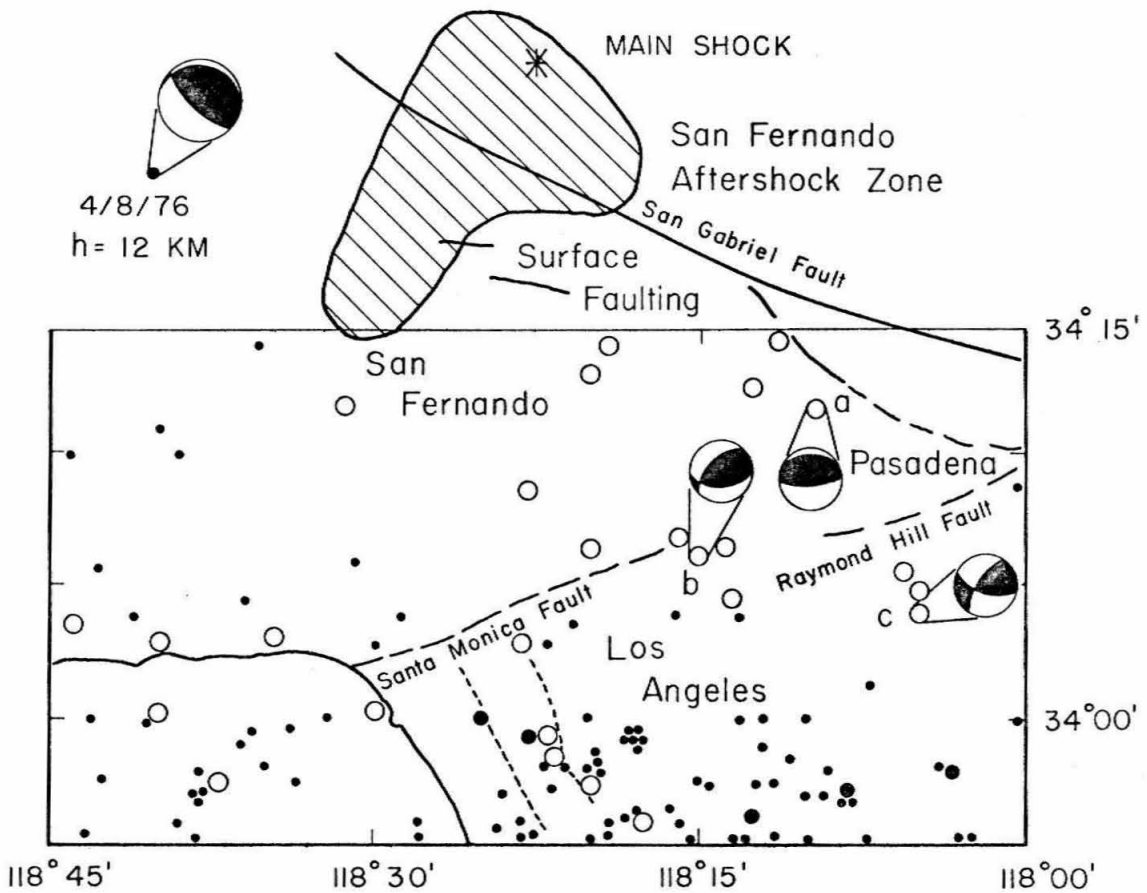


Figure 6.5 Earthquake epicenters ($M_L \geq 3.0$) for the region south of the San Fernando aftershock zone. The events are divided in time by the San Fernando mainshock. The lack of activity in the region around and west of Pasadena in the time interval 1932 - 1970, (solid circles) and the subsequent occurrence of many events, (1971 - September 1977, open circles) suggests a recent increase in the shear stress. Focal mechanism data for the events shown are plotted in Figure 6.6.

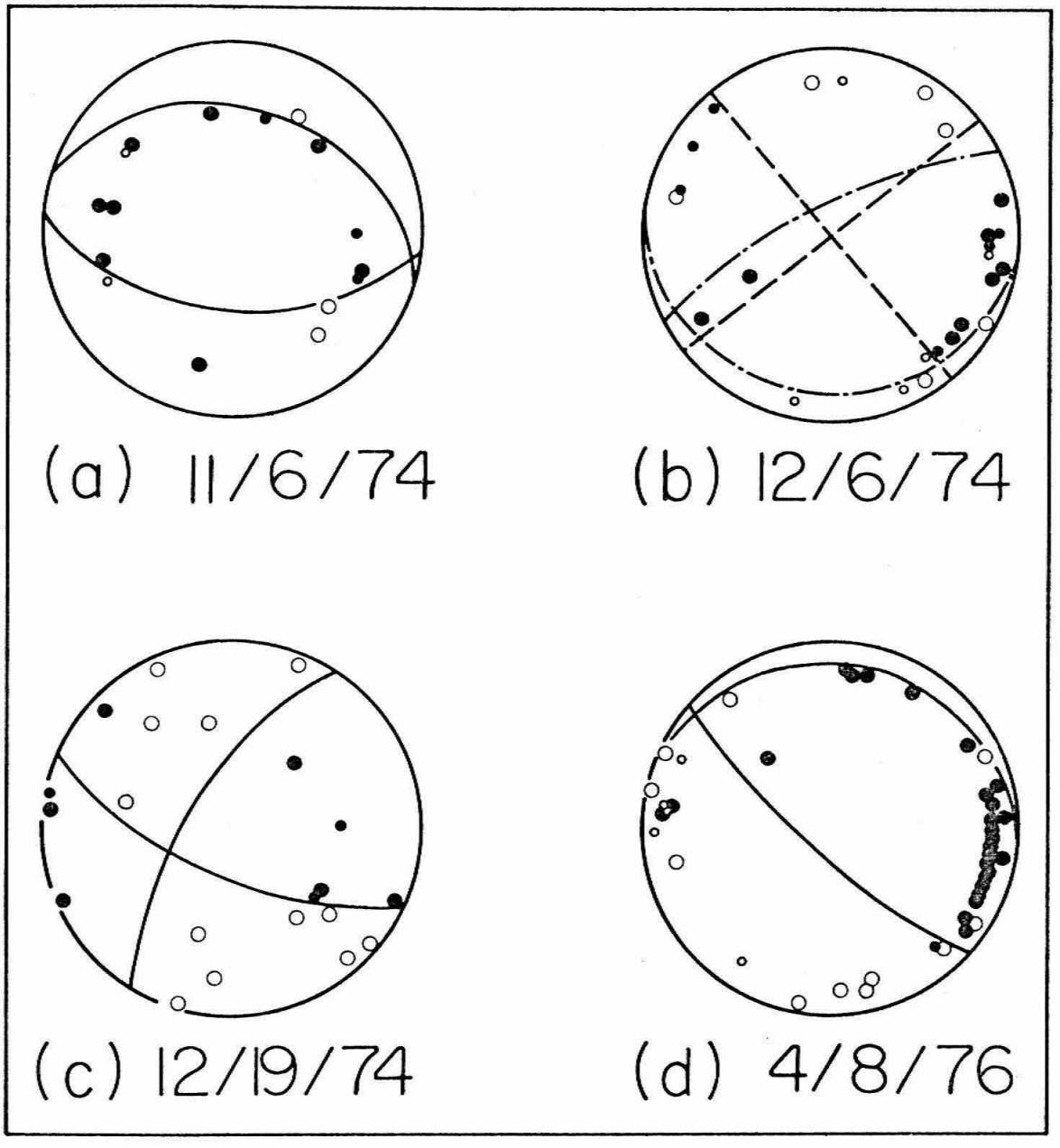


Figure 6.6 Focal data for the mechanisms plotted in Figure 6.5. An alternate solution is shown for event B. The projections are lower hemisphere and solid circles are compressional.

within a subregion of southern California, as discussed in Chapter 5. If this anomaly resulted from a phase change such as garnet-granulite to eclogite a large gravity anomaly would be observed. The absence of any anomaly indicates that the velocity contrast is not accompanied by a significant density contrast. Anderson and Spetzler (1970) have shown that a 1 per cent partial melt can produce the observed velocity contrast. Such a small melt fraction will not affect the gravity. From previous studies (Hadley and Kanamori, 1977; Raikes and Hadley, 1977) there is strong evidence for regional decoupling that is accompanied by large variations in slip direction between the crust and upper mantle. The shallow upper mantle, interpreted as a zone of partial melting, has been suggested as the zone of decoupling. Recent studies of the temperature and compositional effects on the transition from brittle to ductile yielding (Brace and Byerlee, 1970; Byerlee and Brace, 1968) show that these variables may control the depth of the seismic zone within California. Events occurring at the bottom of the seismic zone may be indicative of aseismic deformation within the lower crust. The recent deep seismicity supports the hypothesis of regional shear parallel to a horizontal plane and further suggests that this deformation may not be limited to the upper mantle.

The San Fernando earthquake represents the end result of strain accumulation with the crust. The co-seismic crustal deformations south of San Fernando, considered from either an observational or theoretical base, were small (Alewine, 1973; Castle et al., 1975). The small strain changes require a relatively small change in stress.

If the San Fernando earthquake was the result of very gradual strain accumulation, the regional variations in fault strength and the stress field would control the occurrence of faulting. A regional change in seismicity, particularly in a region not strained by the mainshock, would not be expected. Alternatively, if the stress field changed abruptly, a regional increase in seismicity would be expected. The San Fernando event would represent one of many faults rapidly loaded to failure. Figure 6.5 is a plot of seismicity, $M_L \geq 3.0$, in the region south of San Fernando. The solid symbols are earthquake locations from 1932 through 1970. Open circles are from 1971 to September 1977. Seismicity within the Los Angeles basin shows no increase. However, activity along the southern boundary of the Transverse Ranges, namely at the eastern end of the Santa Monica fault and in the vicinity of the Sierra Madre and Raymond Hill faults, shows a marked increase. The available focal mechanisms for these events, with some diversity, are oblique thrust (Figure 6.6).

The apparent increase in seismicity within this zone of the Transverse Ranges suggests a recent, significant increase in the regional stress. Consistent with this interpretation is the report of Savage and Prescott (1977) of "one east-west geodimeter line near Palmdale... (that shows)... a striking increase in length in the period 1968-1971, a possible precursor to the 1971 San Fernando earthquake." From regional horizontal and vertical geodetic data, Thatcher (1976) similarly concludes that the central Transverse Ranges have recently experienced an episodic strain accumulation.

# CONCLUSIONS

We have systematically relocated the San Fernando mainshock and all ($M_L \geq 3.5$) aftershocks. The cumulative moment sum for the aftershocks shows two distinct sequences of activity. The change in the rate of strain release is accompanied by extension of activity southwest of the surface faulting and by a change in style of faulting from thrust to strike-slip (Whitcomb, 1973). Recent activity is clustered slightly southwest of the mainshock epicenter. The deepest event within the recent activity as well as a separate earthquake 30 km west of the San Fernando earthquake suggest a form of decollement. The relatively abrupt change in seismicity in the region south of the aftershock zone suggests a rapid increase in the stress field. This implies that San Fernando was only one of many faults recently loaded to failure. We speculate that the increase in regional stress is intimately related to inferred aseismic deformation within the lower crust and upper mantle. The few deep events studied to date suggest that this deformation is a horizontal shear with a relative southward transport of the upper portion of the crust.

REFERENCES

Aki, K. (1971). Seismic moment and stress drop, presented at the Annual Meeting of the Seismological Society of America, The San Fernando Earthquake of February 9, 1971, A Symposium, Riverside, California.

Alewine, R. (1973). Application of linear inversion theory toward the estimation of seismic source parameters, Ph.D. thesis, California Institute of Technology.

Anderson, D. L. and H. Spetzler (1970). Partial melting and the low-velocity zone, Phys. Earth Planet. Inter., 4, 62-64.

Allen, C. R., G. R. Engen, T. C. Hanks, J. M. Nordquist, and W. R. Thatcher (1971). Mainshock and larger aftershocks of the San Fernando Earthquake, February 9 though March 1, 1971, U.S. Geol. Surv. Profess. Paper 733, 17-20.

Allen, C. R., T. C. Hanks, J. H. Whitcomb (1972). Seismological studies of the San Fernando Earthquake and their tectonic implications, Calif. Div. Mines Bull., 196, Ch. 20.

Archambeau, C. B., E. A. Flinn, and D. G. Lambert (1969). Fine structure of the upper mantle, J. Geophys. Res., 74, 25, 5825-5865.

Bailey, T. L. and R. H. Jahns (1954). Geology of the Transverse Range province, Southern California, Calif. Div. Mines Bull., 170, Ch. II, 83-106.

Biswas, N. N. and L. Knopoff (1974). The structure of the upper mantle under the United States from the dispersion of Rayleigh waves, Geophys. J. R. Astro. Soc., 36, 515-539.

Brace, W. and J. Byerlee (1970). California earthquakes: Why only shallow focus?, Science, 168, 1573.

Byerlee, J. and W. Brace (1968). Stick-slip, stable sliding and earthquakes--effect of rock type, pressure, strain rate and stiffness, J. Geophys. Res., 73, 6031.

Castle, R. O., J. P. Church, M. R. Elliott, and N. L. Morrison (1975). Vertical crustal movements preceding and accompanying the San Fernando Earthquake of February 9, 1971, Tectonophysics, 29, 127-140.

Crowell, J. C. (1954). Geology of the Ridge Basin area, Los Angeles and Ventura Counties, Calif. Div. Mines Bull., 170.

Earthquake Engineering Research Laboratory (1976). Strong motion earthquake accelerograms, California Institute of Technology, Report No. EERL 76-02.

Hadley, D. and H. Kanamori (1977). Seismic structure of the Transverse Ranges, California, Bull. Geol. Soc. Am., 88, 1469-1478.

Hanks, T. C., T. H. Jordan and J. B. Minster (1971). Precise locations of aftershocks of the San Fernando Earthquake 2300 (GMT) February 10 - 1700 February 11, 1971, U.S. Geol. Surv. Prof. Paper, 733, 21-23.

Hartzell, S. H. and J. N. Brune. Source parameters for the January, 1975 Imperial Valley-Brawley Earthquake swarm, in press.

Hileman, J. A. (1977). A contribution to the study of the seismicity of Southern California, Ph.D. thesis, California Institute of Technology.

Kanamori, H. and D. M. Hadley (1975). Crustal structure and temporal velocity change in Southern California, Pageoph, 113, 257-280.

Johnson, C. E. and D. M. Hadley (1976). Tectonic implications of the Brawley Earthquake swarm, Imperial Valley, California, Bull. Seism. Soc. Am., 66, 1133-1144.

Langston, C. A. (1978). The February 9, 1971 San Fernando Earthquake: A study of source finiteness in teleseismic body waves, submitted to Bull. Seism. Soc. Am.

McKenzie, D. P. (1969). The relation between fault plane solutions for earthquakes and the directions of the principal stresses, Bull. Seism. Soc. Am., 59, 591-601.

Oakeshott, G. B. (1952). Geology and mineral deposits of the San Fernando Quadrangle, Los Angeles County, Calif. Div. Mines Bull., 172.

Raikes, S. A. and D. M. Hadley (1977). Azimuthal variation of teleseismic P-residuals in Southern California: Implications for upper mantle structure, in press.

Savage, J. C. and W. P. Prescott (1977). Geodimeter measurements on the Palmdale Bulge, 1959-77, (abstract), EOS, 58, 1121.

Thatcher, W. (1976). Episodic strain accumulation in Southern California, Science, 194, 691-695.

Whitcomb, J. H. (1971). Fault-plane solutions of the February 9, 1971, San Fernando Earthquake and some aftershocks, U.S. Geol. Surv. Prof. Paper 733, 30-32.

Whitcomb, J. H. (1973). The 1971 San Fernando Earthquake series focal mechanisms and tectonics, Ph.D. thesis, California Institute of Technology.